学位論文

Dynamical Evolution of Quark Degrees of Freedom in the Relativistic Heavy Ion Collision within the Color Glass Condensate Framework

（カラーグラス凝縮による相対論的重イオン衝突におけるクォーク自由度の動的発展）

平成 29 年 12 月博士（理学）申請

東京大学大学院理学系研究科
物理学専攻

モラレス ロドリゲス　パブロ アンドレス

Dynamical Evolution of Quark Degrees of Freedom in the Relativistic Heavy Ion Collision within the Color Glass Condensate Framework

Pablo A. Morales

A Thesis Presented to the Physics Faculty
of the University of Tokyo
in Candidacy for the Degree
of Doctor of Science

December 2017

Abstract

In the context of ultra-relativistic heavy-ion collisions, most of the phenomenological approaches typically assume some initial matter distributions in hydrodynamic simulations. While hydrodynamic models are successful for the late stages of the collision, at early times of the collision the quarks and gluons emerge from the microscopic dynamics of quantum chromodynamics (QCD). On top of the QCD dynamics, during the earliest stages extremely high magnetic fields of the order of $eB \sim 10^{18}$G are expected from peripheral collisions. The existence of such strong magnetic fields leads to a set of novel effects such as the magnetic catalysis of quark matter and exotic transport phenomena. Much of discussion in the recent literature is focused on the exciting possibility to observe the $\mathcal{CP}$-violating effects caused by chiral anomalies: the Chiral Magnetic/Separation Effect (CME/CSE) and the Chiral Vortical Effect (CVE). Anomalous processes as well as the axial charge generation play an important role and are indispensable in understanding the anomalous transport in a quark-gluon plasma (QGP). However the lack of theoretical prediction on a clear-cut signature for anomalous phenomena has frustrated its observation in heavy-ion collision experiments.

This thesis represents an attempt to formulate the axial charge dynamics in an expanding geometry using a simplified setup motivated by the heavy-ion collision. Although most of preceding works assume constant magnetic fields, the lifetime of the magnetic fields is as short as QCD time scales. Therefore precise knowledge on the initial conditions for the heavy-ion collision is required to make a theoretical prediction. This early-time regime with strong magnetic fields is dominated by the coherent gluon fields which can be described well by the Color-Glass-Condensate (CGC) framework. In this thesis, the generation of the axial charge density was studied in systems with the CGC inspired initial conditions for constant background fields. The effect of finite quark masses was given a special attention and the mass suppression of the axial charge generation was numerically confirmed, which is quite non-trivial not directly inferred from the axial Ward identity.

Acknowledgements

First and foremost, I would like to thank my adviser Kenji Fukushima who has helped throughout the development of my Ph.D. thesis as well as for the various advises shaping my formation as a scientist. Without Prof. Fukushima this research would not have been possible. Also, I would like to acknowledge the members of the Hadron group, in particular, Koichi Murase, Shi Pu, Patrick Copinger and Yuuki Fujimoto for various discussions and support. Finally, my wife Midori, who has supported me throughout this long journey and to whom this thesis is dedicated to.

Contents

Chapter 1

Introduction

Behaviour of matter under extreme environments has puzzled us for over half a century, starting with the conjecture of exotic states of matter at high temperatures and density by Fermi during the early 50's. Pomeranchuck in [1] had pointed out that the finite size of hadrons implies a critical density n_c, above which nuclear matter cannot be found in a hadronic state. Hagedorn estimated a critical temperature T_c for nuclear matter around 200 MeV based on the exponential spectrum of hadron masses [2]. At the time, much of the understanding of strong-interacting matter was limited to the parton model which had been confirmed by deep-inelastic scattering processes. It was not until 1973, when the discoveries of asymptotic freedom [3] and infrared slavery [4] lead to the establishment of quantum chromodynamics (QCD) as the fundamental theory of strong interactions.

Based on the asymptotic freedom property Collin and Perry in [5] parallely with Cabibo and Parisi in [6] claimed the transition of hadronic matter to a "*soup*" of deconfined quarks and gluons at high temperatures and densities. This form of matter is now known as a quark-gluon plasma (QGP). The temperatures required to achieve this transition are extremely large comparable to the typical scale of strong interactions $\Lambda_{\mathrm{QCD}} \sim 0.2$ GeV. The ideas of setting up high energy beams as a mean to test this transition phenomenon started at the 1974 Bear Mountain Workshop but did not materialize until the 80's with the Alternating Gradient Synchrotron (AGS) fixed target program at Brookhaven National Laboratory (BNL) and the Super Proton Synchrotron (SPS) at CERN. The AGS was eventually suc-

ceeded by the Relativistic Heavy-Ion Collider (RHIC) at Brookhaven and the SPS by the most recent Large Hadron Collider (LHC) at CERN. RHIC and LHC perform experiments to collide nuclei at center of mass energies $\sqrt{s} = 200A$ GeV and $\sqrt{s} = 5500A$ GeV respectively. The heavy-ion collision events at the RHIC and LHC are of typical length and time scales of order of 10 fm and 1 fm/c, and the produced QGP fireball expands emitting different particles as it cools eventually hadronizing. There are in fact, various striking similarities between studies of the Big-Bang in the early universe and the "Little-Bang" in heavy-ion collision experiments, specially in the thermalization processes from the initial condition with quantum fluctuations prominent examples of this. While the inflation scenario is the most promising candidate for the initial state of the Big-Bang, the Color-Glass-Condensate (CGC) formalism represents a counterpart for the initial state of the heavy-ion collision.

Besides high temperature and density in the ultra-relativistic collisions that realizes QGP formation, extremely strong magnetic fields of the order of 10^{18} G are expected [7] from peripheral collisions. In other words, strongly interacting matter under magnetic fields must be understood to answer some questions in QGP physics relevant electromagnetic probes. This leads to a brand-new field of study combining QCD and QED effects expected to take place in the QGP phase. The strong magnetic field introduces a unique opportunity to study macroscopic manifestations of the quantum anomaly and topological structure of the QCD vacuum. One of the most notable examples of this, is the Chiral Magnetic Effect (CME) [8, 9] which corresponds to a non-dissipative electric current induced by a strong magnetic field at collisions with finite impact parameter on top of chirally imbalanced matter sourced in topologically distinct states. A series of new novel topological effects of increasing interest eventually came along; Chiral Separation Effect (CSE), Chiral Magnetic Wave (CMW) [10] and Chiral Vortical Effect (CVE) [11]. Possible manifestations of these effects are not limited to the ultra-relativistic heavy-ion collisions but also at much lower energy scales in condense matter systems. The observation of a quadratic dependence of the electric conductivity on the magnetic field was the smoking gun for the CME in condense matter systems of the Weyl semimetals [12].

There has been an active search for signatures of the CME in the heavy-ion collisions. Unfortunately, it is a very subtle issue whether an observable in the heavy-ion collisions is a clear-cut signal or not. RHIC and LHC measured electric charge separation at early times by looking at charge dependent azimuthal correlations of produced particles. These results have not been met without controversy and a resolution on a proper observable requires a deeper understanding from the theoretical side. How do we distinguish the signal from background and what are the relevant time and magnitude scales of this effect?. In essence, the CME is the electric current produced in response to an electromagnetic $\boldsymbol{B}$ field on a chirally imbalanced medium and so these two factors of magnetic field and chirality should be carefully addressed. Although the transient magnetic field is strong, the lifetime is short, less than $Q_{sat}^{-1} \sim 0.2$ fm/c for RHIC and $Q_{sat}^{-1} \sim 0.1$ fm/c for the LHC with Q_{sat} being the gluon saturation momentum, that is in fact much shorter than the thermalization time scale. From the chirality imbalance perspective, precise knowledge on the dynamical evolution of the chiral charge is indispensable. Anomalous hydrodynamics [11, 13, 14] and chiral kinetic theory [15, 16] stand out as notable examples of recent theoretical developments in the description of chiral transport; however, these two approaches must be externally supplemented with the initial condition of the heavy-ion collision. Description of the out-of-equilibrium dynamics right after the collision from first principles is important and how to reliably specify the initial conditions of the system is an extremely challenging yet imperative task. Fortunately, by means of perturbative techniques a successful framework has already been developed in the form of an effective field theory of CGC [17, 18]. As the colliding nuclei approach each other at nearly the speed of light, the high energetic partons within the nucleus start to radiate softer gluons carrying a smaller and smaller fraction of the longitudinal momentum of the nuclei, until parton recombination starts to take over and the system reaches parton or gluon saturation. Soft gluons override and so the nucleus in the CGC regime is described by classical coherent color fields associated with these soft partons and quarks are subleading effects. Most quarks are produced almost immediately after the Little-Bang but for most problems, such as how the system thermalization time scale estimate and the produced particle multiplicity computation quarks can be safely neglected.

Quark degrees of freedom introduce chirality onto the system which is a basic ingredient in the generation of the topological current sourced by the quantum anomaly. Searching for experimental signatures for chiral transport phenomena provides us with a unique opportunity to see manifestation of the non-trivial topological QCD vacuum related to the quantum anomaly. Therefore when searching for experimental signatures of CME or CSE, it is of utmost important to come up with a quantitative description of quark production. However it was just very recent when the precise quark field initial condition was resolved in an expanding geometry [19]. With such initial condition at hand, this thesis provides the first attempt to perform the numerical calculation for the axial charge dynamics.

This thesis is structured as follows: The first two chapters are devoted to reviews of background physics; Chapter 2 on the basics of the QCD with an emphasis on the introduction of strong-$\boldsymbol{B}$ induced phenomena and Chapter 3 focused on discussing the theoretical foundations of the small-x physics and the CGC initial condition relevant to our problem. Chapters 4 and 5 will be about elucidating the quark spectrum in the heavy-ion collision setup: Chapter 4 shall explain in all detail the initial condition employed in this work and Chapter 5 contains the original results of this thesis describing the axial charge generation and its mass dependence before finalizing with the conclusions.

Chapter 2

Fundamental Aspects of QCD

Quantum Chromodynamics (QCD) has been accepted to be the theory that explains strong interactions. The QCD degrees of freedom are quark fields and gluon gauge fields, which possess color and charge and, up till now, have not been detected as isolated free particles. It is a non-abelian gauge theory, whose gauge group is the color group SU(3), although it is convenient sometimes to think in the number of colors as a variable N_c, and so in that case the gauge group becomes SU(N_c). There are $N_c^2 - 1 = 8$ gauge bosons for the theory called gluons, and the matter particles are quarks with spin $1/2$ of which we find $N_f = 6$ kinds, or flavors of them. The theory has profound contents to be explored with external parameters such as the temperature, baryon chemical potential and magnetic field, for what it is high desirable to study its phase structure. However, this construction, represents one the most difficult tasks up to date. This purpose of this chapter is to outline some basic concepts of QCD. The underlying gauge group of the theory is color SU(3) (local color symmetry), the Lagrangian of Quantum Chromodynamics reads,

$$\mathscr{L}_{QCD} = \bar{\psi}\left(i\gamma^{\mu}D_{\mu} - M\right)\psi - \frac{1}{4}F^{a}_{\mu\nu}F^{\mu\nu}_{a} \ , \tag{2.1}$$

where the quark fields ψ belong to the color SU(3) triplet and the gluon fields A^{a}_{μ} to the octet of the same group. The field-strength tensor and covariant derivative are given by

$$
\begin{aligned}
F^a_{\mu\nu} &= \partial_\mu A^a_\nu - \partial_\nu A^a_\mu + g f_{abc} A^b_\mu A^c_\nu \\
(D_\mu)_{cc'} &= \delta_{cc'}\partial_\mu - ig\frac{1}{2}(\lambda^a)_{cc'} A^a_\mu \, .
\end{aligned}
\tag{2.2}
$$

It should be noted there is only one coupling constant between quarks and gluons, and that the gluon field can self interact, this self interaction is the main source of asymptotic freedom. Here the indices $\mu, \nu = 0, ..., 3$ refer to Lorentz vector labels; the labels $a, b, c = 1, ..., 8$ belong to the adjoint representation of color SU(3) and $c, c' = 1, ..., 3$ in context are color labels belonging to the fundamental representation of color SU(3) group. In (2.1) M is a matrix color independent which can always be brought to its diagonal form through flavor-mixing transformations, so that the fermion mass contribution to $\mathscr{L}_{QCD}$ may be written as

$$
\mathscr{L}_{mass} = \sum_{\alpha=1}^{N_c} \sum_{f=1}^{N_f} m_f \bar{\psi}^f_\alpha \psi^f_\alpha \, . \tag{2.3}
$$

The Lagrangian (2.1) is invariant under color SU(3) gauge transformations $U(x) = \exp(-i\theta^a(x)\lambda^a)$ that is, $\psi(x) \to U(x)\psi, gA_\mu(x) \to U(x)(gA_\mu(x) - i\partial_\mu)U^\dagger(x)$. This gauge invariance rules out terms like $A^a_\mu A^\mu_a$ and as a result the gluons are massless. On the other hand gauge symmetry does not restrict the quark's mass in any way and they are indeed finite. Within the standard model the quarks mass is described by Yukawa coupling, yet the wide rande of masses among different flavours is not understood.

QCD is a renormalizable quantum field theory, and as such, its coupling constant $\alpha_s(Q^2)$ is a function of the energy scale, the coupling constant of strong interactions (as it can be seen already at a one-loop order calculation)

$$
\alpha_s(Q^2) \equiv \frac{g^2(Q^2)}{4\pi} = \frac{4\pi}{(11 - \frac{2}{3}N_f)\ln\left(\frac{Q^2}{\Lambda^2_{QCD}}\right)} \, ,
$$

goes to zero as energy goes to infinity, or in other words, at short distances the coupling between quarks and gluons becomes small therefore the perturbative treatment developed for quantum elec-

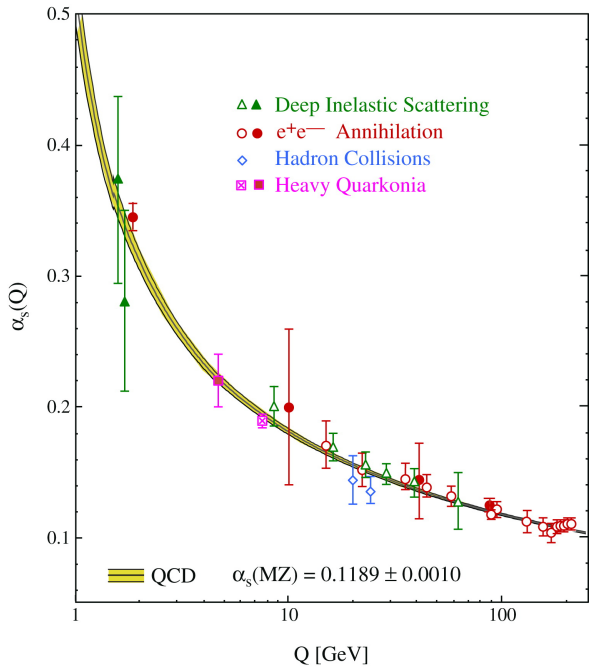

FIG. 2.1: Experimental data contrasted with theoretical prediction of the coupling in constant in QCD, asymptotic freedom. Figure taken from Ref. [3]

trodynamics can be extended to QCD at energies above the QCD energy scale $\Lambda_{\text{QCD}} \simeq 200$ MeV, behavior is known as asymptotic freedom [20]. On the other hand, at low energies, i.e. at low momentum transfers Q^2, or equivalently at great distances, the coupling constant $\alpha_s(Q^2)$ grows to the point that perturbative techniques are no longer valid. And so despite of having a Lagrangian in which all the dynamics of the system is contained, it is not possible to obtain information of many physical processes of interest, like properties of hadrons at low energies and their interactions or the behavior of hadronic matter at high densities. By means non-perturbative frameworks that lead to a deeper understanding of the complicated vacuum structure of QCD and infrared phenomena in QCD. A remarkable example of this is the dynamical breaking of chiral symmetry, mechanism responsible for the mass generation of all visible matter. In order to discuss these subjects, a brief review of QCD symmetries is presented in the following section.

2.1 QCD Symmetries and Their Realization

The QCD Lagrangian is quite rich in symmetries. Besides having SU(N_c) local gauge symmetry and Lorentz invariance as exact symmetries in its core, the QCD Lagrangian also has discrete and approximate symmetries such as isospin symmetry and chiral symmetry which are certainly quite relevant at the moment of studying hadron phenomena. Among the discrete symmetries there is time-reversal $\mathcal{T}$, charge conjugation $\mathcal{C}$ and parity $\mathcal{P}$, however the behavior of QCD at quantum level unravels a much more complicated scenario under $\mathcal{CP}$-transformations, the strong $\mathcal{CP}$-problem. Also, as it shall be discussed to some brief extent, some symmetries that are gained in the massless limit like dilatation and axial are broken at the quantum level, referred as anomalies.

We may conveniently separate $\mathscr{L}_{\text{QCD}}$ for our purposes, with diagonal quark mass matrix in flavor space emphasizing on the lighter quarks *up* and *down* and calling $\mathscr{L}_{scbt}$ to the part of the Lagrangian associated with the heavier quarks, $\mathscr{L}_{QCD} = \mathscr{L}_{ud} + \mathscr{L}_{scbt}$, where

$$\mathscr{L}_{ud} = \bar{q} i\gamma^\mu D_\mu q - (m_u \bar{u}u + m_d \bar{d}d) + \frac{1}{4} F^a_{\mu\nu} F^{\mu\nu}_a, \qquad q = \begin{pmatrix} u \\ d \end{pmatrix}. \tag{2.4}$$

Leaving out the heavy sector, we find that the Lagrangian is invariant under separate global phase for both up and down quarks. The conservation law associated with this invariance is that of baryon number. When $m_u - m_d$ is small compared to the hadronic mass scale then the bilinear present in (2.4) is now invariant under transformations $U\psi \to \psi$ where U can be some unitary 2×2 matrix in flavor or Dirac space or a combination of matrices in both spaces. Unitary transformations $\text{U}(1)_V$ and $\text{SU}(2)_V$ are well known symmetries that result on baryonic and isospin conservation, respectively.

The symmetry grows larger when we neglect the up and down quark mass. To see these more explicit, let us write $\mathscr{L}_{ud}$ projecting ψ into left and right components, i.e. $\psi_{L/R} = \frac{1}{2}(1 \pm \gamma_5)\psi$ the quark sector then reads,

$$\mathscr{L}_{ud} = \bar{\psi}_L i\gamma^\mu D_\mu \psi_L + \bar{\psi}_R i\gamma^\mu D_\mu \psi_R \,, \tag{2.5}$$

where we can see how the vanishing of the mass term implies no crossing term between left and

right quark fields. Consequently, left and right rotations leave the Lagrangian invariant, and thus the symmetry group is upgraded to

$$\mathscr{G} = \mathrm{SU}_L(2) \otimes \mathrm{SU}_R(2) \,. \tag{2.6}$$

The symmetries of and their manifestation in nature are shown in table (2.1). The corresponding currents of $\mathscr{L}_{ud}$ are given by

$$\begin{aligned} \partial^\mu J^j_\mu &= i\bar{\psi}[m, \lambda^j]\psi \\ \partial^\mu J^j_{\mu 5} &= i\bar{\psi}\{m, \lambda^j\}\gamma_5\psi \\ \partial^\mu J^0_{\mu 5} &= \sqrt{\frac{2}{N_f}}\left(i\bar{\psi}m\gamma_5\psi - 2N_f\frac{g^2}{32\pi^2}F^a_{\mu\nu}\tilde{F}^{\mu\nu}_a\right) , \end{aligned} \tag{2.7}$$

where $F^a_{\mu\nu} = \frac{1}{2}\epsilon_{\mu\nu\lambda\rho}F^{\lambda\rho}_a$ corresponds to the dual field strength tensor. The spontaneous breaking of the global SU(2) symmetry, in this limit an exact, to $\mathrm{SU}_V(2)$ is identified with pion triplet (π^-, π^0, π^+). Here we can also see how even in the massless limit the axial charge does not vanishing but from an extra contribution coming from the quantum effect referred as axial anomaly. This extra term comes from an extra contribution from the path integral measure which is not invariant under $\mathrm{U}_A(1)$ axial rotations. The spontaneous breaking of this symmetry predics yet another Goldstone boson, the η' meson. As it turns out, the experimental data revealed that the mass for the η' meson is too large $m_{\eta'} \sim$ 975 MeV, far exceeding the upper bound $\sim \sqrt{3}m_\pi$ to be regarded as a NG boson. This inconsistency implies that there might be a dynamical mechanism that gives the η' its large mass. It was not until in Ref. [21] when t'Hooft revisited the U(1) problem considering the instanton configurations that a resolution was found. To this end let us briefly discuss the QCD θ-vacuum.

2.1.1 Spontaneous Breaking of Chiral Symmetry

The QCD chiral symmetry group governs the dynamics of the light sector, as quarks the actions remains invariant under $U_R U_R$ transformations, equivalently this symmetry group may be expressed as $U_V U_A$. As opposed to vector rotations, axial rotations mix states with different parities, if this symmetry was an exact one then there would be parity degeneracy of states with otherwise the same

Symmetry	Transformation	Currents	Name	Manifestation
$SU_V(2)$	$\psi \to e^{-i\tau\cdot\omega/2}\psi$	$J^k_\mu = \bar{\psi}\gamma_\mu\tau^k\psi$	isospin	approx. conserved
$U_V(1)$	$\psi \to e^{-i\alpha}\psi$	$j_\mu = \bar{\psi}\gamma_\mu\psi$	baryonic	always conserved
$SU_A(2)$	$\psi \to e^{-i\tau\cdot\theta\gamma_5/2}\psi$	$J^k_{5\mu} = \bar{\psi}\gamma_\mu\gamma_5\tau^k\psi$	chiral	CSB; Goldstone mode
$U_A(1)$	$\psi \to e^{-i\beta\gamma_5/2}\psi$	$j_{5\mu} = \bar{\psi}\gamma_\mu\gamma_5\psi$	axial	't Hooft interaction

Table 2.1: Symmetries and their transformation properties associated conserved currents and manifestation in nature for two flavors

quantum numbers. However, as briefly mentioned above, this is not the case and so the observed splittings are large, e.g. the splitting of the vector ρ meson and axial a_1 mesons around ~ 400 MeV.

Let us start by from the Euclidean QCD partition function, for the purposes of our discussion gauge fixing is not relevant and so absorb the contribution from the Fadeev-Popov ghosts $\{\bar{c}^a(x), c^a(x)\}$ to Z into the gauge sector. We do this by the denoting $[\mathscr{D}A]$ for the gauge measure and $\tilde{S}_{g,A}$

$$\begin{aligned} Z_{\text{QCD}} &= \int [\mathscr{D}A]\mathscr{D}\bar{\psi}\mathscr{D}\psi \exp\left[-\tilde{S}_{g,A} + \sum_f^{N_f}\int d^4x_E \psi_f^\dagger(i\not{D} + im_f)\psi_f\right] \\ &= \int [\mathscr{D}A] e^{-\tilde{S}_{g,A}} \prod_f^{N_f} \det(i\not{D} + im_f) \ , \end{aligned} \tag{2.8}$$

the covariant derivative in the Dirac operator is expressed in the semiclassical (WKB) approximation $i\not{D} = \gamma^\mu(\partial + A_{\text{cl}\mu} + a_\mu)$ where the second term corresponds to the classical solution (instanton) subject of the following section and a_μ representing the quantum fluctuations around this solution. With the partition function at hand we can now define correlation functions, of particular interest is the chiral condensate, which for a given flavour is defined as,

$$\langle\bar{\psi}_f\psi_f\rangle = -\lim_{m_f\to 0}\frac{\partial \log Z}{\partial m_f} \ , \tag{2.9}$$

without lose of generality we limit the discussion to a single flavor $N_f = 1$, we proceed integrate the gauge sector out of the functional which means taking the average of the gauge field configurations, i.e. $Z = \overline{\det(i\not{D} + im)}$. The Dirac operator is not hermititian due to the presence of the im term in the determinant but it is nevertheless real. We can rewrite Z in terms of the eigenvalues λ_n and eigenvectors Ψ_n of the massless Dirac operator, if there λ_n is finite then there exists $\Psi_{n'} = \gamma^5 \Psi_n$ whose eigenvalue is $-\lambda_n$. The determinant can thus be rewritten as,

$$\det(i\not{D} + im) = \exp\left[\frac{1}{2}\sum_n \log(\lambda_n + m^2)\right] = \exp\left[\frac{1}{2}\int_{\mathbb{R}} d\lambda\, \xi(\lambda)(\lambda^2 + m^2)\right] , \tag{2.10}$$

in the last part of the equality we have introduced a spectral density function $\xi(\lambda) = \sum_n \delta(\lambda - \lambda_n)$. The resulting expression is real and even with respect to the fermion mass, manifestation of the chiral invariance. The chiral condensate follows then from the fermion determinant.

$$\langle \bar{\psi}\psi \rangle = -\lim_{m_f \to 0} \frac{1}{V}\frac{\partial}{\partial m}\left[\frac{1}{2}\int_{\mathbb{R}} d\lambda\, \overline{\xi(\lambda)} \log(\lambda^2 + m^2)\right] = -\lim_{m_f \to 0} \frac{1}{V}\left[\frac{1}{2}\int_{\mathbb{R}} d\lambda\, \overline{\xi(\lambda)} \frac{m^2}{\lambda^2 + m^2}\right] , \tag{2.11}$$

where the overline bar denotes average of field configurations. From this expression one may be tempted to think that the condensate vanishes at the zero mass limit, such reasoning would certainly justified for the finite volume system. However, it turns out that in the thermodynamic limit the volume goes to infinity faster than the mass goes to zero, and so the integrand is instead given by $\pi \mathrm{sign}(m)\delta(\lambda)$. This translate into the quark condensate,

$$\langle \bar{\psi}\psi \rangle = -\frac{1}{V}\mathrm{sign}(m)\overline{\xi(0)} , \tag{2.12}$$

in other words, only the zero modes of the Dirac operator are relevant to the chiral condensate. The sign function appearing in the expression above denotes the non-analyticity of the QCD partition function with respect to the mass. The partition function is also even in m reflecting the invariance of the action under axial transformations and non-analyticity on the symmetry breaking mass parameter is a typical situation where the symmetry is spontaneously broken.

2.1.2 Explicit Breaking of $U_A(1)$ Symmetry

The non-conservation of the axial current comes from an extra contribution from the path integral measure which is not invariant under $\mathrm{U}_A(1)$ axial rotations. As briefly mentioned on the previous section, the spontaneous breaking of the $\mathrm{U}_A(1)$ symmetry predicts yet another Goldstone boson, the η' meson. The experimental data revealed that the mass for the η' meson is too large $m_{\eta'} \sim 975$ MeV, far exceeding the upper bound $\sim \sqrt{3}m_\pi$ to be regarded as a NG boson [22]. Such inconsistency implies that there must be some dynamical mechanism that gives the η' its large mass. It was not until when the U(1) problem was reconsidered by taking into account instanton configurations that this long standing problem was solved [23]. Let us first briefly review the spontaneous breaking of $\mathrm{U}_A(1)$ symmetry.

The classical action is invariant under local axial transformations $\psi' = e^{-i\beta(x)\gamma_5/2}\psi$ at the zero masses limit, this symmetry is manifested as the conservation of the axial current manifests as the Noether's theorem implies. However, as previously explained, the quantum dynamics lead to non-conservation, more precisely the very invariance of the quantum action against local axial transformations implies a non-vanishing anomalous divergence. The chiral anomaly has been derived in various different contexts, here let us sketch its path integral derivation first introduced by Fujikawa [24, 25]. The generating functional for this system is

$$\begin{aligned} Z &= \int \mathscr{D}\bar{\psi}'\mathscr{D}\psi' \det\left[e^{2i\gamma^5\beta}\right] e^{-S(\bar{\psi}',\psi')} \exp\left[\int d^4x\,\beta(x)\partial_\mu J_{5\mu}\right] \\ &= \int \mathscr{D}\bar{\psi}\mathscr{D}\psi\, e^{-S(\bar{\psi},\psi)} \exp\left[2i\,\mathrm{Tr}(\gamma^5\beta) - \int d^4x\,\beta(x)\partial_\mu J_{5\mu}\right], \end{aligned} \tag{2.13}$$

where $J_{\mu 5}$ denotes the axial vector current. As this is a mere change of coordinates Z should remain unchanged, we can explicitly see this by expanding the exponential term which leads us to the Ward-Takashi (WT) identity,

$$\int \mathscr{D}\bar{\psi}\mathscr{D}\psi\, e^{-S(\bar{\psi},\psi)}\left[-2i\,\mathrm{Tr}(\gamma^5\beta) + \int d^4x\,\beta(x)\partial_\mu J_{5\mu}\right] = 0\,. \tag{2.14}$$

Naively one may expect that being the trace of γ^5 above is vanishes, however, this operator does not only trace over spin space but also over the infinite dimensional space of eigenmodes which requires careful treatment. Expanding in terms of the eigenfunctions the trace can be understood as an alternating sum of the eigenvalues of γ^5 implying that the result is sensitive to the way in which the sum is performed. Gauge invariance tells us that this quantity must not diverge, hence a regulator a Gaussian regulator is introduced. In this way, one arrives to $\mathrm{tr}(\gamma^5\beta) = \frac{1}{8\pi^2}\int_{S^4}\beta\,\mathrm{tr}\,F^2$. Hence the effective action is not invariant. It is quite interesting that one arrives to the exact same result when looking at the index theorem for the Dirac operator or studying fermions on top of an instanton background, spelling out an intimate relation to topology.

Indeed diving deeper into the relation between the quantum anomaly and the topology, it is perhaps illuminating to look at the properties of the Dirac operator itself. The spinors on a manifold $\mathscr{M}$ may be decomposed by chirality $\psi = \mathcal{P}_+\psi + \mathcal{P}_-\psi = \phi_+ + \phi_-$ with the chirality projector $\mathcal{P}_\pm = \frac{1}{2}(1 \pm \gamma^5)$ allowing us to define two vector bundles for the normalizable spinors modes associated with chirality $\pm$ on $\mathscr{M}$ as $S_\pm$. We may also rearrange the Dirac operator in a similar way $\not{D} = D - D^\dagger$ where $D = \not{D}\mathcal{P}_+$ which in turn implies that $D^\dagger = -\not{D}P_-$. The γ^μ matrix has the effect to change chirality and in fact they provide a one to one map between the chirality spaces. On the other hand, with D one may construct the Laplacian operator $\Delta_+ = D^\dagger D$ and $\Delta_- = DD^\dagger$ which do not, in other words,

$$\Delta_+ \circlearrowright C^\infty(S_+) \underset{D^\dagger}{\overset{D}{\rightleftarrows}} C^\infty(S_-) \circlearrowleft \Delta_- \tag{2.15}$$

These operators are elliptic, and since the manifold $\mathscr{M}$ is compact, the spectrum of $\Delta_\pm$ is discrete and the degeneracy of each eigenvalue is finite. Therefore the Laplacians have a well-defined eigenvalue problem, this is very helpful since we cannot define the eigenmodes for D and $D^\dagger$ because as shown in (2.15) they connect different spaces, but the Laplacians defined by them don't. So by looking at the eigenvalue problem $\Delta_+\varphi_{+\lambda} = \lambda\varphi_{+\lambda}$ with $D\varphi^+ = \varphi^-$ which is an eigenfunction of the Δ_- we can see share the same eigenvalue and thus the spectrum of the Laplacians for non-zero λ is the same. Denoting the space of eigenfunctions $E_\pm(\lambda) = \{\varphi_{\pm\lambda}\}$, we have that their dimensions for finite λ is the same $\dim E_+(\lambda) = \dim E_-(\lambda)$, the operators act,

$$\Delta_+ \circlearrowright E_+(\lambda) \underset{D^\dagger}{\overset{D}{\rightleftharpoons}} E_-(\lambda) \circlearrowleft \Delta_- \tag{2.16}$$

this is not the case for the zero-modes $\lambda = 0$. The zeros however of the pair of operators $\{D, \Delta_+\}$ and $\{D^\dagger, \Delta_-\}$ are the same, and thus $\ker \Delta_+ = \ker D$ and $\ker\Delta_- = \ker D^\dagger$. We can now write the index of the Dirac operator defined as $\text{index}(\not{D}) = \dim\ker[D^\dagger D] - \dim\ker[DD^\dagger]$, which tells us the difference of the number of linearly independent zero-modes of the Laplacians. It is remarkable that we can in fact relate this quantity to the Fujikawa's method of regularization for the trace of γ_5 when deriving the chiral anomaly via path integrals as previously shown described. This is done via Heat Kernel, the functional trace

$$\begin{aligned}
\text{tr}_{E_+}(e^{-t\Delta_+}) - \text{tr}_{E_-}(e^{-t\Delta_-}) &= \sum_\lambda e^{-t\lambda}\left[\sum_{\varphi_\lambda^+}\langle\varphi^+|\varphi^+\rangle - \sum_{\varphi_\lambda^-}\langle\varphi^-|\varphi^-\rangle\right] \\
&= \sum_\lambda e^{-t\lambda}\left[\dim E_+(\lambda) - \dim E_+(\lambda)\right] \\
&= \dim E_+(0) - \dim E_-(0)\ ,
\end{aligned} \tag{2.17}$$

but $\dim E_\pm(0) = \dim\ker\Delta_\pm$ which means that the trace difference above is the index of the Dirac operator as the mentioned above the ker of the Laplacians and the D operators. In this way we can write the index as,

$$\begin{aligned}
\text{index}(\not{D}) &= \text{tr}_{S_+}\left(e^{-tD^\dagger D}\right) - \text{tr}_{S_-}\left(e^{-tDD^\dagger}\right) = \text{tr}_{S_+}\left(e^{-t\not{D}^2}\mathcal{P}_+\right) - \text{tr}_{S_-}\left(e^{-t\not{D}^2}\mathcal{P}_-\right) \\
&= \text{tr}_{S=S_+\otimes S_-}\left[e^{-t\not{D}^2}(\mathcal{P}_+ - \mathcal{P}_-)\right] = \text{tr}_S\left[\gamma_5 e^{-t\not{D}^2}\right]\ ,
\end{aligned} \tag{2.18}$$

which is exact same Gaussian regulator chosen in Fujikawa's method. This expression can be computed by the Heat Kernel method, expanding and taking the limit to zero t arriving to the very same result. In general the one obtains,

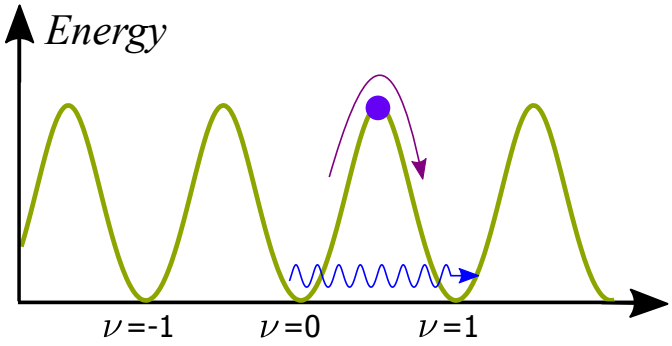

FIG. 2.2: Transition between two topologically different vacuum states by the instanton corresponding to the winding number $Q_W = 1$. Sphaleron configuration despicted by the dot on the peak.

$$\text{index}(\not{D}) = \frac{1}{n!}\left(\frac{i}{2\pi}\right)^n \int_{\mathscr{M}^{2n}} \text{tr}\, F^n \,, \tag{2.19}$$

known as the Atiyah-Singer index theorem.

2.2 QCD θ-Vacuum – Instantons and Sphalerons

One of the most fundamental quantity in a quantum field theory is the vacuum to vacuum transition amplitude, embodied by the Euclidean partition function. For the evaluation of this quantity we must first obtain the local minimum of the Euclidean action. For simplicity let us consider the SU(2) gauge theory the Euclidean 4-dimensional space $E^4 = \mathbb{R}^4$ and discuss the SU(3) case afterwards in this subsection. The action reads,

$$S_E = \frac{1}{4}\int d^4x_E\, F^a_{\mu\nu}F^{a\mu\nu} = -\int_{\mathrm{E}^4} \text{tr}\{F^2\} \,, \tag{2.20}$$

in the last line we have expressed in a language more proper to geometry and topology, where the field strength 2-form $F = \frac{1}{2}F^a_{\mu\nu}(x)\mathrm{T}^a dx^\mu \wedge dx^\nu$, T^a the group generator and the trace defined under this group. As we are looking for a configuration for which the action remains finite it is obvious that F must vanish at infinity. One way to satisfy such condition is having the gauge field vanish at infinity, however the provides a trivial solution, a more interesting scenario for the vanishing of F is

also achieved when A becomes a pure gauge, i.e.

$$A(x) \xrightarrow{|x|\to\infty} U^{-1}(x)\mathrm{d}U(x)\ , \tag{2.21}$$

in this way F does not vanish in E^4 but on its boundary $\partial\mathrm{E}^4 = S^3$ (3-dimensional sphere) where A is a pure gauge. This produces a situation where the gauge elements $U(x) \in \mathrm{SU}(2)$ represent a mapping $U : S^3 \to \mathrm{SU}(2) \simeq S^3$, these mapping are classified under the homotopy classes $\Pi_3(\mathrm{SU}(2)) \simeq \Pi_3(S^3) \simeq \{n\} = \mathbb{Z}$, determined by the topological winding number $n \in \mathbb{Z}$. That is to say, for a given gauge element U we can define over the manifold, an invariant quantity called Pontryagin index or Chern-Simons number,

$$\nu[U] = \frac{1}{24\pi^2}\int_{\mathscr{M}} d\alpha^1 d\alpha^2 d\alpha^3 \epsilon^{ijk}\mathrm{tr}\left[U^{-1}\partial_i U U^{-1}\partial_j U U^{-1}\partial_k U\right]\ , \tag{2.22}$$

in this way the $U^{(0)}(x) = 1$ corresponds to zero, the identity map $U^{(1)}(x) = \frac{1}{r}(x_4 + i\boldsymbol{x}\cdot\sigma)$ yields $\nu = 1$, and higher order elements $U^{(n)}(x) = [U^{(1)}(x)]^n$ correspond to $\nu = n$. The mappings fall into disjoint homotopy classes and so a gauge configuration of a given ν cannot be continuously deformed into another of ν'. We can rewrite the above quantity in terms of the field strength,

$$\nu[U] = -\frac{1}{16\pi^2}\int d^4x_E\,\mathrm{tr}\{\tilde{F}_{\mu\nu}F^{\mu\nu}\} = -\frac{1}{8\pi^2}\int_{S^4}\mathrm{tr}\{F * F\}\ , \tag{2.23}$$

where we have compactified E^4 to the 4-dimensional sphere S^4. The Pontryagin index represents the *winding number* of the mapping SU(2). It is certainly a remarkable quantity, only sensible to the topology of the underlying fiber bundle and so it does not change under diffeomorphisms nor under local variations of U, i.e. $\delta_U\nu[U] = 0$, for this reason $\nu[U]$ it is also referred as topological charge Q_W. The integrand of the topological charge is a closed form $\mathrm{d}\,\mathrm{tr}\{F^2\} = 0$ which follows from the Bianchi identity. Therefore, by the Poincare theorem we know that it is locally exact on for instance the upper hemisphere of S^4, H_+. This allows us to write,

$$Q_W = \frac{1}{32\pi^2}\int_{\mathrm{S}^3} dS\, n_\mu K^\mu = \frac{1}{32\pi^2}\int_{\mathrm{E}^4} d^4x\partial_\mu K^\mu\ , \tag{2.24}$$

in the last equality, Stokes theorem was applied. Given that Q_W denotes the topological charge, K is fairly enough referred as the topological current. It is a is 3-form, it reads,

$$K_\mu = \epsilon_{\mu\nu\rho\sigma}\mathrm{tr}\left(A_\nu F_{\rho\sigma} + \frac{2i}{3}A_\nu A_\rho A_\sigma\right) . \tag{2.25}$$

The analytical continuation to imaginary time of the Yang-Mills theory puts the imaginary unit in E^a field, this allows for a zero Euclidean energy configuration when $E^a = \pm B^a$ or in the covariant language in Euclidean space this means, $\frac{1}{2}\epsilon^{\mu\nu\rho\sigma}F_{\rho\sigma} = \tilde{F}^{\mu\nu} = \pm F^{\mu\nu}$ or in differential forms simply, $F = \pm * F$. Configurations that while keeping the action finite satisfy this condition are called self-dual or anti self-dual instantons. The YM equations of motion are automatically satisfied by virtue of the Bianchi identity. Since the Euclidean YM action can be rewritten as

$$S_E = \frac{1}{4}\int_{\mathrm{E}^4} d^4x_E\,\mathrm{tr}\{(F_{\mu\nu} \pm \tilde{F}_{\mu\nu})^2\} \mp \frac{1}{2}\int_{\mathrm{E}^4} d^4x_E\,\mathrm{tr}\{\tilde{F}_{\mu\nu}F^{\mu\nu}\} , \tag{2.26}$$

we have that the action may be brought to an utterly simple and elegant form $S_E = 8\pi|Q_W|$. In this way an explicit solution that satisfy the boundary condition at infinity as well as the self-duality of F may found with help of the ansatz, $A(x) = f(r^2)U^{-1}(x)\mathrm{d}U(x)$. The simplest function that achieves this and is regular at the origin is $f(r^2) = r^2/(r^2 + \rho^2)$ with ρ being a constant which specifies the instanton size.

Thus, SU(N) Yang-Mills theories allow for the existence of localized configurations in space-time that keep the action finite (named instantons by t'Hooft in 1974). Since the Pontryagin term may be expressed as total derivarive, it does not alter the equations of motion in any way, nevertheless, it is need to render all physical states gauge invariant. Specifying a classical gauge theory implies that we must fix a group, however the quantized theory also requires a θ-phase which stems from the topological properties. The θ-term has thus profound effects at the non-perturbative level leading to the formation of the gluon condensate and the topological susceptibility solving the $U_A(1)$ puzzle. We can defining QCD vacuum which may now be characterized by the Pontryagin index $\nu[U] \in \mathbb{Z} \to |n\rangle$. This vacuum state, corresponds to an instanton configuration with index $\nu = n$. However a gauge field configuration with a given Prontryagin number n can be brought down into another by a gauge

transformation G_m of homotopy class $\nu = m$. More concretely using the additive property of the winding number we can see that the vacuum state $|n\rangle$ changes into $|n+m\rangle$ under the action of G_m and so the vacuum defined in this way is not gauge invariant. On the other hand we can build a proper vacuum state in terms of the linear combination,

$$|\theta\rangle = \sum_{\nu=-\infty}^{\infty} e^{i\theta\nu}|\nu\rangle \ , \tag{2.27}$$

called θ-vacuum, we can see that we only pick up a complex phase when applying a gauge transformation physical observables are gauge invariant. It reshapes our understanding of the QCD vacuum as the superposition of the many quasi-vacua corresponding to a Q_W, where the θ-parameter is introduced as phase characterizing each state. The only quantum path that can tunnel to another is the instanton, θ-vacuum. There are several analogies to Bloch states in condense matter physics that one can spot here; identifying large gauge transformations as lattice translations and the just shown θ-phase with the Bloch momentum, we can see how the quantum states associated with the θ-vacuum behave as Bloch waves in a periodic lattice. The θ-phase, arises from quantum tunneling in the gauge field space [26].

In this regard the Yang-Mills theory is truly exceptional as it allows paths in field space that avoid the infinitely large energy barriers often encountered in other field theories eventually translating into spontaneous symmetry breaking. Such paths are the instantons configuration, quantum tunneling paths that arise in the semiclassical approximation by looking at classical EOM in imaginary time including classically degenerate vacua while keeping the action finite. For the θ state to be a good vacuum, we should first see the transition from $\theta \to \theta'$,

$$\begin{aligned} \langle\theta|e^{-H_{\rm QCD}T}|\theta'\rangle &= \sum_{n,m} e^{-i(n\theta - m\theta')}\langle m|e^{-H_{\rm QCD}T}|n\rangle \\ &= \delta(\theta-\theta')\int [\mathscr{D}A]_{Q_W}\mathscr{D}\bar{\psi}\mathscr{D}\psi e^{-(S_{\rm QCD}+S_\theta)} \ , \end{aligned} \tag{2.28}$$

where $S_\theta = iQ_W\theta$. Implying on the one hand that thus theta is unique, i.e. there is no transition

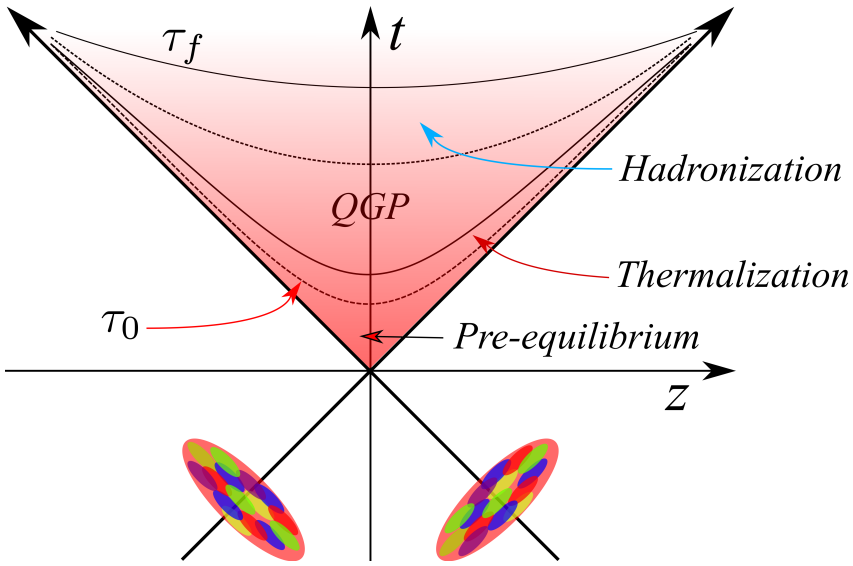

FIG. 2.3: Temporal evolution of a heavy ion collision in the light cone. Hyperbolic lines denote some critical proper times at each a transition of the produced matter takes place. In particular, the transition to thermalized matter by τ_0, the formation of QGP and the freezeout proper time τ_f are shown.

between vacuum states and so the definition above is that of a proper vacuum. And on the other that QCD action should be modified to accommodate the effective interaction in Minkowski space,

$$S_\theta = -\frac{g^2}{32\pi}\int d^4x\theta F^a_{\mu\nu}\tilde{F}^{a\mu\nu} \ . \tag{2.29}$$

2.3 Relativistic Heavy Ion Collision

Most of our knowledge on hadron structure had been achieved by colliding fundamental particles electron/positron with hadrons. However, as one may anticipate, the collision of two nuclei belongs to a whole different plane of complexity. Gluons of one nucleus interacting with the gluons of the other in various ways at very high temperatures and densities behaving like as an almost perfect dense fluid, a plasma of quarks and gluons. High energy beams collision experiments such as RHIC and LHC where constructed with the very aim of detecting this exotic and extreme form of matter.

2.3.1 Establishment of a Quark-Gluon Plasma

Evidence appeared soon enough in the shape of *jets*, which we can understand as particles very located in space. What was observed in the heavy ion collision experiments was that in the numerous collision events jets would be detected however some of them would be much more energetic than the rest. These particles are formed as the product of the most energetic collisions in the nuclei. In particular, the collisions near the center of the QGP were observed to produce to highly energetic beams on opposite sides of the detector, these correlated beams are known as "back-to-back" jets traveling 180 degrees with respect to the other. The situation is very different however for those jets that were produced as we get near the edge of the QGP, in this situation the beam only needs to cross a small portion, when the beam crosses a large portion of it loses energy as a product of the interaction with the QGP medium. Therefore, a particular, signature for the production of the QGP was established in this form as some of the jets were observed to be more energetic than their counterpart.

2.3.2 Magnetic Probe to the QCD θ-Vacuum

Understanding phenomena in the Early Universe, quark matter inside neutron stars, magnetars and quark gluon plasma in heavy ion collisions, implicates complications beyond the finite temperature and density scenario as strong magnetic fields are involved. In a certain type of compact stars called magnetars, the surface magnetic fields reach up to the order of 10^{15} G while the interior is predicted to exhibit $eB \sim 10^{18}$ G. The most prominent magnetic fields, however, are formed in non-central relativistic heavy ion collisions. We can obtain a good estimate merely by classical considerations. Let us approximate the incoming nuclei as a point charges Fig. 2.4, then from the Lienard-Wiechert potential, the magnetic field at the origin reads,

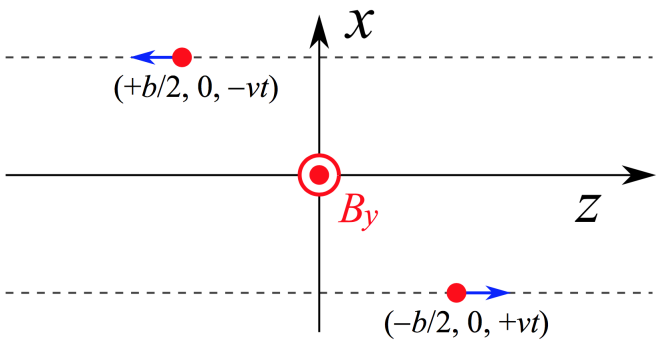

FIG. 2.4: (*left side*) Amplitude of the magnetic fields in non-central collision as a function of impact parameter. (*right side*) Time evolution of the magnetic field at finite impact parameter $b = 4$ fm. Amplitude in units of the pion mass squared, where $m_\pi = 140$ MeV. Fig. taken from Ref. [27]

$$
\begin{aligned}
e\mathbf{B}(\boldsymbol{x},t) &= \frac{Ze^2}{4\pi}\frac{b\beta(1-\beta^2)\mathbf{e}_y}{[(\beta t)^2+(1-\beta^2)(b/2)^2]^{3/2}} = eB_0\frac{\mathbf{e}_y}{[1+(t/t_0)^2]^{3/2}} \\
eB_0 &= \frac{8Z\alpha_e}{b^2}\sinh(Y) = (47.6\text{MeV})^2\left(\frac{1fm}{b}\right)^2 Z\sinh(Y) \\
t_0 &= \frac{b}{2\sinh(Y)}\,,
\end{aligned}
\tag{2.30}
$$

where B_0 corresponds to the maximum intensity of the magnetic field and t_0 the typical time scale of the decaying field. These quantities are expressed in terms of the beam rapidity Y rather than the velocity β which are related by $\beta = \sinh(Y)$. One can now give an estimate using typical values at Au-Au at RHIC provide an estimate; $Z = 79$ and $\sinh(Y) \simeq 0.23$ and impact parameter $b = 10$ fm implies $eB_0 \simeq 3.2 \times 10^{19}$ G and $t_0 = 0.05$ fm/c. The resulting perpendicular magnetic field reaches values up 10^{18} G [7, 28], Fig 2.5.These values are comparable with the QCD scale $\Lambda_{QCD} \simeq 200$ MeV thus are expected to have a significant influence on the physics governed by the strong interaction. It turns out to be exactly the case; the produced $\boldsymbol{B}$ in relativistic heavy ion collisions is responsible for an observed charge asymmetry attributed to the chiral magnetic separation effect. The composition of compact stars could be importantly affected by the strong $\mathbf{B}$ produced. From the field theory side, magnetically induced QCD effects such as the chiral magnetic effect, chiral magnetic separation

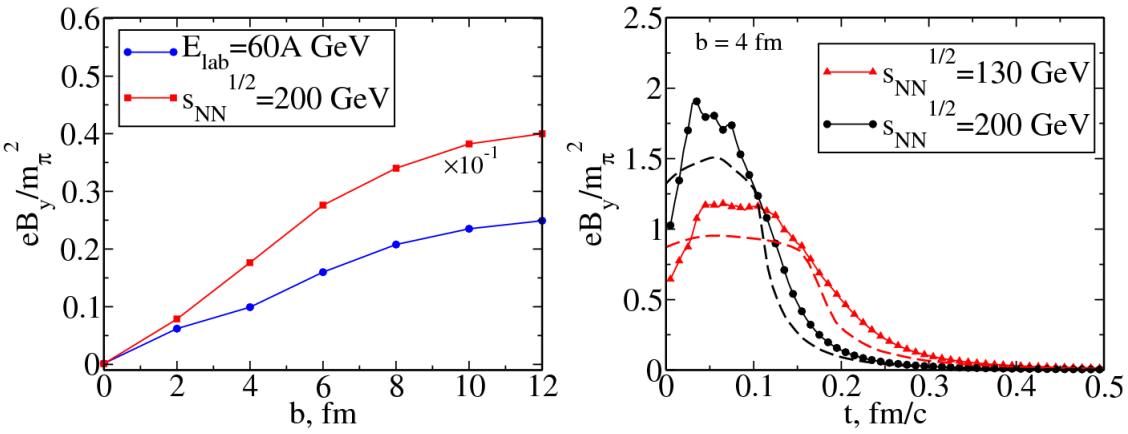

FIG. 2.5: (*left side*) Amplitude of the magnetic fields in non-central collision as a function of impact parameter. (*right side*) Time evolution of the magnetic field at finite impact parameter $b = 4$ fm. Amplitude in units of the pion mass squared, where $m_\pi = 140$ MeV. Taken from Ref. [7]

effect, and chiral vortical effect are subjects of increasing interest to which these chapter will focus on.

The existence of topological excitations such as the instanton and sphaleron configurations in the SU(3) Yang-Mills theory implies the modification of the QCD action by a $\mathcal{P}$ and $\mathcal{CP}$ violating Lorentz invariant θ-term. The QCD θ angle violates induces an neutron dipole moment with magnitude proportional to θ. The latter has been eventually observed by experiments and found to be as low $|d_n| < 2.9 \times 10^{-26}$ e cm [29]. This smallness of the θ parameter represents the so called "strong $\mathcal{CP}$ problem". A solution around this problem has been proposed by Peccei and Quinn [30, 31] by the Introducing a dynamical field substitute to the θ parameter. This field should take a zero value at the low energy regime, this particle was latter identified as a light spin zero particle named *axion* [32, 33]. Therefore, while it is argued that the θ parameter is zero, it is believed that topological fluctuations take place in the heavy-ion collisions allowing for a space-time inhomogeneous θ [34]. If we permit an axion-like term in the action, we find that upon an axial transformation couples the $\theta(x)$ to the field strength through $\frac{\theta(x)e^2}{16\pi^2}\epsilon_{\mu\nu\alpha\beta}F^{\mu\nu}F^{\alpha\beta}$. After integration by parts we arrive to the vector current,

$$j_\mu = -\frac{e^2}{4\pi^2}\mu_5\epsilon_{0\mu\rho\sigma}F^{\rho\sigma} \ , \tag{2.31}$$

where the definition for the chiral chemical potential $\mu_5 = \partial_0\theta$ has been introduced. The generation of this vector current is known as the chiral magnetic effect.

Non-trivial topological configurations of the gauge field play a pivotal role when understanding the QCD vacuum structure. It is necessary to solve the U(1)-problem, it is crucial in the formation of the gluon condensate and above all it is at the heart of the mechanism of dynamical mass generation by the spontaneous breaking of chiral symmetry. Now, this begs the question on whether there is a direct way to detect these topological excitations with experiments. Well, this was exactly one of the motivations that eventually lead to the discovery of a very novel effect combining QCD and QED, the chiral magnetic effect. There are in fact many motivations, for one, the detection of the CME current would imply chiral symmetry restoration.

In fact, quarks in QGP phase are necessary for the CME. The electric current of the CME can be induced only in the situation that chiral symmetry is restored because if not, then the net chiralities vanished. That quarks are not confined because quarks flow individually in the system. In this sense, the CME might be the order parameter for the transition between hadronic and QGP phase.

Interaction between the fermions and the $Q_W \neq 0$ fields produce nonzero parity $\mathcal{P}$ and charge parity $\mathcal{CP}$ odd effects. In relativistic heavy ions collisions color flux tubes naturally arise at the initial state, strong color electromagnetic fields, in addition to this, perpendicular to the color flux tube a magnetic field is also present. As a result the spin of the particles align in the direction of the magnetic field resulting in production of chirality this asymmetry corresponds

$$\frac{d(N_R - N_L)}{dt} = -\frac{g^2 N_f}{32\pi^2} \int d^3x F_a^{\mu\nu} \tilde{F}^a_{\mu\nu} \,. \tag{2.32}$$

Right after the nuclei collides color flux tubes are formed, these tubes play the role of Q_W. Under a strong magnetic field **B** the particle under these tubes have a characteristic momentum distribution as predicted by CME. The finiteness of the above expression can thus be understood as arising from the vacuum boundary conditions of the integrated the chiral anomaly, a realization of the index theorem.

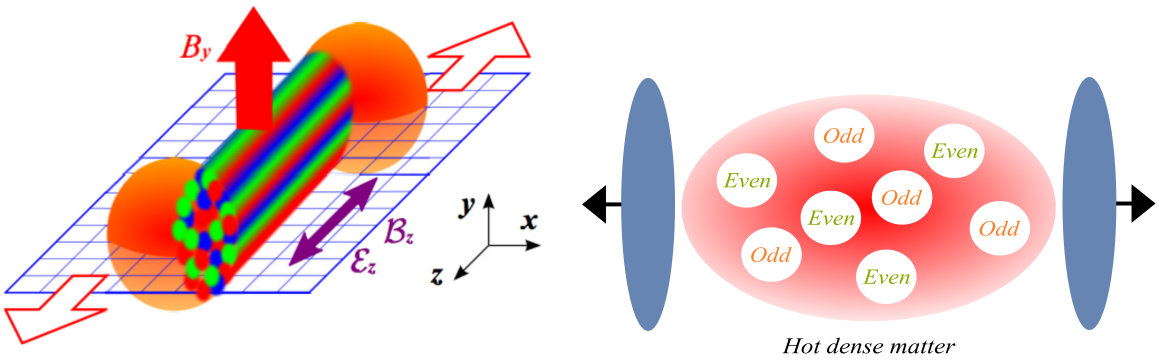

FIG. 2.6: (*On the left*) Cartoon representing a relativistic heavy ion collision event. The formation of flux tubes and the produced color electromagnetic field is depicted. Figure taken from [35]. (*On the right*) Schematic representation of local parity violation, depicting the formation of parity even and parity odd bubbles within the matter produced after the collision.

The non-zero topological charge induces a transition between different classical vacua, as described in the previous section, at the zero temperature vacuum this implies the tunneling through a potential barrier that suppresses the transition rate by an exponential factor, the instanton configuration. However, the number of transitions induced by $Q_W = 1$ per unit of volume becomes severely impaired at finite temperature,

$$\frac{dN}{d^3x dt d\rho} = e^{-2\pi^2\rho T^2 - 18A(\pi\rho T)} \frac{dN}{d^3x dt d\rho}\bigg|_{T=0} , \tag{2.33}$$

with $A(x)$ being a function with asymptotics $-\log(x)/6$ when $x \to \infty$ and $-x^2/36$ in the $x \to 0$ limit [36]. This implies that the transitions related to instantons at high temperatures are negligible. This is the exactly the case for ultrarelativistic heavy ion collision experiments and what occurs in the electroweak theory. In the latter, the transition between different vacua results into the violation the baryon plus lepton number relevant for baryogenesis problem. Nevertheless in the SU(2) Yang-Mills theory also allows for static solutions of finite energy associated with the real-time transitions between field configurations and half-integer winding number called sphalerons. As it turns out the sphaleron transitions rate is not suppressed with temperature like the instanton but enhanced, $\Gamma_{\rm sph} \sim T^4$ behaviour shared with QCD [37, 38]. Hence the sphaleron expected to play a main role in QCD

[39] and in the CME current generation.

The CME provides a way to probe strong interacting matter in response to a strong magnetic field in much the same way as a current is induced in response to an external electric field according in Ohm's law. In the latter proportionality constant is given by electrical conductivity of the medium σ. The QGP medium with electrically charged quarks may be regarded as a conductor but a parallel to Ohm's law is not straight forward. In fact, solely by symmetry one may argue that because the vector current is an $\mathcal{P}$-odd quantity and the $\boldsymbol{B}$ is an $\mathcal{P}$-even quantity, the conductivity must vanish ruling out the CME current. However, as discussed above the chiral charge of the medium is not conserved due to the anomaly, the CME is a *quantum* effect. One intuitively way to understand the formation of the electric vector CME current is as a polarization effect. Namely, the quark spins align in the direction of the magnetic field, then the momentum of the nearly massless quarks may be either parallel or antiparallel to their spin direction Fig. 2.7. The CME is $\mathcal{CP}$-odd effect, let's say we are in one of the parity bubbles as depicted in Fig. 2.6, then the previous statement translates into chirallity imbalance parametrized by μ_5, which in turn implies that the net momentum distribution along the direction of the magnetic fields. In this picture, we have introduced chiral imbalance parametrized by a finite chiral chemical potential μ_5, however, this quantity and thereby the chiral conductivity coefficient must be determined dynamically. This will be explicitly shown in terms of particle distributions in a following chapter.

There are several remarkable features of the CME current that should be pointed out. The origin of the electric current in the CME is topological, therefore it does not dissipate at high temperature nor it changes at the limit of strong coupling, as shown by holographic computation, where it has been shown to have profound effects in its QCD phase structure [40]. The produced current and dipole moment in the CME are exact at the operator level, this can be understood from its intimate relation to the quantum anomaly which receives no perturbative corrections. Finally, the magnetic field is also known to trigger the production of axial current under the presence of finite vector density, a dual effect to the up until now discussed CME known as the Chiral Separation Effect (CSE). The

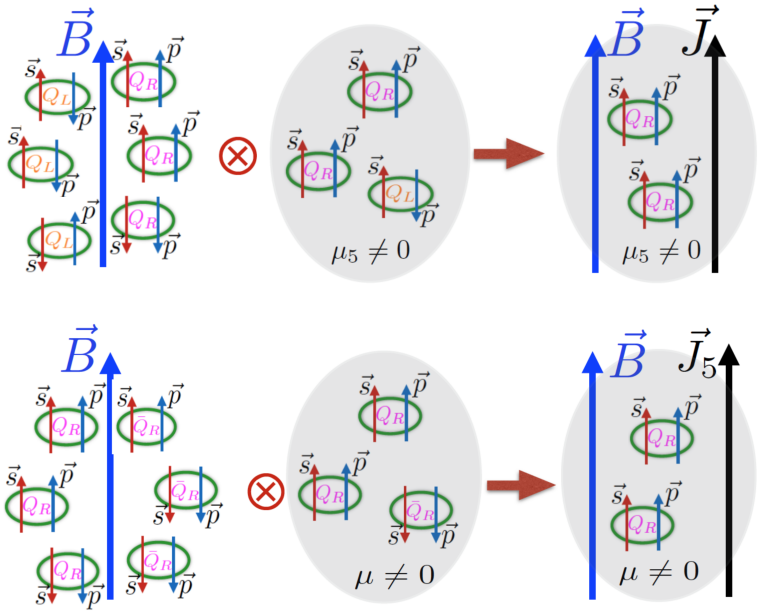

FIG. 2.7: (*On the top*) Schematic representation of the Chiral Magnetic Effect. (*On the bottom*) Schematic representation of the Chiral Separation Effect. Figures taken from Ref. [28]

collisions of heavy ions at RHIC and LHC are not only endowed with strong magnetic fields but also angular momentum where the coupling to vorticity $\omega = \frac{1}{2}\nabla \times \mathbf{u}$, manifested as a current induced along the direction of the local angular velocity of the medium ω, known as the Chiral Vortical Effect (CVE). Along with the CME and CSE, the CVE is also rooted in the quantum anomaly, and so it enjoys many of the properties discussed above. As it was discussed in this chapter, there is mounting evidence in the literature connecting the CME and CSE to the chiral anomaly. In the same way, it is now is widely accepted that the CVE current arises from the gravitational anomaly as first pointed out by the holographic QCD dual computations at [41]. However, the microscopic mechanism of currents realization is well known only in the case of chiral magnetic transport while its vortical cousin has more subtle description at the level of the underlying theory, in any case more research is needed along this direction. Studies on the anomalous transport phenomena of the chiral medium was soon enhanced with a richer picture considering the above mentioned effects along with their manifestation through new type of collective excitations such the Chiral Magnetic Wave (CMW) and its vortical counterpart, the Chiral Vortical Wave (CVE).

Nevertheless, it is far from trivial how to see their manifestation in an experimental set-up. The effect has been realized within condense matter systems studying the response to of Dirac and Weyl under a magnetic field where a quadratic dependence of the magnetoconductivity on the magnetic field was observed. However, the situation has been quite different in heavy ion collision experiments. mostly due to the lack of prediction from the theoretical side on a clear-cut observable.

2.3.3 Charge Separation and the CME

The azimuthal distribution of particles in their final state contains the information of the charge separation. This comes however at the price of interpreting a $\mathcal{P}$-even observable which is sensible to background effects as well [42]. Let us start by describing the proposed observable.

$$\frac{dN^{\alpha}}{d\phi} \propto 1 + 2v_1^{\alpha}\cos(\phi - \Psi_{\rm RP}) + 2a_1^{\alpha}\sin(\phi - \Psi_{\rm RP}) + \sum_{n>1} 2v_n^{\alpha}\cos[n(\phi - \Psi_{\rm RP})]\ , \tag{2.34}$$

where $\alpha \in \{+,-\}$ representing the charges of the particles. The Fourier coefficients v_n^{α} of the above azimuthal-angle distribution characterize the flow of particles in momentum space. The lower schematic picture in Fig. 2.8 depicts the first coefficients of the expansion. The $n = 1$ coefficient of the series corresponds to the directed flow, which has been decomposed into two parts, one associated to the portion of the flow parallel to the reaction plane v_1 and another perpendicular to it, denoted by a_1^{α}. In a similar way v_2 represents to elliptic flow [43], an schematic visualization of the first harmonics v_1 and v_2 is shown in Fig. 2.8, higher order harmonics v_n are not relevant to this discussion. $\Psi_{\rm RP}$ corresponds to the angle of the of the reaction plane shown in the upper part of Fig. 2.8. Let us now suppose now that a local domain of positive/negative axial charge is produced by the collision. If the collision is peripheral then a CME vector current is expected to be induced in the direction (or opposite) of the induced magnetic field perpendicular to the collision plane. One would thus expect, that the CME vector current drives the flow of opposite charge particles leading to the formation of a charged dipole. In this way, a_1^{α} should be sensible to the CME, in the shape of charge separation.

To quantify the magnitude of such $\mathcal{P}$-odd fluctuations, the two particle correlator $\gamma_{\alpha,\beta} \equiv \langle\cos(\phi_{\alpha} + \phi_{\beta} - \Psi_{\rm RP})\rangle$ observable has been proposed [44], $\alpha \in \{+,-\}$ representing the charges of the particles.

This comes at the cost of interpreting a now $\mathcal{P}$-even observable that is vulnerable to background effects. To suppress the background effects, we make a subtraction between the desired out-of-plane correlation and the in-plane correlation:

$$\begin{aligned}\gamma_{\alpha,\beta} \equiv&\langle\cos(\phi_\alpha + \phi_\beta - \Psi_{\rm RP})\rangle = \langle\cos\Delta\phi_\alpha\cos\Delta\phi_\beta\rangle - \langle\sin\Delta\phi_\alpha\sin\Delta\phi_\beta\rangle \\ &= [\langle v_{1,\alpha}v_{1,\beta}\rangle + B_{\rm IN}] - [\langle a_\alpha a_\beta\rangle + B_{\rm OUT}] \simeq -\langle a_\alpha a_\beta\rangle + [B_{\rm IN} - B_{\rm OUT}]\ .\end{aligned} \tag{2.35}$$

where B_{in} and B_{out} correspond to $\mathcal{P}$-even background processes. This quantity was first measured by the STAR Collaboration Fig. 2.9 as a function of centrality and corroborated by PHENIX Collaboration [45] and the ALICE Collaboration [46] with qualitative agreement. The STAR data shows charge asymmetry which vanishes at head-on collisions in line with CME-based expectations.

The fireball produced in the aftermath of the high energy collision provides the perfect environment for the study of the previously discussed anomalous transport. In order to accurately describe these effects within the nucleus-nucleus collision setup, it is imperative that their manifestation is disentangled from background effects. The complex structure of the space-time evolution of the system clouds any attempt to quantitative describe the CME and related phenomena. There are increasing efforts along the direction on how to reduce uncertainties from the observables, and there is current consensus on the theoretical origin of these recently summarized in the shape of a CME force task report [48].

To model and constrain for the initial condition is a crucial challenge that must be dealt in the search of the manifestation of anomalous effects. The theoretical approach to describe charge asymmetry requires the use of the relativistic hydrodynamical simulations enhanced by anomaly induced transport. The relativist hydrodynamics with the triangle anomaly describes the transport of a system of $\mathrm{U(1)_V}$ vector current and the non-conserved $\mathrm{U(1)_A}$ axial current j_5 by the chiral anomaly. The hydrodynamic equations represent the (non-)conservation laws of energy momentum, vector and axial currents.

$$\partial_\mu T^{\mu\nu} = eF^{\nu\lambda}j_\lambda, \quad \partial_\mu j^\mu = 0, \quad \partial_\mu j_5^\mu = -\mathrm{C}E_\mu B^\mu\ , \tag{2.36}$$

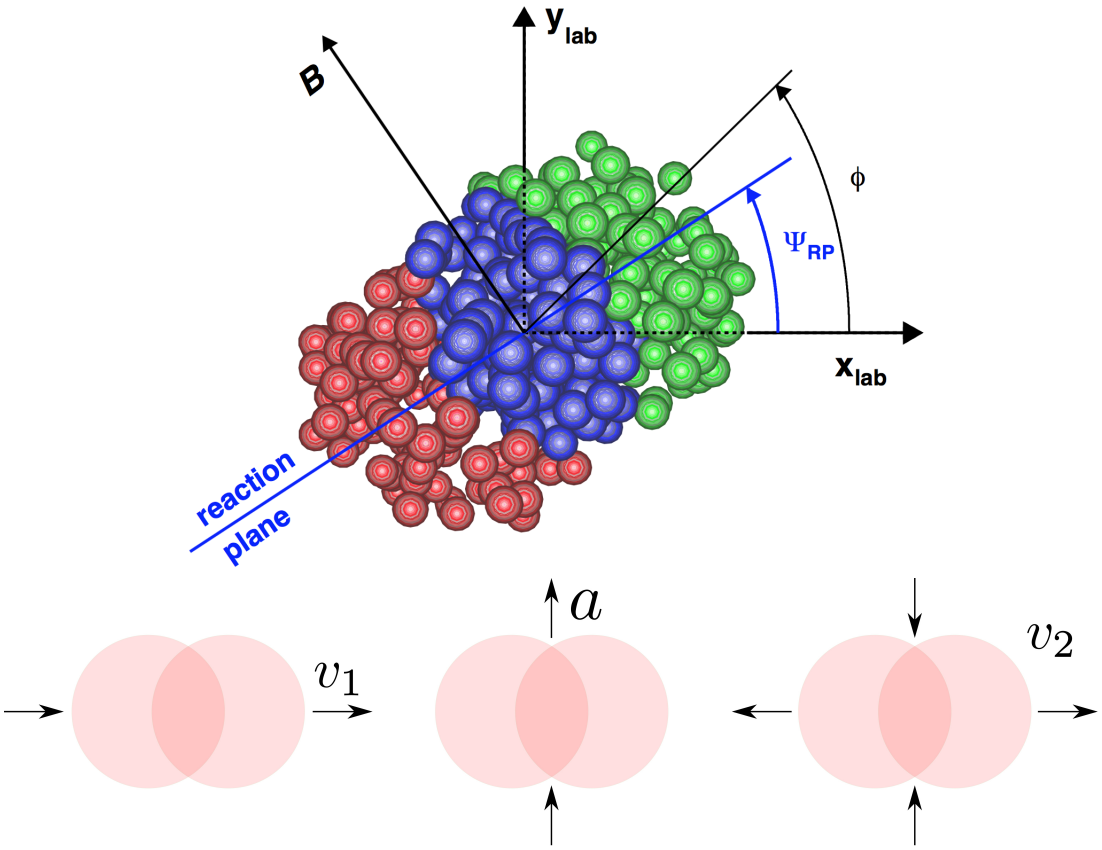

FIG. 2.8: (*On the top*) Schematic depiction of the transverse plane for a heavy ion collision, where the left ion emerges from the page and the right one goes into the page. The produced particles are shown in the overlap region, the blue-colored nucleons [47]. (*On the bottom*) Schematic picture of Fourier coefficients v_1 and v_2 describing directed and elliptic flow respectively.

where C is a constant determined by the chiral anomaly $\mathrm{C} = \frac{N_c}{2\pi^2}\sum_f q_f^2$, and the definitions $E^\mu = F^{\mu\nu}u_\nu$ and $B^\mu = \tilde{F}^{\mu\nu}u_\nu$ should be understood, u^μ being the four velocity. The fluid is assumed to be dissipationless as the CME is non-dissipative current. The energy-momentum tensor along with the vector and axial currents read,

$$\begin{aligned} T^{\mu\nu} &= (\epsilon + p)u^\mu u^\nu - p\eta^{\mu\nu}, \\ j^\mu &= nu^\mu + \kappa_B B^\mu, \\ j_5^\mu &= n_5 u^\mu + \xi_B B^\mu. \end{aligned} \tag{2.37}$$

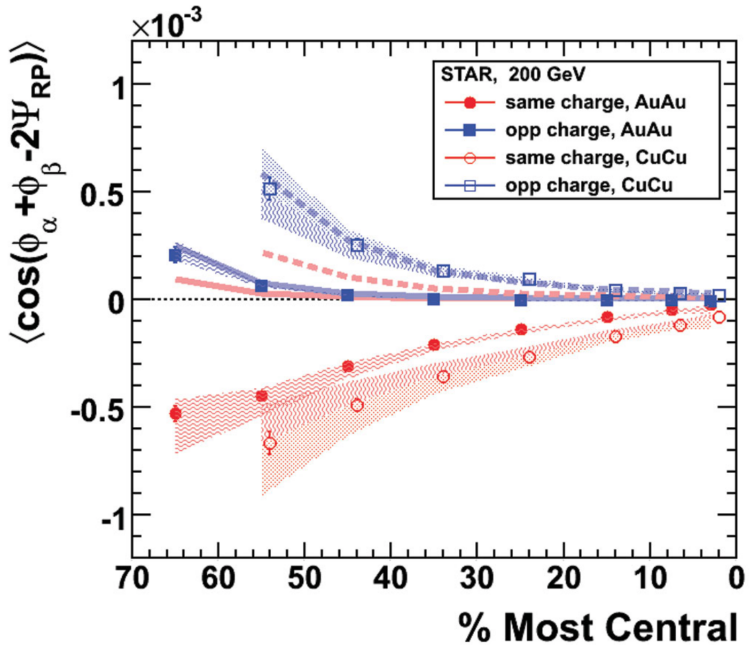

FIG. 2.9: STAR Collaboration results for the three-point correlator, $\gamma_{\alpha\beta}$, measured with 1st and 2nd harmonic event planes versus centrality for Au+Au and Cu+Cu collisions. Figure taken from [47].

where ϵ corresponds to energy, p to the hydrodynamic pressure and $\eta^{\mu\nu}$ to the Minkowsky metric. The second term in the vector and axial current provides correspond to the chiral magnetic and separation effects respectively. The specific values for the transport coefficients κ_B and ξ_B are determined by requiring that either the entropy does not increase or by imposing the condition of no entropy production from the anomalous current yielding the same results. In order to make the connection to the hadron particle spectrum one needs to switch from hydrodynamic degrees of freedom to individual particles via Cooper-Frye formula at freeze-out temperature. The Cooper-Frye formula [49] reads,

$$E\frac{dN}{d^3p} = \frac{1}{(2\pi)^3}\int_{\Sigma_{\tau_f}} \frac{p^\mu d\sigma_\mu}{\exp[(p^\mu u_\mu - \mu)/T_{\rm fo}] \mp 1}\,, \tag{2.38}$$

where the sign in the integrand depends on whether the thermal spectrum corresponds to fermion or bosons and $T_{\rm fo}$ denotes the freeze-out temperature. The hydrodynamics allows us to evolve freeze-out hypersurface at $T_{\rm fo} = 160$ MeV which is affected by the currents and with by integrating the over the thermal distribution of particles in their final state, we can obtain the Fourier coefficients associated to the above defined observable (2.34).

There is however, a consensus from the theoretical side as from where these uncertainties originate, as recently summarized in the shape of a CME force task report [48] these are: The initial distribution of charges, the evolution of the magnetic field, the dynamics of the CME during the pre-equilibrium stage and the uncertainties from the hadronic phase and the freeze out.

There are different mechanisms that could be responsible for the generation of chirality imbalance which feeds the CME current. Topological transitions in particular sphalerons, local fluctuations in the topological density at the longitudinal color flux tubes, as well as local axial current associated with the CSE current, are all viable sources local chirality imbalance that must be addressed. The main production of quark is expected to take place during the pre-equilibrium regime [19], suggesting that the main source of axial charge must be produced during this stage.

Chapter 3

Small-x and Saturation Physics

The study of chiral transport phenomena has profound consequences in our understanding of the topological properties of strong interacting matter. In the search for the smoking gun on these effects, firm theoretical estimations of the experimental observables are crucial. In this sense, a better understanding on the physics governing at early-time regime prior QGP formation is essential. The non-equilibrium early-times dynamics of the collision involves an extremely hard task, in fact, not possible to describe from first principles. However, an effective description for the nuclei at this stage is known where particles are from quantum fluctuations on top of coherent fields, called Color Glass Condensate (CGC) which shall be one of the main aim of chapter. CGC theory arises in the context of gluon saturation physics and so we devote this chapter to some basic concepts regarding this subject as well.

QCD is the quantum field theory that governs the dynamics of strong interacting matter. Hadrons are understood as bound states of quarks and gluons which due the confining property of the theory have never been directly detected. In fact, it was by means of the deep inelastic scattering (DIS) of fundamental particles with protons that lead to Bjorken scaling and culminated with the discovery of quarks as fundamental constituents in QCD. The scattering cross-section σ for instance, the electron-proton scattering (Fig. 3.1), can be expressed as the product $\sim L^{\mu\nu}W_{\mu\nu}$ of the lepton tensor $L^{\mu\nu}$ and the hadronic tensor $W_{\mu\nu}$. The latter containing all the strong interacting dynamics and from where the structure functions are extracted and with these the quark and gluon distributions within the hadron.

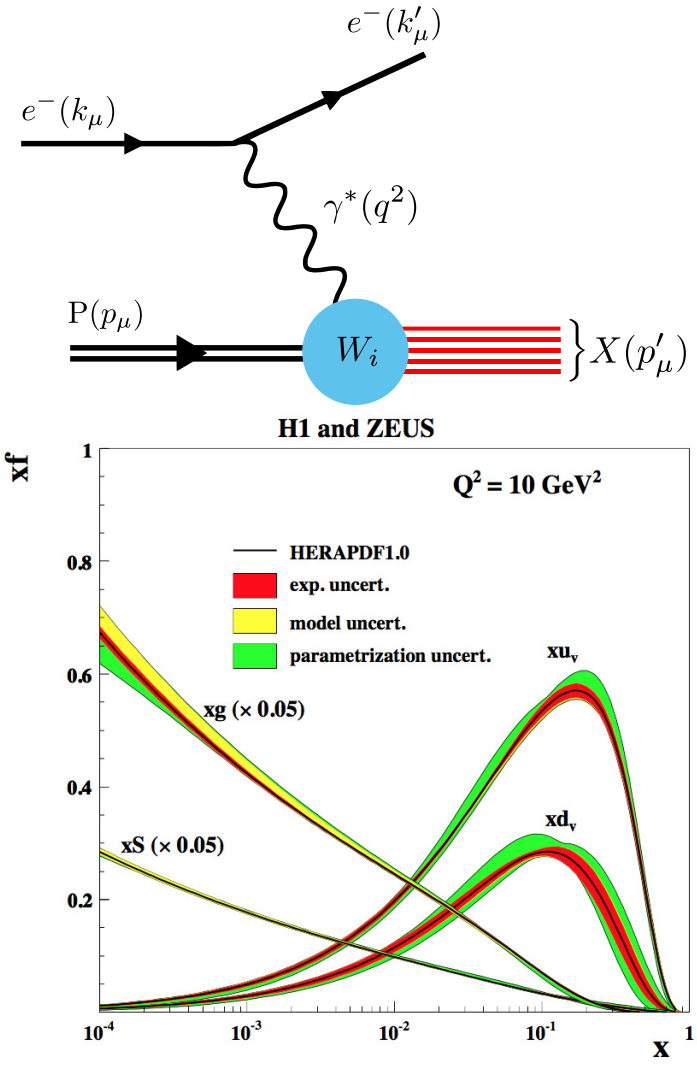

FIG. 3.1: (*On the top*) Deep inelastic scattering of $e^- p \to e^- X$ via exchange of a virtual photon. On the left hand side, valence quarks of the proton seen by the probed photon. (*On the bottom*) Parton distribution functions (PDFs) within the proton plotted as a function of x at $Q^2 = 10$GeV. Valence quark distributions denoted by xu_V, xd_V and sea quark and gluon distribution functions denoted by xS and xG respectively. Figure taken from [50].

3.1 Evolution of the Parton Distribution Functions

The Hadron Electron Ring Accelerator (HERA) has made precise measurements for the quark and gluon structure of the proton by means of electron/positron with proton scattering. Hitting the proton target with a long-wave photon reveals at first three valence quarks, however with increasing momentum transfer a more complex picture arises as the exchanged photon perceives a larger number of sea quarks and antiquarks carrying a smaller fraction of the proton's longitudinal momentum. The hadronic structure strongly depends on the scale resolved by the external probe and so what might appear as an isolated quantum at some resolution scale could be seen as much more complex set of processes at another. In perturbative QCD (pQCD), the evolution equations describe the change in the hadron wave function with respect to the resolution scale at which they are probed. The kinematics of the collision is best described in the infinite momentum frame (IMF), also it is convenient to define the following Lorentz invariants: the virtual photon momentum $q^2 = -Q^2 < 0$ exchanged between the electron and proton target, the center-of-mass energy squared s, ratio of the photon energy to the electron energy in the proton rest frame y and the longitudinal momentum fraction of a parton in the proton x. This quantities can $x = Q^2/ys$, Bjorken's x variable. In terms of these variables two limits are worth mentioning at this point, one taking $Q^2 \to 0$ while keeping x fixed (Bjorken limit) and the other at going to smaller and smaller x while keeping Q^2 fixed (Regge-Gribov limit). Typical values at the LHC and RHIC at central rapidity involve x $\sim 10^{-2}$ and x $\sim 10^{-4}$. We also know from data obtained at HERA that the gluon distribution is completely dominant over the that of quarks as we approach the Regge-Gribov limit see Fig. 3.1 Therefore, before any attempt at describing what is observed at the ultra-relativistic heavy ion collision experiments, it is imperative to have deep understanding of the dynamics of small x gluons. Observable at these experiments are as sensible to the bulk properties of the QGP as they are to the initial state. Although proven to be a powerful tool when describing the QGP system evolution Relativistic Hydrodynamics has not been successful into predicting the medium transport coefficients, reflection of our lack of knowledge on the initial state.

One could imagine a proton at rest revealing three valence quarks and then as the proton energy

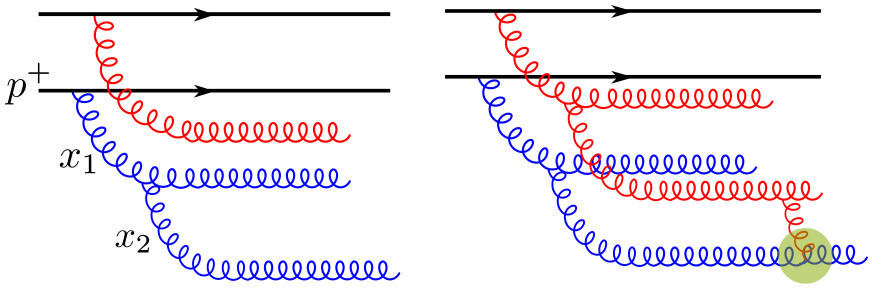

FIG. 3.2: (*Left side*) soft gluon emission within the hadron via bremsstralung, single gluon in red and cascade of n-subsequent gluons where $x_1 \gg x_2 \gg x_3 \cdots \gg x_n$. (*Right side*) gluon recombination starts to take place represented by the green shaded area.

increases gluons start to be emitted. We are thus interested evolution of the gluon distribution on x, $xG(x, Q^2)$. The basic mechanism that governs the parton evolution in perturbative QCD (pQCD) is the branching of partons. At the lowest order the emission of small-x partons takes place via bremstrahlung, the probability of a single gluon emission is,

$$d\mathcal{P}_{\text{Brem}} \simeq \frac{C_R \alpha_s}{\pi^2} \frac{d^2\boldsymbol{k}_\perp}{\boldsymbol{k}_\perp} \frac{d\mathrm{x}}{\mathrm{x}} \,, \tag{3.1}$$

where C_R is the SU(N_c) Casimir corresponding to N_c for gluons and $(N_c^2 - 1)/2N_c$ for quarks. This differential probability is divergent at $\mathrm{x} \to 0$, manifestation of the soft singularity of the QCD splitting functions and also divergence at $\boldsymbol{k}_\perp \to 0$. The probability per one gluon emission then proportional to $\alpha_s \log(1/\mathrm{x})$, similarly the emission of collinear gluons is logarithmically enhanced. Small x translates into small value of the coupling constant however the log-enhancement completely overrides and so successive emissions start to take place. Each radiated gluon further suppresses the probability by α_s until the cascade ends, and so an $n-$gluon emission process involves

$$\alpha_s^n \int_{\mathrm{x}}^1 \frac{d\mathrm{x}_n}{\mathrm{x}_n} \int_{\mathrm{x}_n}^1 \frac{d\mathrm{x}_{n-1}}{\mathrm{x}_{n-1}} \cdots \int_{x_2}^1 \frac{d\mathrm{x}_1}{\mathrm{x}_1} = \frac{1}{n!} \left(\alpha_s \log \frac{1}{\mathrm{x}} \right)^n \,, \tag{3.2}$$

pQCD evolution equations provide us with a systematic way to perform the resummation of these ladders to all orders. RG equations such as the Dokshitzer-Gribov-Lipatov-Altarelli-Parisi (DGLAP) or Balitsky-Fadin-Kuraev-Lipatov (BFKL) [51, 52] achieve on taking these log contributions in the

the scale dependence of the parton distributions. For the Bjorken limit it is relevant to know how the parton functions change with the Q^2 scale once x is fixed, the DGLAP equation provides a set of differential equations describing the evolution of parton functions with Q^2, it describes a dilute system. The x dependence is modulated by the splitting functions, at small x only the gluon splitting function matters and it translates into an explosive growth of the gluon distribution function. On the other hand, the BFKL equation describes the parton evolution with the scale x while keeping Q^2 fixed. We can compactly express this equation as,

$$\frac{\partial \phi(\mathrm{x}, \boldsymbol{k}_\perp)}{\partial \log(1/x)} = \mathscr{K} \otimes \phi(\mathrm{x}, \boldsymbol{k}_\perp), \tag{3.3}$$

here ϕ represents the unintegrated gluon distribution which as the name suggests is given by $\mathrm{x}G(\mathrm{x}, Q^2) = \int^{Q^2} d^2\boldsymbol{k}_\perp \phi(\mathrm{x}, k_\perp)$, and on the right we have the convolution of the BFKL kernel $\mathscr{K}$ with ϕ. To leading order in $\alpha_s \log(1/x)$, this equation admits the solution $\mathrm{x}^{-\alpha_s(4N_c \log 2)/\pi}$ implying the exponential growth of the gluon distribution in rapidity $\log(1/\mathrm{x})$ for small x similar behaviour to what is observed by the DGLAP equations. Of course, radiation of softer and softer gluon cannot continue indefinitely as unitary of the theory would be violated. What is it eventually found is that as the system reaches the high-density regime at smaller and smaller x the non-linear dynamics of the soft gluons start to become relevant taming the avalanche of gluons and thereby restoring unitarity. This phenomenon implies the emergence of a dimensionful scale Q_{sat}, embodying the concept of gluon saturation.

As an improvement of BFKL equation, the Balisky-Kovchegov (BK) equation takes non-linearities responsable are taken into account by means of gluon recombination [53, 54]. At heart, the DGLAP as well as the BFKL equations assume a dilute system at each step and so their linear character does not allow for the interference between cascades. Indeed non-linear contributions stemming from gluon recombination should be taken into account introduced as a quadratic term in the BFKL evolution equation Fig. (3.2). In this picture, we can now understand the saturation momentum $Q_{sat}(\mathrm{x})$ as the dynamically generated momentum transverse momentum scale at which the linear effects coming from gluon emission and the non-linear corrections stemming from recombination become of the

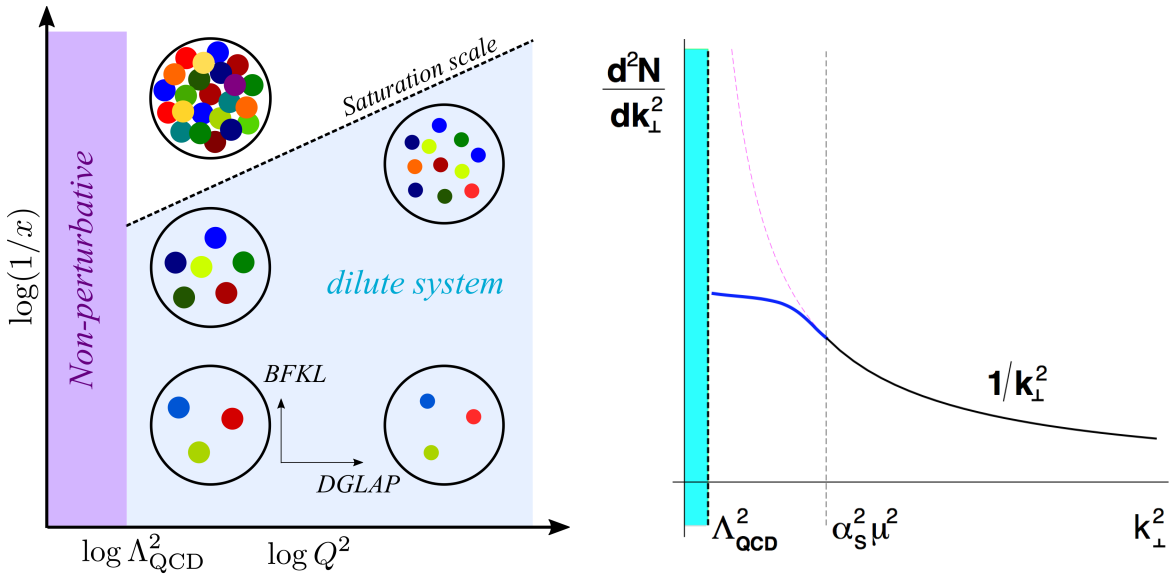

FIG. 3.3: (*On the left*) Phase diagram of High-Energy QCD in (x, Q^2) plane. Horizontal and vertical lines represent the DGLAP and BFKL regimes where as the diagonal line corresponds to saturation scale and the left stripe to the non-perturbative region. Schematic picture of the nucleon at that region is presented. (*On the right*) Saturation of the gluon density at small transverse momentum. Figure taken from Ref. [55]

same order.

$$\frac{\partial}{\partial \mathrm{Y}}\mathcal{N}_{\mathrm{Y}}(\mathrm{x}, \boldsymbol{k}_\perp^2) = \alpha_s \mathscr{K}_{\mathrm{BFKL}} \otimes \left\{\mathcal{N}_{\mathrm{Y}}(\mathrm{x}, \boldsymbol{k}_\perp^2) - \mathcal{N}_{\mathrm{Y}}(\mathrm{x}, \boldsymbol{k}_\perp^2)^2\right\}, \tag{3.4}$$

where $\otimes$ denotes convolution. The very presence of the non-linear term in the equation above already implies the emergence of a dimensionful scale, known as the gluon saturation scale Q_{sat}, which signals the transverse momentum scale at which the emission contribution corresponding to the linear term becomes of the same order as of gluon recombination contribution associated with the non-linear. The onset of saturation effects also leads to a geometrical interpretation as due to the overlap of gluons in the transverse plane, known as geometric scaling.

3.2 Gluon Saturation and the Color Glass Condensate

As described in the previous section the density of gluons within the parton grows as α_s^{-1} at the relativistic heavy-ion collision. In this section, we will introduce the basics behind the McLerran-Venegopalan model (MV) model, the precursor to the color-glass condensate (CGC) formulation. This model comes as an effective theory aiming to describe the gluon correlations in the hadron wave-function measured in small-x DIS. The relevant degrees of freedom are hard (large x) and soft (small x) partons. It is therefore useful to introduce an intermediate scale Λ allowing us to distinguish between these modes in the hadron wave function. Fast modes are identified as excitations with longitudinal momentum $p^+ \gg \Lambda^+$ and soft modes with $p^+ \ll \Lambda^+$. Hard partons are treated as quantum but perturbatively integrated out and in this way the classical source ρ emerges as a way to describe the fast modes whereas the soft partons are non-perturbative because of their large occupation numbers, yet can be regarded as classical for this reason. The difference in longitudinal momentum between slow and fast partons translates into a difference in light cone energies and light cone time scales between them. That means that the lifetime of the soft gluons is much shorter their fast counterparts. It is in this sense that, from the soft partons perspective fast gluons appear as colored on-shell propagating particles. The soft gluons are thus taken as localized static color charge sources moving along the light cone in the x^+ direction, namely

$$\mathcal{D}_\mu \mathcal{F}^{\mu\nu} = \delta^{\nu+}\rho^{(1)}(x^-, \boldsymbol{x}_\perp). \tag{3.5}$$

in the saturation regime the source and fields are strong and $\sim 1/g$ and thus the classical problem becomes fully non-linear. Once an exact solution for the classical Yang-Mills equation of motion is obtained, gluon correlation functions can be computed by taking the average over color charges randomly distributed according to the probability distribution function $W[\rho]$.

Our current task is to thus solve the classical Yang-Mills equation of motion for the current (3.17), namely

$$\mathcal{D}_\mu \mathcal{F}^{\mu\nu} = \delta^{\nu+}\rho^{(1)}(x^-, \boldsymbol{x}_\perp). \tag{3.6}$$

To solve this equation we choose light-cone gauge $\mathcal{A}^+ = 0$, however we shall first assume $\mathcal{A}^- = 0$ and then perform a gauge rotation onto the solution back to $\mathcal{A}^+ = 0$. With $\mathcal{A}^- = 0$ the solution is simply,

$$\mathcal{A}^+(x^-, \boldsymbol{x}_\perp) = -\nabla^{-2}\rho(x^-, \boldsymbol{x}_\perp), \qquad \mathcal{A}^i = 0\,. \tag{3.7}$$

We gauge rotate back to the light-cone using $\mathcal{A}^\mu = V^\dagger \mathcal{A}^\mu V + (i/g)V^\dagger \partial^\mu V$, in this way we rewrite the solution in terms of the color matrix V, i.e. $\mathcal{A}^\pm = 0$ and $\mathcal{A}^i = -\frac{1}{ig}V^\dagger(x^-, \boldsymbol{x}_\perp)\partial^i V(x^-, \boldsymbol{x}_\perp)$ where the rotation matrix V being found to be

$$V^\dagger(x^-, \boldsymbol{x}_\perp) = \mathscr{P}\exp\left[-\int_{-\infty}^{x^-} d\xi^- \nabla^{-2}\rho(\xi^-, \boldsymbol{x}_\perp)\right], \tag{3.8}$$

with $\mathscr{P}$ corresponding to the path-ordering operator.

To describe the quantum evolution of the theory in terms of gluon correlators we first need to write down the partition function,

$$Z[J] = \int \mathscr{D}\rho\, W_\Lambda[\rho]\left\{\frac{\int^\Lambda \mathscr{D}A^\mu_a\, \delta(A^+_a)e^{iS[A,\rho]-iJ\cdot A}}{\int^\Lambda \mathscr{D}A^\mu_a\, \delta(A^+_a)e^{iS[A,\rho]}}\right\}. \tag{3.9}$$

The action in this expression for the partition function is composed by the gluon's kinetic term and an interaction term,

$$S[\rho, A] = -\frac{1}{4}\int d^4x F^a_{\mu\nu}F^{\mu\nu}_a - \frac{i}{N_c}\int d^2\boldsymbol{x}_\perp dx^- \delta(x^-)\rho^a(\boldsymbol{x}_\perp)\mathrm{tr}\{T_a V^\dagger_{-\infty,\infty}[A^-](\boldsymbol{x}_\perp)\}\,, \tag{3.10}$$

where the Wilson operator has been evaluated at $x^+ \to \infty$. and color charge density ρ corresponds to a $\mathbb{C}$-number stochastic variable on the sheet. The action above the contains the solution (3.7) to the Yang-Mills equation and so the classical saddle point represents the tree level contribution. This separation between soft and hard gluons introduces a momentum separation scale and as a consequence one can expect that any physical observable from the above effective action will inherit this cut-off.

The color charges are described by $W_{\Lambda^+}[\rho]$, i.e. we only have probabilistic knowledge on the hard gluons and so, ultimately what determines the dynamics of the color charges is the evolution of $W[\rho]$. The Wilsonian renormalization group equation provides a way out this problem, the strategy is the following. We start off with a generating functional at some scale Λ^+ with some initial source distribution, usually a Gaussian profile is assumed for such initial probability distribution. We are interested in gluon correlation in the softer scale $\Lambda^{'+}$ which means that we should focus on obtaining $W_{\Lambda^{'+}}[\rho]$. Such weight function should contain the semi-fast gluons with longitudinal momentum between these two scales. To obtain the distribution, we take fluctuations around the classical background modes of the effective action,

$$A_b^\mu = \mathcal{A}_b^\mu[\rho] + a_b^\mu + \delta A_b^\mu \,, \tag{3.11}$$

calligraphic fonts will be reserved for the classical fields. $\mathcal{A}_b^\mu[\rho]$ represents the tree-level contribution, a_b^μ the semi fast fluctuations and δA_b^μ are unwanted modes outside this strip. There is a problem with small fluctuations in the effective action, there are large corrections to the classical effective action, this implies that the Gaussian weight functional is fragile under the quantum evolution of the sources. The Jalilian-Iancu-McLerran-Weigert-Leonidov-Kovner (JIMWLK) renormalization group equation provides a way out this problem [56, 57, 58]; We attain invariance of the partition function (3.9) on the momentum cut-off Λ by allowing this probability function on it,

$$\Lambda^+ \frac{\partial Z[J]}{\partial \Lambda^+} = 0 \,, \tag{3.12}$$

where Λ^+ is related to x by $\Lambda^+ = \log(1/\mathrm{x})$. The dependence of the $W_{\mathrm{x}}[\rho]$ on x is dictated by the JIMWLK renormalization group equation.

$$\frac{\partial W_{\mathrm{x}}[\rho]}{\partial \log(1/\mathrm{x})} = \alpha_s \left\{ \frac{1}{2} \frac{\delta^2}{\delta \rho_{\mathrm{x}}^a(\boldsymbol{x}_\perp) \delta \rho_{\mathrm{x}}^b(\boldsymbol{y}_\perp)} [W_{\mathrm{x}}[\rho] \chi_{\boldsymbol{xy}}^{ab}] - \frac{\delta}{\delta \rho_{\mathrm{x}}^a(\boldsymbol{x}_\perp)} [W_{\mathrm{x}}[\rho] \sigma_{\boldsymbol{x}}^a] \right\} \,. \tag{3.13}$$

This equation has clearly the structure of a diffusion Fokker-Planck equation: It is a second-order (functional) differential equation whose r.h.s. is a total derivative (as necessary to conserve the total

probability). In fact, the quantum evolution of the probability weight function can be interpreted as the diffusion of probability density. The coefficients σ, χ correspond to one- (two-) point functions of the color charge and must explicitly computed [55]. Eq. (3.13) describes a diffusion in the functional space spanned by ρ from where we can interpret $\alpha_s \rho$ as the -drift velocity- and $\alpha_s \chi$ as the associated diffusion constant. It is often more useful to rewrite the RG equation in terms of a gauge field α in which case the JIMWLK equation can be expressed as,

$$\frac{\partial W_x[\alpha]}{\partial \log(1/\mathrm{x})} = \frac{\alpha_s}{2} \int d^2\boldsymbol{x}_\perp d^2\boldsymbol{y}_\perp \frac{\delta}{\delta \alpha^a_{\mathrm{x}}(\boldsymbol{x}_\perp)} \left\{ \eta^{ab}_{xy}[\alpha] \frac{\delta}{\delta \alpha^b_{\mathrm{x}}(\boldsymbol{y}_\perp)} W_x[\alpha] \right\} \equiv -\mathcal{H} W_{\mathrm{x}}[\alpha] \tag{3.14}$$

where $\mathcal{H}$ is the JIMWLK Hamiltonian. In this way, we are in position to calculate observables of interest accordingly,

$$\frac{\partial \langle \mathscr{O}[\alpha] \rangle_{\mathrm{x}}}{\partial \log(1/\mathrm{x})} = \frac{\alpha_s}{2} \left\langle \int d^2\boldsymbol{x}_\perp d^2\boldsymbol{y}_\perp \frac{\delta}{\delta \alpha^a_{\mathrm{x}}(\boldsymbol{x}_\perp)} \left\{ \eta^{ab}_{xy}[\alpha] \frac{\delta}{\delta \alpha^b_{\mathrm{x}}(\boldsymbol{y}_\perp)} \mathscr{O}[\alpha] \right\} \right\rangle_{\mathrm{x}} \tag{3.15}$$

Usually the x dependence is traded by the rapidity $Y = \log(1/\mathrm{x})$. It is important to remark at the JIMWLK equation describes how the probability distribution changes for different x but does not determine the $W_x[\rho]$ itself for a given target. In order to do so, one must be provided an initial condition at a given value of the cut-off, such value is non-perturbative in nature and must be thus modelled. In fact, it is the Gaussian ansatz assumed for the profile of color charges at $W_x[\rho]$ that defines the MV model. Such Gaussian form is equivalent to requiring the correlator of color charge densities,

$$\langle \rho^a(x^-, \boldsymbol{x}_\perp) \rho^b(y^-, \boldsymbol{y}_\perp) \rangle = \mu^2_{\mathrm{x}} g^2 \delta(x^- - y^-) \delta^{(2)}(\boldsymbol{x}_\perp - \boldsymbol{y}_\perp). \tag{3.16}$$

3.3 Initial Condition for the Relativistic Heavy Ion Collision

In this thesis, we will be interested in the collision of two nuclei. For simplicity of exposition, let us focus first in the case of one nuclei moving along the x^+-axis of the light cone.

$$J^{\mu} = \delta^{\mu+}\delta(x^{-})\rho(\boldsymbol{x}_{\perp}) \tag{3.17}$$

The $\delta^{\mu+}$ enforces the fact that the source is moving near the speed of light whereas the second one depicts the source as a this sheet. Similar treatment for its color source living in the other side of the light-cone. We have now the tools to address the relativist heavy-ion collisions set-up by modelling the collision of two color sources, i.e.

$$\mathcal{D}_{\mu}\mathcal{F}^{\mu\nu} = \delta^{\nu+}\rho^{(1)}(x^{-}, \boldsymbol{x}_{\perp}) + \delta^{\mu-}\rho^{(2)}(x^{+}, \boldsymbol{x}_{\perp}) \tag{3.18}$$

the notation $(i), i = 1, 2$ is reserved for labeling between the incoming nuclei from the opposite regions of the light-cone, I and II. For the next step we are interested into solving the Yang-Mills equation in the forward light-cone, in the particular in the $\tau \to 0^{+}$ surface. We adopt the following ansatz,

$$\mathcal{A}^{i} = \alpha^{i}_{\perp}(\tau, \boldsymbol{x}_{\perp}), \qquad \mathcal{A}^{\pm} = \pm x^{\pm}\alpha(\tau, \boldsymbol{x}_{\perp}) \tag{3.19}$$

where the specific form of the introduced functions α, α_i should be determined by the Yang-Mills equation of motion. This ansatz is, by construction, consistent with the Fock-Schwinger gauge and on explicitly drops dependence on the space-time rapidity as we are looking for a boost invariant solution,

$$\begin{aligned}
\mathcal{A}^{+}(x) &= \Theta(x^{+})\Theta(x^{-})x^{+}\alpha(\tau, \boldsymbol{x}_{\perp}), \\
\mathcal{A}^{-}(x) &= -\Theta(x^{+})\Theta(x^{-})x^{-}\alpha(\tau, \boldsymbol{x}_{\perp}), \\
\mathcal{A}^{i}(x) &= \Theta(x^{+})\Theta(-x^{+})\alpha^{i}_{(1)}(\tau, \boldsymbol{x}_{\perp}) + \Theta(x^{+})\Theta(-x^{-})\alpha^{i}_{(2)}(\tau, \boldsymbol{x}_{\perp}) \\
&\quad + \Theta(x^{+})\Theta(x^{-})\alpha(\tau, \boldsymbol{x}_{\perp})
\end{aligned} \tag{3.20}$$

From this expression, one would naively expect singular terms stemming out from the derivatives in the EOM $[\mathcal{D}_{\mu}, \mathcal{F}^{\mu\nu}] = 0$ as the product of deltas. However, these singularities are avoided altogether, provided that $\mathcal{A} = \mathcal{A}_1 + \mathcal{A}_2$. In the same way, matching the singular terms from both sides in the

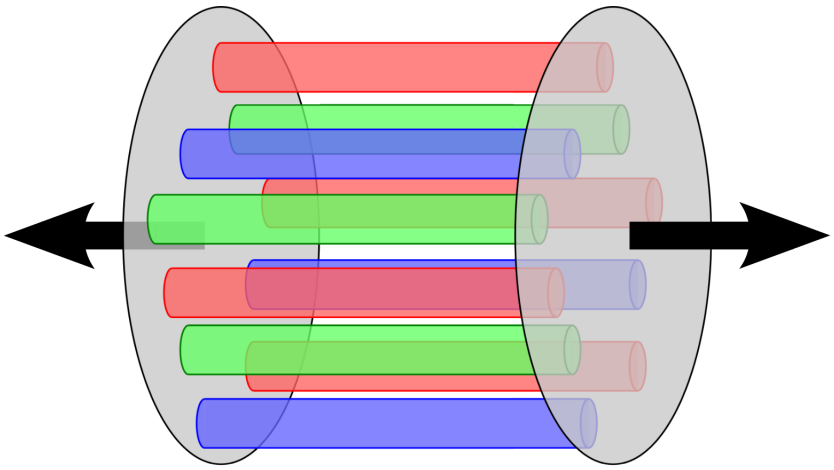

FIG. 3.4: Schematic representation of the glasma initial condition. Showing the longitudinal color electric and magnetic fields, or color flux tubes after the collision. Figure taken from Ref. [59]

remaining EOM $\mathcal{D}_\mu \mathcal{F}^{\mu\nu} = J^\nu$ yields the initial conditions,

$$\alpha_i^3(0, \boldsymbol{x}_\perp) = \alpha_i^{(1)}(\boldsymbol{x}_\perp) + \alpha_i^{(1)}(\boldsymbol{x}_\perp) \tag{3.21}$$

$$\alpha(\tau, \boldsymbol{x}_\perp)\Big|_{\tau=0} = -\frac{1}{2}[\alpha_i^{(1)}(\boldsymbol{x}_\perp), \alpha^{(2)i}(\boldsymbol{x}_\perp)] \tag{3.22}$$

While the transverse component of the resulting gauge field is simply given by a linear superposition, a finite longitudinal component stems out as a result of the non-abelian character of the color fields. From the explicit form of the YM equations exhibits a singularity in the $\tau = 0$ surface, hence, for regular solutions we should also require that the derivatives $\partial_\tau \alpha^i$ and $\partial_\tau \alpha$ vanish at $\tau = 0$. Although one may find an analytical solution by perturbative methods via power expansion of the $\{\alpha^i, \alpha\}$, the classical solutions in the non-perturbative regime are only accessible by numerical means. For this purpose, it is useful to translate the problem to construct the Hamiltonian for this system. The initial conditions are boost invariant by construction therefore it is only natural that the same holds for general solution and thus the solution does not depend on η.

$$S = \int d\tau d^2\boldsymbol{x} d\eta\, \tau\, \mathrm{tr}\left\{(\partial_\tau A_i)^2 - \frac{1}{2}F_{ij}F_{ij} + \frac{1}{\tau^2}(\partial_\tau \phi)^2 - \frac{1}{\tau^2}[D,\phi][D,\phi]\right\} \tag{3.23}$$

The explicit τ factors arise from the Bjorken metric, specifically from the overall τ in the above expression appears from $\sqrt{|g|}$ in volume factor. For the YM Hamiltonian, the canonical conjugate momenta given $E^i = \tau\partial_\tau A_i$ and $E^i = \tau^{-1}\partial_\eta A_\eta$ are needed. While the longitudinal component has the right mass dimension for an electric field, the transverse component does not. The Hamiltonian density can be straightforwardly obtained from (3.23), leading to a 1+2 dimensional YM Hamiltonian coupled to an adjoint scalar field whose discretized version is corresponds to the well known Kogut-Susskind Hamiltonian. The Hamiltonian classical equations for the continuum version are,

$$\begin{aligned}\partial_\tau \mathcal{E}^i &= \tau[D_j, \mathcal{F}_{ji}] - \frac{ig}{\tau}[\phi,[D,\phi]] \\ \partial_\tau \mathcal{E}^\eta &= -\frac{1}{\tau}[D_i,[D_i,\phi]]\end{aligned} \tag{3.24}$$

From here we can extract the CGC initial conditions for the chromo-electric and -magnetic fields.

$$\mathcal{B}^i = 0; \qquad \mathcal{B}^\eta = \mathcal{F}_{12} = -ig\epsilon^{ij}[\alpha_i^{(1)}, \alpha_j^{(1)}] \tag{3.25}$$

After taking the color average assuming a assuming a Gaussian probability distribution, one finds that the expectation values for the chromo electric and magnetic fields are eventually the same.

Chapter 4

Quark Production

As described by the CGC theory right after the collision, the coherent background fields produce longitudinal color flux tubes whose effective diameter is of order Q_{sat}^{-1}. These topological flux tubes play the role of Q_W of the CME integrated current and so the particles that are produced inside these tubes possess a characteristic momentum distribution with respect to the direction of the strong magnetic field that stems during the collision [60, 61]. To address on how this phenomenon takes place better, it is necessary to develop a deeper understanding of the real-time dynamics of the CME, in a framework that allows us to understand the formation of these topological currents in terms of the quark production process, including the Schwinger mechanism. A serious simulation of quark production during the early-time regime with the glasma background is indispensable in the prediction of a concrete experimental signal. To perform our simulation, it is crucial that we know the initial condition of the quark fields in the presence of the proper CGC background, which is to what this chapter shall be devoted to. First, lets us start by the study of the topological current production in the context of quark production and in the finite box and then we shall proceed to the study the quark spectrum in the expanding geometry.

We are ultimately interested in the quark spectrum and the induced observables associated with it. The basic ingredients for such computation are the time-evolved quark wave functions from $x^0 \to -\infty$ into the forward light-cone. Thus, our first task will be able to solve the Dirac equation in the presence of color sources. This chapter will be devoted to this purpose, in particular, to derive an expression

for the initial condition of the quark fields proper to the CGC setup.

4.1 General Formalism

The interactions of a quantum field with a time-dependent background, whether it be an external gravitational or electromagnetic field, modifies the fields energy manifesting into the spontaneous creation of quanta with respect to the initial vacuum. For instance, let us consider the evolution in time of a quantum field from its vacuum state that starts to interact with the background at some initial time t_i. If a measurement is performed at a latter time t_f revealing the number of particles in this state then, we interpret that the interaction has translated into the creation of particles. Let us illustrate the above by considering a fermion field $\psi(x)$ coupled to a classical gauge field. Since the Dirac equation is linear in the field operator we can expand it by a complete set of orthonomal modes $\{f_{ini}, f^*_{ini}\}$ associated with *in* state,

$$\hat{\psi}(t_{\rm ini}, \boldsymbol{x}) = \sum_{\boldsymbol{k}} (f^{ini}_{\boldsymbol{k}} a_{ini}(\boldsymbol{k}) + f^{ini*} a^{\dagger}_{ini}(\boldsymbol{k})) \tag{4.1}$$

Let us assume that there is no electromagnetic field at asymptotic times and take $\lim_{t\to-\infty} A_\mu(x) = 0$ for the initial condition. Let us also fix the gauge $A^0 = 0$. Although a gauge condition has been set, a residual gauge invariance remains corresponding to spatially dependent gauge transformations. The *in*-mode functions expanding the fermion field are free plane waves at $t \to -\infty$. Similarly one may also expand can do the same for the final *out* states, by means of the orthonormal modes $\{\psi_{out}, \psi^*_{out}\}$. Because the scalar field may represented by both of the complete sets, one can relate one in terms of the other. The *out* modes in terms of the *in* modes can thus be expressed as,

$$\hat{\psi}(t_{\rm out}, \boldsymbol{x}) = \sum_{\boldsymbol{k}} (f^{out}_{\boldsymbol{k}} a_{out}(\boldsymbol{k}) + f^{ini*} a^{\dagger}_{out}(\boldsymbol{k})) \ , \tag{4.2}$$

for instance let's consider that the background is vanishes at both $t_i \to -\infty$ or some other finite time and at $t_f \to \infty$ or some other finite time. Then by means of the orthonormal relation of this set one

can define a Bogoliubov tranformation relating the *in* and *out* vacuum.

For a system of massless fermion particles, the problem of net particle production can be tackled with 2-component Weyl spinors using only its right-handed sector. Due to symmetry, the chiral imbalance can be addressed in this way by means of (*right-handed*) particle and antiparticles. However, the inclusion of finite mass breaks the symmetry and thus both sectors must be taken into account, Dirac spinors are more appropriate for this task. As mentioned in order to compute net-particle production, first we are to solve the Dirac equation in real-time. The Dirac equation with a gauge field A_μ reads,

$$\Big(i\gamma^\mu\partial_\mu - e\gamma^\mu A_\mu - m\Big)\psi(x) = 0\ . \tag{4.3}$$

For the gauge field a homogeneous step profile is considered and a gauge where $A_0 = 0$ is chosen. The solution of the Dirac equation in such a background is nothing but the free solution with displaced momenta, and so it is straight forward to write down. The positive energy solution reads $\psi = u^h(\boldsymbol{p};\boldsymbol{A})\, e^{-iE_{\boldsymbol{p},A}x^0 + i\boldsymbol{p}\cdot\boldsymbol{x}}$,

$$u^h(\boldsymbol{p};\boldsymbol{A}) = \begin{pmatrix} \sqrt{(p_A\cdot\sigma)}\,\xi^h \\ \sqrt{(p_A\cdot\bar{\sigma})}\,\xi^h \end{pmatrix}\ . \tag{4.4}$$

Where we have defined p_A as the displaced four-momentum with $\boldsymbol{p}_{\pm A} = \boldsymbol{p} \mp e\boldsymbol{A}$ and $E_{\boldsymbol{p},\boldsymbol{A}} = \sqrt{\boldsymbol{p}_A^2 + m^2}$ and h denotes helicity. This 4-spinor solution is obtained from boosting the rest frame solution and its manifestly Lorentz invariant so it constitutes the most general solution to the Dirac equation, ξ^s is a 2-spinor normalized as $\xi^{h\dagger}\xi^h = \mathbf{1}_2$. Since we are dealing with helicity eigenstates a concrete expression for ξ^h can be worked out by computing the square root operator in the above matrix. Consider for instance the second component of a positive energy 4-spinor with + helicity,

$$u_2^+(\boldsymbol{p};\boldsymbol{A}) \equiv \sqrt{(p_A\cdot\bar{\sigma})}\,\xi^+ = \frac{1}{\sqrt{2(E_{\boldsymbol{p},A}+m)}}(p_A\cdot\bar{\sigma}+m)\xi^+\ , \tag{4.5}$$

In order to go further, we have to obtain an expression for ξ^+ which is chirality eigenstate. To see this

clearly, let us first consider massless fermions. In this case,

$$u_2^+(\boldsymbol{p};\boldsymbol{A}) = \frac{1}{\sqrt{2E_{\boldsymbol{p},A}}}(E_{\boldsymbol{p},A} + \boldsymbol{p}_A \cdot \boldsymbol{\sigma})\xi^+ = \sqrt{\frac{|\boldsymbol{p}_A|}{2}}(1+\Sigma)\xi^+ \tag{4.6}$$

This spinor is also eigenstate of helicity, thus $[\Sigma, (p\cdot\bar{\sigma})] = 0$ and so $\Sigma\,\xi = +\xi$ which constrains sigma and the explicit form for this positive energy spinor is follows as,

$$u_2^+(\boldsymbol{p};\boldsymbol{A}) = \sqrt{2|\boldsymbol{p}_A|}\xi^+ = \begin{pmatrix} \sqrt{|\boldsymbol{p}_A| + p_A^3} \\ e^{i\theta(p)}\sqrt{|\boldsymbol{p}_A| - p_A^3} \end{pmatrix}, \qquad e^{i\theta(p_A)} = \frac{p_A^1 + ip_A^2}{\sqrt{(p_A^1)^2 + (p_A^2)^2}}, \tag{4.7}$$

where we note that $u_2^+(\boldsymbol{p};\boldsymbol{A})$ has a well-defined chirality. Similarly, the corresponding spinor solution to the negative energy Dirac solution can be obtained. The 2 component spinor ξ^h also normalized $\xi^{h\dagger}\xi^s = \mathbf{1}_2$ where $E_{\boldsymbol{p},\boldsymbol{A}} = \sqrt{\boldsymbol{p}_A^2 + m^2}$. The complete explicit expression for the + helicity spinor reads,

$$u^+(p_A) = \frac{1}{\sqrt{4|\boldsymbol{p}_A|E_{\boldsymbol{p},A}}}\frac{1}{\sqrt{2(E_{\boldsymbol{p},A}+m)}}\begin{pmatrix} \gamma_-\begin{pmatrix} \sqrt{|\boldsymbol{p}_A| + p_A^z} \\ e^{i\theta(\boldsymbol{p}_A)}\sqrt{|\boldsymbol{p}_A| - p_A^z} \end{pmatrix} \\ \gamma_+\begin{pmatrix} \sqrt{|\boldsymbol{p}_A| + p_A^z} \\ e^{i\theta(\boldsymbol{p}_A)}\sqrt{|\boldsymbol{p}_A| - p_A^z} \end{pmatrix} \end{pmatrix}. \tag{4.8}$$

Where $\gamma_\pm = (E_{\boldsymbol{p},A} + m \pm |\boldsymbol{p}_A|)$ has been introduced and the phase factor $e^{\pm i\theta(\boldsymbol{p}_A)}$ is given by $\tilde{\boldsymbol{p}}_A/|\tilde{\boldsymbol{p}}_A|$ with $\tilde{\boldsymbol{p}}_A = p_A^x \pm ip_A^y$. In an exact analogy the negative energy solution $\psi = v^h(\boldsymbol{p};\boldsymbol{A})\,e^{iE_{\boldsymbol{p},A}x^0 - i\boldsymbol{p}\cdot\boldsymbol{x}}$ is given by the same expression as Eq (4.4) but with the lower 2-components negative. Following the same logic, we obtain an explicit expression for the negative energy free spinor,

$$v^+(p_A) = \frac{1}{\sqrt{4|\boldsymbol{p}_A|E_{\boldsymbol{p},A}}}\frac{1}{\sqrt{2(E_{\boldsymbol{p},A}+m)}}\begin{pmatrix} -\gamma_-\begin{pmatrix} \sqrt{|\boldsymbol{p}_{-A}| + p_{-A}^z} \\ e^{-i\theta(\boldsymbol{p}_{-A})}\sqrt{|\boldsymbol{p}_{-A}| - p_{-A}^z} \end{pmatrix} \\ \gamma_+\begin{pmatrix} \sqrt{|\boldsymbol{p}_{-A}| + p_{-A}^z} \\ e^{-i\theta(\boldsymbol{p}_{-A})}\sqrt{|\boldsymbol{p}_{-A}| - p_{-A}^z} \end{pmatrix} \end{pmatrix}. \tag{4.9}$$

The quantized fermionic field operator in this representation can be expanded as,

$$\hat{\psi}_+(x) = \int \frac{d^3\boldsymbol{p}}{(2\pi)^3}\left[\hat{a}^+_{\boldsymbol{p}}\,\frac{u^+(\boldsymbol{p}_A)}{\sqrt{2\,E_{\boldsymbol{p},A}}}\,e^{-iE_{\boldsymbol{p},A}x^0+i\boldsymbol{p}\cdot\boldsymbol{x}} + \hat{b}^{+\dagger}_{\boldsymbol{p}}\,\frac{v^+(\boldsymbol{p}_{-A})}{\sqrt{2\,E_{\boldsymbol{p},-A}}}\,e^{iE_{\boldsymbol{p},-A}x^0-i\boldsymbol{p}\cdot\boldsymbol{x}}\right]. \tag{4.10}$$

The idea is to evolve the field in in time allowing it to interact and project out its positive energy part. Each wave function evolves and changes through interaction effects induced by a change in our vector gauge potential $\boldsymbol{A} \to \boldsymbol{A}'$. The temporal profile of the electromagnetic pulse considered, specifically the electric field allows us to define these two asymptotic states. As advertised earlier once we have well defined asymptotic states the problem of net particle production is well-defined. Assuming both "in/out" vector gauge fields constant the associated Hilbert space is complete and we can quantize our fermion fields. What we are doing corresponds to this change of basis between these two representations, this defines our Bogoliubov transformation operators. As expected the expectation value of the particle density operator vanishes in vacuum for the free particle case. As we shall see this is not the case when we introduce the homogeneous gauge $\boldsymbol{A}'$. Explicit computation will be performed through a Bogoliubov transformation of in and out states picking up a non-trivial contribution coming these coefficients. Let us now assume a Schwinger problem and postulate that the wave-functions change through interaction effects

$$\begin{aligned}
\frac{u^+(\boldsymbol{p}_A)}{\sqrt{2\,E_{\boldsymbol{p},A}}}\,e^{-iE_{\boldsymbol{p},A}x^0+i\boldsymbol{p}\cdot\boldsymbol{x}} \longrightarrow \int \frac{d^3\boldsymbol{q}}{(2\pi)^3}\Bigg[&\alpha_{\boldsymbol{q},\boldsymbol{p}}\frac{u^+(\boldsymbol{q}_{A'})}{\sqrt{2\,E_{\boldsymbol{q},A'}}}\,e^{-iE_{\boldsymbol{q},A'}x^0+i\boldsymbol{q}\cdot\boldsymbol{x}} \\
&- \beta^*_{-\boldsymbol{q},-\boldsymbol{p}}\frac{v^+(-\boldsymbol{q}_{A'})}{\sqrt{2\,E_{\boldsymbol{q},A'}}}\,e^{iE_{\boldsymbol{q},A'}x^0+i\boldsymbol{q}\cdot\boldsymbol{x}}\Bigg], \\
\frac{v^+(\boldsymbol{p}_{-A})}{\sqrt{2\,E_{\boldsymbol{p},-A}}}\,e^{iE_{\boldsymbol{p},-A}x^0-i\boldsymbol{p}\cdot\boldsymbol{x}} \longrightarrow \int \frac{d^3\boldsymbol{q}}{(2\pi)^3}\Bigg[&\bar{\alpha}^*_{\boldsymbol{q},\boldsymbol{p}}\frac{v^+(\boldsymbol{q}_{-A'})}{\sqrt{2\,E_{\boldsymbol{q},-A'}}}\,e^{iE_{\boldsymbol{q},-A'}x^0-i\boldsymbol{q}\cdot\boldsymbol{x}} \\
&+ \beta_{-\boldsymbol{q},-\boldsymbol{p}}\frac{u^+(-\boldsymbol{q}_{-A'})}{\sqrt{2\,E_{\boldsymbol{q},-A'}}}\,e^{-iE_{\boldsymbol{q},-A'}x^0-i\boldsymbol{q}\cdot\boldsymbol{x}}\Bigg].
\end{aligned} \tag{4.11}$$

Concrete expressions for the introduced Bogoliubov coefficients can and will be worked out, however let us keep them for the moment. The "particle" number, $(\alpha_{\boldsymbol{p}}\hat{a}_{\boldsymbol{p}} + \beta_{\boldsymbol{p}}\hat{b}^\dagger_{-\boldsymbol{p}})^\dagger(\alpha_{\boldsymbol{p}}\hat{a}_{\boldsymbol{p}} + \beta_{\boldsymbol{p}}\hat{b}^\dagger_{-\boldsymbol{p}})$, then picks up a contribution from $|\beta_{\boldsymbol{p}}|^2\hat{b}_{-\boldsymbol{p}}\hat{b}^\dagger_{-\boldsymbol{p}}$, which shall be relevant for non-vanishing of the quantities

we are to compute. Imposing anti-commutation relation on the Bogoliugov transformed operators results into the normalization condition:

$$|\alpha_{\boldsymbol{p}}|^2 + |\beta_{\boldsymbol{p}}|^2 = 1 \ . \tag{4.12}$$

preserving the fermi statistics. Let us consider a more conventional way to calculate the vacuum expectation value of the current operator directly: We now proceed to work out a concrete expression for the current operator J'^{μ} produced by the given change in the gauge potential and calculate its expectation value with respect to the initial vacuum state. It reads, where all exponentials have been integrated out yielding the corresponding delta functions,

$$\begin{aligned} J'^{\mu}_{+} = e \int \frac{d^3\boldsymbol{p}}{(2\pi)^3} \Bigg\{ & \frac{\hat{b}'_{-\boldsymbol{p}} \hat{a}'^{+}_{\boldsymbol{p}}}{2\, E_{\boldsymbol{p},A'}} [\bar{v}^{+}(-\boldsymbol{p}_{A'}) \gamma^{\mu} u^{+}(\boldsymbol{p}_{A'})]\, e^{-2iE_{p,A'}x^0} + \frac{\hat{a}'^{\dagger}_{\boldsymbol{p}} \hat{a}'_{\boldsymbol{p}}}{2\, E_{\boldsymbol{p},A'}} [\bar{u}^{+}(\boldsymbol{p}_{A'}) \gamma^{\mu} u^{+}(\boldsymbol{p}_{A'})] \\ & + \frac{\hat{b}'_{\boldsymbol{p}} \hat{b}'^{\dagger}_{\boldsymbol{p}}}{2\, E_{\boldsymbol{p},-A'}} [\bar{v}^{+}(\boldsymbol{p}_{-A'}) \gamma^{\mu} v^{+}(\boldsymbol{p}_{-A'})] + \frac{\hat{a}'^{\dagger}_{\boldsymbol{p}} \hat{b}'^{\dagger}_{-\boldsymbol{p}}}{2\, E_{\boldsymbol{p},A'}} [\bar{u}^{+}(\boldsymbol{p}_{A'}) \gamma^{\mu} v^{+}(-\boldsymbol{p}_{A'})]\, e^{2iE_{p,A'}x^0} \Bigg\} \ . \end{aligned} \tag{4.13}$$

The first and last term vanish due to the orthogonal relations of the Dirac spinors and thus can be discarded,

$$J'^{\mu} = e \int \frac{d^3\boldsymbol{p}}{(2\pi)^3} \left\{ \frac{\hat{a}'^{\dagger}_{\boldsymbol{p}} \hat{a}'_{\boldsymbol{p}}}{2\, E_{\boldsymbol{p},A'}} [\bar{u}^{+}(\boldsymbol{p}_{A'}) \gamma^{\mu} u^{+}(\boldsymbol{p}_{A'})] + \frac{\hat{b}'_{\boldsymbol{p}} \hat{b}'^{\dagger}_{\boldsymbol{p}}}{2\, E_{\boldsymbol{p},-A'}} [\bar{v}^{+}(\boldsymbol{p}_{-A'}) \gamma^{\mu} v^{+}(\boldsymbol{p}_{-A'})] \right\} , \tag{4.14}$$

$$= e \int \frac{d^3\boldsymbol{p}}{(2\pi)^3} \left\{ \frac{p^{\mu}_{A}}{E_{\boldsymbol{p},A'}} \hat{a}'^{\dagger}_{\boldsymbol{p}} \hat{a}'_{\boldsymbol{p}} + \frac{p^{\mu}_{-A}}{E_{\boldsymbol{p},-A'}} \hat{b}'_{\boldsymbol{p}} \hat{b}'^{\dagger}_{\boldsymbol{p}} \right\} . \tag{4.15}$$

Now, we are interested in the expectation values of these operators, let us first take the normal ordering before proceeding. As mentioned earlier, equivalent to anti-symmetrizing the bilinear of the current operator we consider normal ordering and thus,

$$\begin{aligned} : J'^{\mu} : &= e \int \frac{d^3\boldsymbol{p}}{(2\pi)^3} \left\{ \frac{p^{\mu}_{A}}{E_{\boldsymbol{p},A'}} : \hat{a}'^{\dagger}_{\boldsymbol{p}} \hat{a}'_{\boldsymbol{p}} : + \frac{p^{\mu}_{-A}}{E_{\boldsymbol{p},-A'}} : \hat{b}'_{\boldsymbol{p}} \hat{b}'^{\dagger}_{\boldsymbol{p}} : \right\} \\ &= e \int \frac{d^3\boldsymbol{p}}{(2\pi)^3} \left\{ \frac{p^{\mu}_{A}}{E_{\boldsymbol{p},A'}} \hat{a}'^{\dagger}_{\boldsymbol{p}} \hat{a}'_{\boldsymbol{p}} - \frac{p^{\mu}_{-A}}{E_{\boldsymbol{p},-A'}} \hat{b}'^{\dagger}_{\boldsymbol{p}} \hat{b}'_{\boldsymbol{p}} \right\} . \end{aligned} \tag{4.16}$$

However the quantity we to compute is the expectation value associated with the initial state, that is,

$$\begin{aligned}\left\langle :\hat{J}'^{\mu}_{A'}: \right\rangle_{\boldsymbol{A}} &= e\int \frac{d^3\boldsymbol{p}}{(2\pi)^3}\left\{\frac{p^{\mu}_{A}}{E_{\boldsymbol{p},A'}}\langle \hat{a}'^{\dagger}_{\boldsymbol{p}}\hat{a}'_{\boldsymbol{p}}\rangle_{\boldsymbol{A}} - \frac{p^{\mu}_{-A}}{E_{\boldsymbol{p},-A'}}\langle \hat{b}'^{\dagger}_{\boldsymbol{p}}\hat{b}'_{\boldsymbol{p}}\rangle_{\boldsymbol{A}}\right\} \\ &= e\int \frac{d^3\boldsymbol{p}}{(2\pi)^3}\left\{\frac{p^{\mu}_{A}}{E_{\boldsymbol{p},A'}}|\beta_{\boldsymbol{p}}|^2\langle \hat{b}_{-\boldsymbol{p}}\hat{b}^{\dagger}_{-\boldsymbol{p}}\rangle_{\boldsymbol{A}} - \frac{p^{\mu}_{-A}}{E_{\boldsymbol{p},-A'}}|\bar{\beta}_{\boldsymbol{p}}|^2\langle \hat{a}_{-\boldsymbol{p}}\hat{a}^{\dagger}_{-\boldsymbol{p}}\rangle_{\boldsymbol{A}}\right\} \\ &= e\int \frac{d^3\boldsymbol{p}}{(2\pi)^3}\left\{\frac{p^{\mu}_{A}}{E_{\boldsymbol{p},A'}}|\beta_{\boldsymbol{p}}|^2 - \frac{p^{\mu}_{-A}}{E_{\boldsymbol{p},-A'}}|\bar{\beta}_{\boldsymbol{p}}|^2\right\},\end{aligned} \tag{4.17}$$

from where the charge and vector expectation values follow as

$$\begin{aligned} j^0 &= \left\langle :\hat{Q}_{A'}: \right\rangle_{\boldsymbol{A}} = e\int \frac{d^3\boldsymbol{p}}{(2\pi)^3}\left\{|\beta_{\boldsymbol{p}}|^2 - |\bar{\beta}_{\boldsymbol{p}}|^2\right\}, \\ \boldsymbol{j} &= \left\langle :\hat{\mathbf{J}}^{i}_{A'}: \right\rangle_{\boldsymbol{A}} = e\int \frac{d^3\boldsymbol{p}}{(2\pi)^3}\left\{\frac{\boldsymbol{p}_{A}}{E_{\boldsymbol{p},A'}}|\beta_{\boldsymbol{p}}|^2 - \frac{\boldsymbol{p}_{-A}}{E_{\boldsymbol{p},-A'}}|\bar{\beta}_{\boldsymbol{p}}|^2\right\}. \end{aligned} \tag{4.18}$$

The natural next step in this computation of particle densities and their currents towards a more general setup where more complicated time evolutions are involved is the inclusion of a magnetic field and thus spatial inhomogeneity, in this case the evolution of the wave functions are given by, Once again comparing the wave function in both bases allows us identify the change in the creation and annihilation operators, i.e. their corresponding Bogoliubov transformation,

$$\begin{aligned} \hat{a}^{\sigma}_{\boldsymbol{p}} \longrightarrow \hat{a}'^{\sigma}_{\boldsymbol{p}} &= \int \frac{d^3\boldsymbol{q}}{(2\pi)^3}\left(\alpha_{\boldsymbol{p},\boldsymbol{q}}\hat{a}^{\sigma}_{\boldsymbol{q}} + \beta_{\boldsymbol{p},\boldsymbol{q}}\hat{b}^{\sigma\dagger}_{-\boldsymbol{q}}\right) \\ \hat{b}^{\sigma\dagger}_{\boldsymbol{p}} \longrightarrow \hat{b}'^{\sigma\dagger}_{\boldsymbol{p}} &= \int \frac{d^3\boldsymbol{q}}{(2\pi)^3}\left(\bar{\alpha}^{*}_{\boldsymbol{p},\boldsymbol{q}}\hat{b}^{\sigma\dagger}_{\boldsymbol{q}} - \bar{\beta}^{*}_{\boldsymbol{p},\boldsymbol{q}}\hat{a}^{\sigma}_{-\boldsymbol{q}}\right). \end{aligned} \tag{4.19}$$

As we saw in the previous section, only $\beta_{\boldsymbol{p},\boldsymbol{q}}$ is needed for the desired observables, and so what remains is to write down a concrete expression for the Bogoliubov coefficient. To compute $\beta_{\boldsymbol{p},\boldsymbol{q}}$, we evaluate the transition amplitude from a negative (positive) energy state to a positive (negative) energy state for particle (anti-particles) after the system has been evolved to a time t_f. For definiteness, let us define $f^{r}_{-\boldsymbol{p}}(x^0,\boldsymbol{x})$ and $\bar{f}^{r}_{-\boldsymbol{p}}(x^0,\boldsymbol{x})$ as the numerical solutions to the Dirac equation at a time x^0 for particle and

anti-particle respectively.

$$
\begin{aligned}
f^{+}_{-\boldsymbol{p}}(x^0 \sim -\infty, \boldsymbol{x}) &= \frac{v^{+}(-\boldsymbol{p}_A)}{\sqrt{2\,E_{\boldsymbol{p},A}}}\, e^{iE_{p,A}x^0 + i\boldsymbol{p}\cdot\boldsymbol{x}} \longrightarrow \\
&\int \frac{d^3\boldsymbol{q}}{(2\pi)^3}\left[\alpha^{*}_{-\boldsymbol{q},-\boldsymbol{p}}\frac{v^{+}(-\boldsymbol{q}_{A'})}{\sqrt{2\,E_{\boldsymbol{q},A'}}}\, e^{iE_{q,A'}x^0 + i\boldsymbol{q}\cdot\boldsymbol{x}} + \beta_{\boldsymbol{q},\boldsymbol{p}}\frac{u^{+}(\boldsymbol{q}_{A'})}{\sqrt{2\,E_{\boldsymbol{q},A'}}}\, e^{-iE_{q,A'}x^0 + i\boldsymbol{q}\cdot\boldsymbol{x}}\right]. \\
\bar{f}^{+}_{-\boldsymbol{p}}(x^0 \sim -\infty, \boldsymbol{x}) &= \frac{u^{+}(-\boldsymbol{p}_{-A})}{\sqrt{2\,E_{\boldsymbol{p},-A}}}\, e^{iE_{p,-A}x^0 - i\boldsymbol{p}\cdot\boldsymbol{x}} \longrightarrow \\
&\int \frac{d^3\boldsymbol{q}}{(2\pi)^3}\left[\bar{\alpha}_{-\boldsymbol{q},-\boldsymbol{p}}\frac{u^{+}(-\boldsymbol{q}_{-A'})}{\sqrt{2\,E_{\boldsymbol{q},-A'}}}\, e^{-iE_{q,-A'}x^0 - i\boldsymbol{q}\cdot\boldsymbol{x}} - \bar{\beta}^{*}_{\boldsymbol{q},\boldsymbol{p}}\frac{v^{+}(\boldsymbol{q}_{-A'})}{\sqrt{2\,E_{\boldsymbol{q},-A'}}}\, e^{iE_{q,-A'}x^0 - i\boldsymbol{q}\cdot\boldsymbol{x}}\right].
\end{aligned}
\tag{4.20}
$$

where the arrows denote the change that a shift on the gauge field has on the wave functions. From here the explicit expression for the $\beta_{\boldsymbol{p},\boldsymbol{q}}$ Bogoliubov coefficient is trivial; using the proper orthogonality and normalization of the spinors above. The coefficients read,

$$
\beta_{\boldsymbol{q},\boldsymbol{p}} = \int d^3x \frac{u^{+\dagger}(\boldsymbol{q}_{A'})}{\sqrt{2\,E_{\boldsymbol{q},A'}}}\, e^{iE_{q,A'}x^0 - i\boldsymbol{q}\cdot\boldsymbol{x}} f^{+}_{-\boldsymbol{p}}(x^0, \boldsymbol{x}) \tag{4.21}
$$

similarly, the corresponding expression for antiparticles gives,

$$
\bar{\beta}_{\boldsymbol{q},\boldsymbol{p}} = \int d^3x \frac{v^{+\dagger}(\boldsymbol{q}_{-A'})}{\sqrt{2\,E_{\boldsymbol{q},-A'}}}\, e^{-iE_{q,-A'}x^0 + i\boldsymbol{q}\cdot\boldsymbol{x}} \bar{f}^{+}_{-\boldsymbol{p}}(x^0, \boldsymbol{x}) \tag{4.22}
$$

4.2 Test Simulations in a Finite Box

The essential ingredient to compute the above defined currents and distribution is the time-evolved fermionic wave function under a certain background gauge field. We are therefore, in need to solve Dirac's equation on top of a discrete lattice. The Dirac equation for + helicity fermion field under external electromagnetic reads,

$$
\Big[\Big(i\gamma^0\partial_0 - e\gamma^0 A_0\Big) + \Big(i\gamma^i\partial_i - e\gamma^i A_i\Big) - m\Big]\psi_{+}(x) = 0\,. \tag{4.23}
$$

The interaction is contained in the covariant derivative, to this end we are in the need of link variables,

$$U_\mu(x) = e^{-ia^\mu eA_\mu(x)} \,, \tag{4.24}$$

with these we can approximate the derivatives

$$\begin{aligned} dt(\partial_0 - ieA_0)\psi_+(x) &\approx U_0(x)\psi_+(x+\hat{0}) - \psi_+(x) \\ a^i(\partial_i - ieA_i)\psi_+(x) &\approx \frac{1}{2}\left[U_i(x)\psi_+(x+\hat{i}) - U_i^\dagger(x-\hat{i})\psi_+(x-\hat{i})\right] \,, \end{aligned} \tag{4.25}$$

allowing us to rewrite the discretized version of the Dirac equation. The updated field is,

$$\psi_+(x+\hat{0}) \approx U_0^\dagger(x)(1 - im\,dt\gamma^0)\psi_+(x) + \frac{dt}{2}U_0^\dagger(x)\gamma^0\gamma^i\left[U_i(x)\psi_+(x+\hat{i}) - U_i^\dagger(x-\hat{i})\psi_+(x-\hat{i})\right] \,. \tag{4.26}$$

With this algorithm, we numerically solve the Dirac equation under an external electromagnetic field allowing us to compute the desired observables.

We will first check the consistency of our formulation with Schwinger pair production by applying an homogeneous electric field in the z direction, to this end we consider a time-dependent $A_3 = -E_0 t$. The duration of the electric step to be applied is $t_E = \sqrt{10/E_0}$. Even when no external magnetic field is applied, the sole presence of an external electric field can trigger particle production via the Schwinger mechanism. In this case $\mathcal{CP}$-symmetry is conserved and although pairs are produced no net current can be observed. Particle and antiparticle distributions are shown for a pulsed electric field at zero mass in Fig. 4.1. Both distributions correspond to an step in the p_z axis from 0 to $t_E \cdot E_0$. The particle/anti-particle pair production rate is given by,

$$\Gamma = e^2\frac{E_0 B_\parallel}{4\pi^2}\coth\left(\frac{B_\parallel}{E_0}\pi\right)e^{-m^2\pi/|eE_0|} \,, \tag{4.27}$$

$$\Gamma \xrightarrow{B_\parallel \to 0} \Gamma_{\text{Schwinger}} e^{-m^2\pi/|eE_0|} \,, \qquad \Gamma_{\text{Schwinger}} = e^2\frac{E_0^2}{4\pi^3} \,, \tag{4.28}$$

corresponding to the Schwinger pair production rate [62, 63]. The net currents will be presented

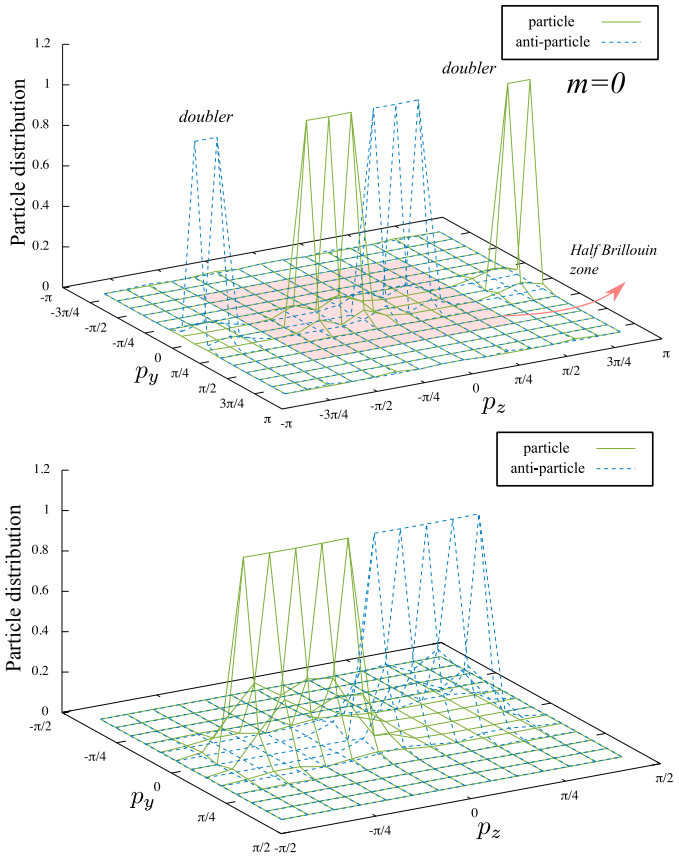

FIG. 4.1: Particle and anti-particle momentum distributions in the Schwinger mechanism. Lattice size was set to 24^3 and the applied electric field to 0.1 for massless fermions. (*Above*) Full Brillouin zone with unsupressed doublers. (*Below*) Half Brillouin zone cut-off corresponding to the shaded region in the figure above

later on are normalized in units of $n_0 = \Gamma_{\text{Schwinger}} \cdot t_E$. The inclusion of finite fermionic mass results into a suppression of the particle antiparticle distributions. When only the electric field is present this mass damping affects particle and antiparticle distributions alike as it can be appreciated in Fig. 4.2. In order to make an more explicit comparison with (4.28), let us compute the pair production rate defined $\Gamma_{\text{rate}} = \frac{n_{\text{pair}}}{t_E}$, where we have defined pair number density as,

$$n_{\text{pair}} = \int \frac{d^3\boldsymbol{p}}{(2\pi)^3} \left\{ |\beta_{\boldsymbol{p}}|^2 + |\bar{\beta}_{\boldsymbol{p}}|^2 \right\}. \tag{4.29}$$

In Fig. 4.3 the numerical pair production rate is shown to agree with the analytical expectation (4.28) revealing an exponential damping from the fermion's mass. The computation of observables once

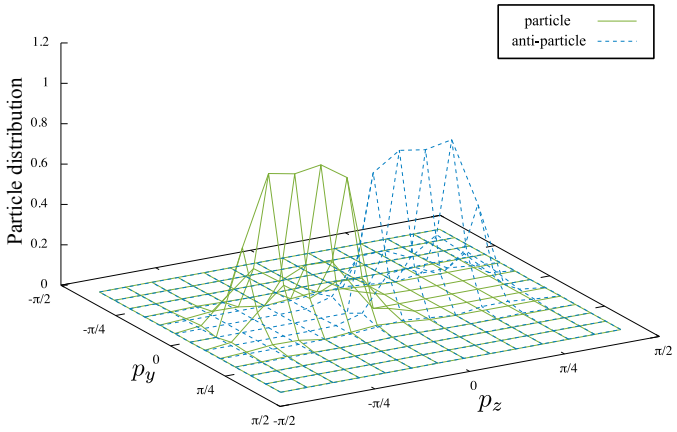

FIG. 4.2: Particle and anti-particle momentum distributions in the Schwinger mechanism. Lattice size was set to 24^3 and the applied electric field to 0.1. On the right massless particles and on the left a system with $m = E_0/2$ was considered.

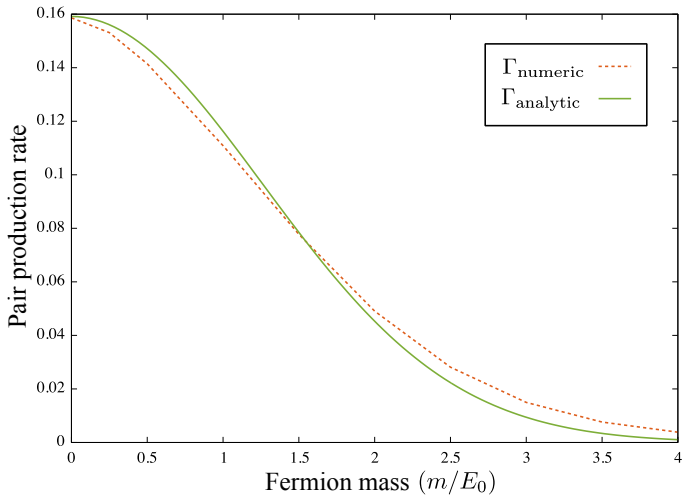

FIG. 4.3: Pair production rate (4.29) revealing exponential damping by the mass in agreement with (4.28). The considered lattice size is 17^3 and electric field fixed at $E_0 = 0.1$.

a finite magnetic field is turned on is much numerically expensive than our previous case dealing only with E. Now non-diagonal components of the $\beta_{\boldsymbol{p},\boldsymbol{q}}$ must be calculated for every lattice point in momentum space. The homogeneous magnetic field included on top of this picture is considered to have the same time pulse profile as that of the electric field. Such magnetic field is implemented by introducing the vector potential $A^x = (B_\perp z - B_\parallel y)\epsilon(t)$ and $A^y = 0$, where $\epsilon(t)$ defines the time profile as $\epsilon(t) = 1$ when $-t_E/2 \leq t \leq t_E/2$ and zero otherwise as prescribed in Ref. [64].

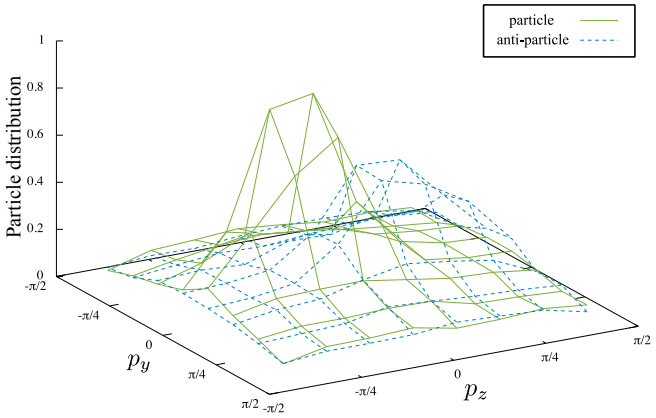

FIG. 4.4: Particle and anti-particle distributions under a finite magnetic field parallel to the background electric field, $B_{\parallel} = E_0/2$. The lattice considered in this figure is 17^3 and the applied electric field $E_0 = 0.1$.

In particular a configuration in which the magnetic field and electric fields are orthogonal, particle and antiparticle distributions are smeared and spread across momentum space as the intensity increases. This spreading is symmetrical and as it can be read from Eq. (4.17), the four-current expression is zero for all components in the orthogonal configuration. Also, as observed in the massive Schwinger case mass damps but maintains the symmetry altogether. On the other hand, any departure from the orthogonal EB-background results the breaking of the particle-antiparticle symmetry. Indeed, the inclusion of a finite magnetic field can break the $\mathcal{CP}$-invariance of the system when $E \cdot B$ is finite, i.e. the magnetic field has a non-vanishing component parallel to the background electric field. The breaking of the symmetry is manifested through an enhancement of the particle momentum distribution over its antiparticle counterpart Fig. 4.4. This imbalance results thus, in an increment of charge carriers of the systems, a flow of helicity in the system as shown in figure 4.5. For instance, in a system of massless fermions where chirality is well-defined quantum number, particle number conservation is broken through the Adler-Bell-Jackiw quantum anomaly which is turned on in a $\mathcal{CP}$ breaking background, such as the one considered. We can in this sense observe a dynamically induced μ_5 with this background. The anomaly equation becomes non-trivial. Such imbalance from the particle and antiparticle is often parametrized through the inclusion of an axial chemical potential μ_5, which we have set in dynamical way. However as the expression which summarizes CME shows, finite μ_5 alone

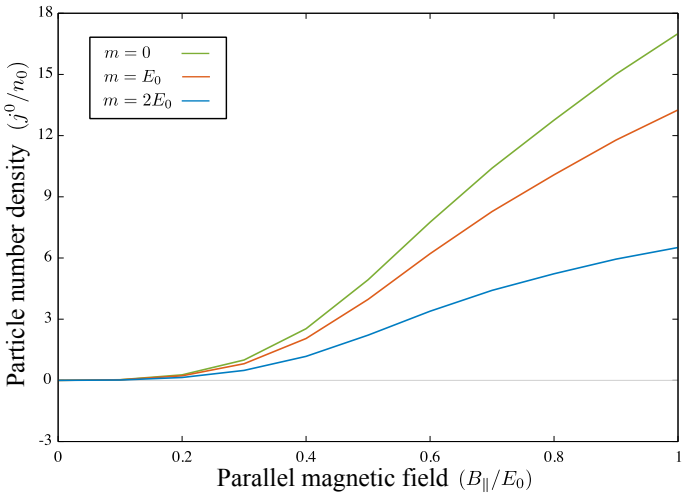

FIG. 4.5: Induced axial charge density by finite $\boldsymbol{E} \cdot \boldsymbol{B}$ for fixed intensity of the electric field set at $E_0 = 0.1$ and increasing $B_\parallel$. Suppression by finite fermion mass is shown. The considered lattice size is 17^3.

is not enough trigger the current, A magnetic field on top is needed. This fact can be observed in the case in which E and B are exactly parallel to each other: although the number of charge carriers available increase with the magnitude of $B_\parallel$ the current along the y-direction, corresponding to j_{CME} remains zero. Therefore becomes non-trivial as the angle between the E and B, $\theta \in [0, \pi/2]$ achieving a maximum when $\pi/2$. Fig. 4.6 displays the time evolution of the produced currents for various masses consistent with the results [64] when $m = 0$.

The sharp localized distributions spread across momentum space more and more as the magnitude of magnetic field grows. And so, it is not unlikely that contribution coming from spurious states would eventually interfere with the physical distribution on the inner portion of the BZ. Thus it becomes important to quantify such effect for the reliability of simulation results with UV and IR cut-off approach. To this end we will perform simulations considering Wilson fermions on top of the full BZ instead of the naive fermion approach taken until now.

In solving the discretized Dirac equation one encounters, as an inevitable consequence of approximating the derivatives as finite differences operators, spurious states in the high momentum region and low energy. Such states cannot be gotten rid off by improving precision on the lattice model and remain as we approach the continuum limit. Furthermore, a no-go theorem for this phenomenon,

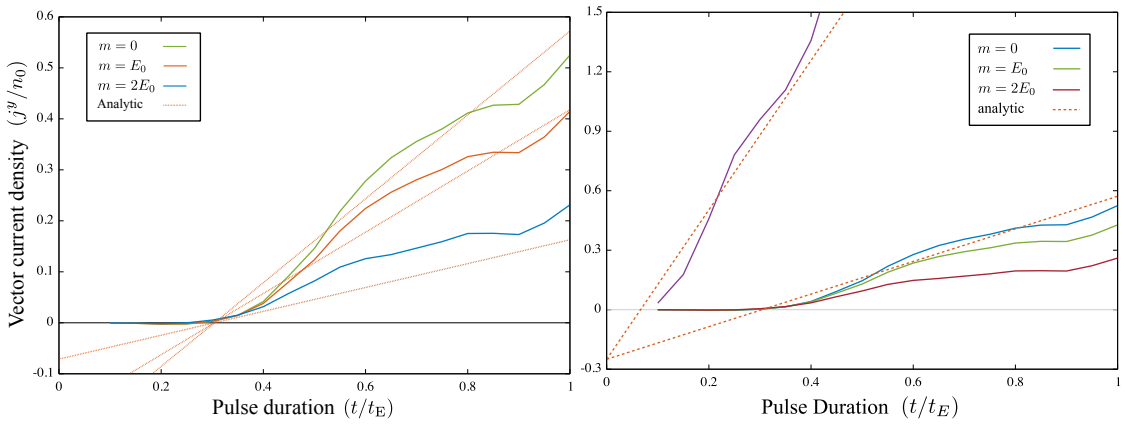

FIG. 4.6: Real time evolution of y-component of vector current j^y/n_0 corresponding to the chiral magnetic effect for $B_\parallel = B_\perp = E_0/2$ and different fermion masses. The purple line corresponds to particle density j^0/n_0 at $m = 0$ and is left as reference. The analytical values for both, anomaly equation and the chiral magnetic current at $m = 0$ are shown by the dotted orange line with a common offset of -0.25. Lattice size is taken as $N_i = 8$.

termed as the *fermion doubling problem*, was formulated by Nielsen and Ninomiya [65]. Several approaches around the fermion doubling problem have been developed by the lattice community. One method to eliminate these unphysical contributions was proposed by K. G. Wilson in [66] and consists in the addition of an extra term to the action, the Dirac-Wilson action reads,

$$S = S_f - \frac{r}{2} \sum_{h=\pm} \int d^4x \, \bar{\psi}_h D_i D^i \psi_h \, , \tag{4.30}$$

where D^i corresponds to the spatial covariant derivative. The inclusion of this term is allowed as it preserves lattice gauge symmetry and also enables us to get rid of the unwanted spurious states; This extra term contributes as $\boldsymbol{p}^2$ to the dispersion relation lifting the minimum that spawns at the edge of the BZ and thus raising the energy for the unphysical doublers. This is, the mass term becomes develops a momentum dependence,

$$M_W(p^i) = m + \frac{2r}{a} \sum_i (1 - \cos(p^i a)) \, . \tag{4.31}$$

This modification to the dispersion relation is of course expected to vanish at the continuum when

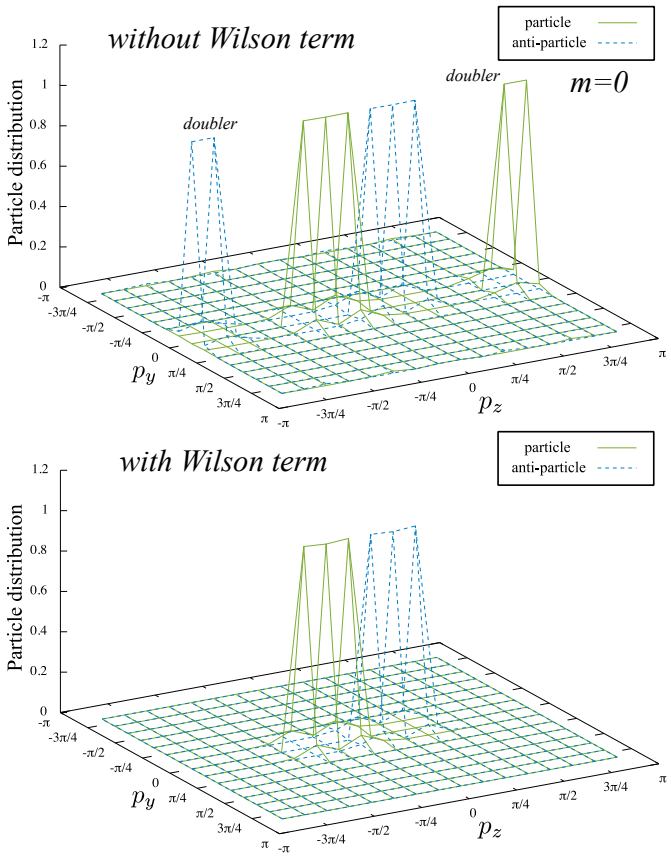

FIG. 4.7: Fermion doublers in the Schwinger mechanism. (*Above*) particle and antiparticle distribution are displayed over the full BZ using naive fermions. (*Below*), The same setup implemented for Wilson fermion with $r = 0.2$ coupling. Lattice size was set to 17^3 and the applied electric field to 0.1.

$a \to 0$ implies the generation of a momentum dependent mass. The spinors in the initial conditions of our Cauchy problem are thus accordingly modified by the replacement ($m \to M_W(p^i)$). From this expression one can appreciate how Wilson fermions become massive at the edge of the BZ, rising the energy of spurious states and at same time how it also affects physical states although in a much diminished way as fermions get lighter and lighter as we get away from the edges. In fact, because of this, the chiral limit $m = 0$ cannot be attained as physical states are perturbed by the momentum dependent contribution and thus chiral symmetry is inevitably broken. Therefore, the implementation of Wilson fermions inevitably breaks chiral symmetry. A temporal component of the Wilson term would turn the Dirac equation to second order in time, however $dt \ll a_i$ and so we do not need to deal with doublers in the temporal direction. The corresponding equation of motion leads us to the field

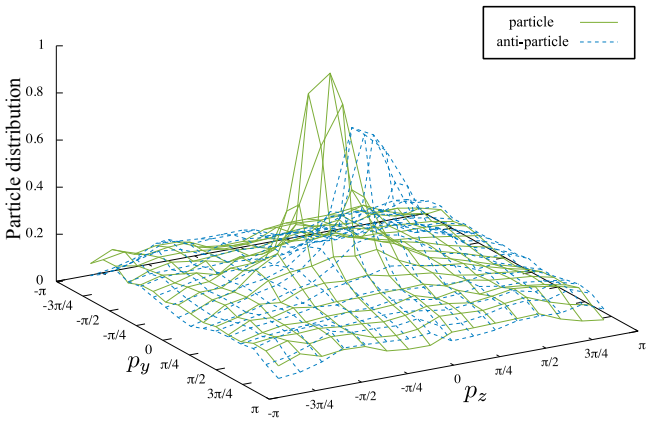

FIG. 4.8: Particle and anti-particle momentum distributions at $B_{\parallel} = B_{\perp} = E_0/2$ for Wilson fermions with $r = 0.5$. Lattice size is taken as $N_i = 8$ and electric field $E_0 = 0.1$.

update algorithm,

$$\begin{aligned}\psi_+(x+\hat{0}) = U_0^\dagger(x)[1 - idt(m+3r)\gamma^0]\psi_+(x) \\ + \frac{dt}{2}\gamma^0 U_0^\dagger(x)\left[(\gamma^i + ir)U_i(x)\psi_+(x+\hat{i}) - (\gamma^i - ir)U_i(x-\hat{i})\psi_+(x-\hat{i})\right]\end{aligned} \tag{4.32}$$

In a sense, the Wilson-term contribution acts as an inhomogeneous mass term and so a light damping on the currents is to be expected. In Fig. 4.9 we compare the anomalous current production from this two approaches in order to test the reliability of the approximation of introducing a UV and IR cut-off on the BZ.

4.3 Formulation in the Expanding Geometry

To describe the time-evolution of observables in the forward light-cone, the Bjorken chart suits us best. This is $\mathbb{R}^2 \times H^2$ equipped with the following Lorenzian metric,

$$ds^2_{\text{Bjorken}} = d\tau^2 - d\boldsymbol{x}_\perp^2 - \tau^2 d\eta^2, \tag{4.33}$$

it trades time t and the longitudinal coordinate z for proper time τ and rapidity η, which are related by $t = \tau\cosh\eta$, $z = \tau\sinh\eta$ depicted in Fig. 4.10. The Bjorken chart represents an expanding

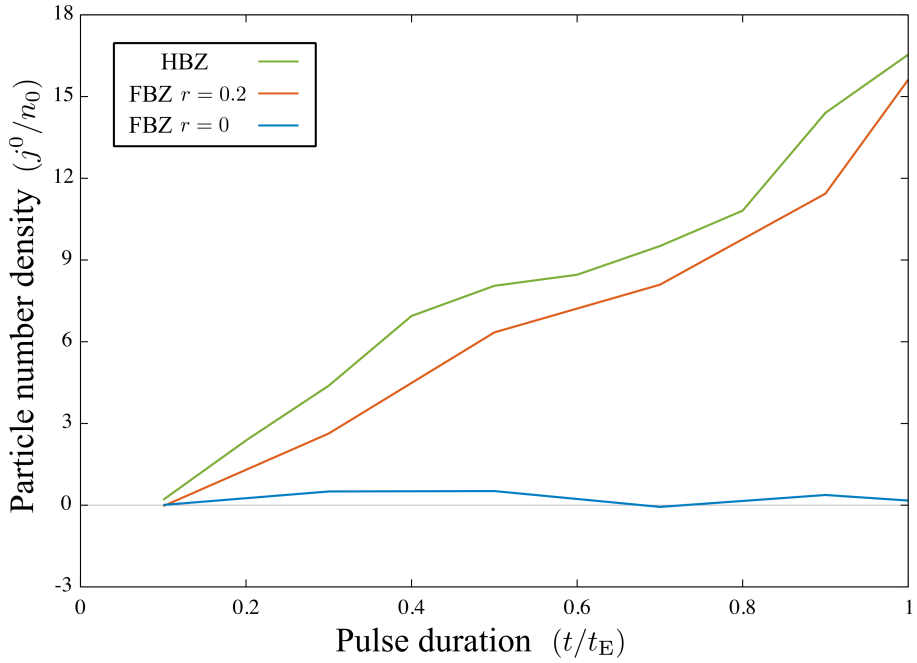

FIG. 4.9: Comparison between the two approaches. The upper two curves correspond to the net particle number density produced as a result of the anomaly; The green curve is obtained by considering naive fermions on a BZ with lower and upper cut-offs and the orange curve to net particle number considering Wilson fermions with $r = 0.2$ coupling over the full BZ. The blue curve corresponds to the case of naive fermions over the FBZ, which is consistent with the Nielsen-Ninomiya theorem. Lattice size is $N_i = 8$ and parallel E and B equal to E_0 are considered.

1 + 1-dimensional geometry in the longitudinal direction. From the metric it seems as if there is a singularity at $\tau = 0$. This is nothing but a coordinate artifact since the metric is flat and it can always be brought back to the regular Minkowski metric by a suitable coordinate transformation. However, as in the case of other hyperbolic space-times (e.g. Rindler), it is incomplete. This implies that two causal patches will be needed to express the initial condition. The Dirac equation is linear and this allows us to look for a solution written as the sum of left- and right- movers, like one usually would in other incomplete manifolds.

Given that the partial waves live in disconnected regions of the light-cone, they are completely independent. This provides us with the freedom to choose a different gauge for the background field

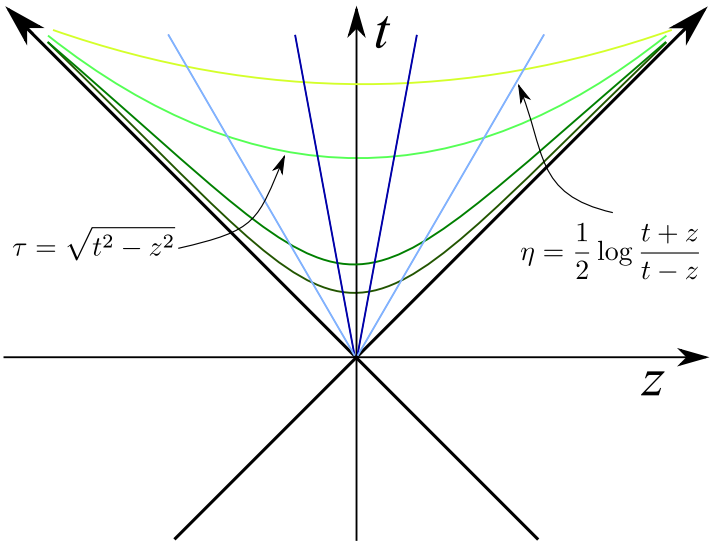

FIG. 4.10: Forward light cone in the Bjorken coordinate chart. Hyperbolic green lines denote constant proper time τ and the straight blue lines denote constant space-time rapidity η. Magnitude in both cases increases from the darker to lighter shades.

on each patch of the manifold, simplifying the problem. And finally, bring them to a common gauge at τ_0 by a gauge rotation; The light-cone gauge $A^- = 0$ can be used for the right moving partial wave and $A^+ = 0$ for the left mover. Once an explicit expression for the spinors is obtained, the solution is rotated to the Fock-Schwinger gauge at the forward light-cone. Before going on with this program, it should be emphasized that the singularity at $\tau = 0$ is physical, though it does come from geometry but from the color sources themselves.

4.4 Initial Conditions on the Light Cone

Owing to the symmetry between left and right movers it is enough to solve for one the partial waves (say the right mover). The starting point is a free negative energy spinor at $x^\pm < 0$. This spinor interacts with the gauge field produced by the nucleus moving in the $-z$. Evolving into the $x^+ > 0$, $x^- < 0$ region, we must deal with the pure background gauge field $A_2^i = \frac{i}{g} U_2^\dagger \partial^i U_2$. The covariant derivative in this region can thus be written as $D^\mu = U_2^\dagger \partial^\mu U_2$, this allows us to define a spinor $U_2\psi$

obeying the free Dirac Equation. For this initial value problem, ψ should be evolved from the $x^- = 0^+$ surface, this admits a formal solution written in terms of the retarded quark propagator,

$$\psi = i \int_{y=0^+} dy^- d^2\boldsymbol{y}_\perp S_{\rm R}^0(x,y)\psi^{(-)} \tag{4.34}$$

denoting the propagation of the spinor field from the $y = 0^+$ surface. The y^- integration produces a delta, the transverse $\boldsymbol{y}_\perp$ is absorbed in the definition of the Fourier conjugate of the Wilson line defined below and so the pole integration from the retarded propagator can be computed in a straightforward way yielding,

$$\begin{aligned}\psi^{(-)}_{\boldsymbol{k}sa}(x) = U_2^\dagger(\boldsymbol{x}_\perp) \int \frac{d^2\boldsymbol{p}_\perp}{(2\pi)^2} e^{i\boldsymbol{p}_\perp\cdot\boldsymbol{x}_\perp} e^{i(k^+x^- + \frac{M_p^2}{2k^+}x^+)} \widetilde{U}_2(\boldsymbol{p}_\perp + \boldsymbol{k}_\perp) \\ \times \left(1 - \gamma^+ \frac{p^i\gamma^i + m}{2k^+}\right) \mathscr{P}^+ v_s(\boldsymbol{k})\end{aligned} \tag{4.35}$$

In this expression $M_{\boldsymbol{p}}$ has been defined as the transverse mass, and the projector $\mathscr{P}^+$ has been introduced. The Fourier transform for the Wilson line conjugated to the transverse variable $x_\perp$ has been defined as $\widetilde{U}$. For the final expression for this partial wave, one must consider the spinor evolution across the $x^+ > 0$, $x^- = 0^+$ stripe of the light cone. This implies a contribution from the nuclei moving along the x^- as well. Given that the associated gauge field involved has no A_1^- component, we can decouple the Dirac equation into two, one for each projection $\mathscr{P}^\pm = \gamma^\mp\gamma^\pm/2$ of the spinor.

$$\begin{aligned} i\partial^- \mathscr{P}^+ \psi^{(-)}_{\boldsymbol{k}sa} &= \frac{m - i\gamma^i D^i}{2} \gamma^- \mathscr{P}^- \psi^{(-)}_{\boldsymbol{k}sa} \\ i(\partial^+ - igA_1^+)\mathscr{P}^- \psi^{(-)}_{\boldsymbol{k}sa} &= \frac{\gamma^+(i\gamma^i D^i + m)}{2} \psi^{(-)}_{\boldsymbol{k}sa} \end{aligned} \tag{4.36}$$

One of which is independent of A_1. These pair of equations can be trivially decoupled resulting into a second-order differential equation. Here, the derivative ∂^+ and A_1^+ are large, inversely proportional to the thickness of the stripe that supports the A_1^+ field. On the other hand $-D_\perp^2 + m^2$ is associated with the transverse diffusion, however in the limit in which the thickness of the

shock wave goes to zero, this term can be safely neglected. This all simply implies that the covariant derivative $i(\partial^+ - igA_1^+)\mathscr{P}^-\psi^{(-)}_{\boldsymbol{k}sa} = 0$ and so the solution of this projection is trivially given by $U_1(x^-, \boldsymbol{x}_\perp)\mathscr{P}^-\psi^{(-)}_{\boldsymbol{k}sa}(0, x^+, \boldsymbol{x}_\perp)$. The remaining projection is given by the line in Eq. (4.36).

As previously mentioned, before adding the two partial waves in the forward light-cone region, they must be brought down to a common gauge. The chosen gauge for this region is the Fock-Schwinger gauge, we achive by a

$$\begin{aligned}
\mathscr{P}^-\psi^{(-)}_{\boldsymbol{k}sa\mathrm{FS}}(x) &= U_2^\dagger(\boldsymbol{x}_\perp)\int\frac{d^2\boldsymbol{p}_\perp}{(2\pi)^2}e^{i\boldsymbol{p}_\perp\cdot\boldsymbol{x}_\perp}e^{i\frac{M_p^2}{2k^+}x^+} \\
&\qquad\times\widetilde{U}_2(\boldsymbol{p}_\perp+\boldsymbol{k}_\perp)\frac{p^i\gamma^i-m}{2k^+}\gamma^+v_s(\boldsymbol{k}) \\
\mathscr{P}^+\psi^{(-)}_{\boldsymbol{k}sa\mathrm{FS}}(x) &= \Big(i\gamma^iD^i_{\mathrm{FS}}-m\Big)U_2^\dagger(\boldsymbol{x}_\perp)\int\frac{d^2\boldsymbol{p}_\perp}{(2\pi)^2}e^{i\boldsymbol{p}_\perp\cdot\boldsymbol{x}_\perp}e^{i\frac{M_p^2}{2k^+}x^+} \\
&\qquad\times\widetilde{U}_2(\boldsymbol{p}_\perp+\boldsymbol{k}_\perp)\frac{p^i\gamma^i-m}{2k^+}\gamma^+v_s(\boldsymbol{k})
\end{aligned} \tag{4.37}$$

Taking the $\mathscr{P}^-$-projection of this expression and replacing $\mathscr{P}^-\psi$ at Eq. (4.36).

$$\begin{aligned}
\mathscr{P}^-\psi^{(-)}_{\boldsymbol{k}sa\mathrm{FS}}(x) &= \sqrt{\tau}U_2^\dagger(\boldsymbol{x}_\perp)\int\frac{d^2\boldsymbol{p}_\perp}{(2\pi)^2}\times e^{i\boldsymbol{p}_\perp\cdot\boldsymbol{x}_\perp} \\
&\qquad\int_{-\infty}^{\infty}dy'\exp\left[i\frac{M_p\tau}{2}e^{-(y'-\eta)}\right]\widetilde{U}_2(\boldsymbol{p}_\perp+\boldsymbol{k}_\perp) \\
&\qquad\times e^{iy'}\frac{p^i\gamma^i-m}{\sqrt{2}M_p}e^{-y'}\gamma^+[e^{\frac{y+\eta}{2}}\mathscr{P}^+ + e^{-\frac{y'+\eta}{2}}\mathscr{P}^-]v_s(\boldsymbol{k}_\perp,0) \\
&= \sqrt{\tau}\int\frac{d^2\boldsymbol{p}_\perp}{(2\pi)^2}e^{i\boldsymbol{p}_\perp\cdot\boldsymbol{x}_\perp}U_2^\dagger(\boldsymbol{x}_\perp)\widetilde{U}_2(\boldsymbol{p}_\perp+\boldsymbol{k}_\perp)\int_{-\infty}^{\infty}dy'\exp\left[i\frac{M_p\tau}{2}e^{-(y-\eta)}\right] \\
&\qquad\times e^{iy'}\frac{p^i\gamma^i-m}{\sqrt{2}M_p}e^{-\frac{1}{2}(y'-\eta)}\gamma^+v_s(\boldsymbol{k}_\perp,0)
\end{aligned} \tag{4.38}$$

As we are now in the forward light-cone the Bjorken coordinate chart $(\tau, \boldsymbol{x}_\perp, \eta)$ suits us best. They are related to light-coordinates by $\boldsymbol{x}^\pm = \frac{\tau}{\sqrt{2}}e^{\pm\eta}$ and $p^\pm$ traded for momentum rapidity in a similar way, $p^\pm = \frac{y}{\sqrt{2}}e^{\pm\eta}$. In the first line we have explicitly spelled out the rapidity dependance of the spinor $e^{\frac{y}{2}\gamma^0\gamma^3}v_s(\boldsymbol{k}_\perp,0)$ from where the $e^{\frac{y+\eta}{2}\gamma^0\gamma^3}$ term appears. This term is rewritten in terms of projectors

$$
\begin{aligned}
e^{\frac{y+\eta}{2}\gamma^0\gamma^3} &= \cosh(\frac{y+\eta}{2}) + \gamma^0\gamma^3 \sinh(\frac{y+\eta}{2}) \\
&= (\mathscr{P}^+ + \mathscr{P}^-)\cosh(\frac{y+\eta}{2}) + (\mathscr{P}^+ - \mathscr{P}^-)\sinh(\frac{y+\eta}{2}) \\
&= e^{\frac{y+\eta}{2}}\mathscr{P}^+ + e^{-\frac{y+\eta}{2}}\mathscr{P}^-
\end{aligned}
\tag{4.39}
$$

In the second line of (4.38), the momentum rapidity can be integrated out, from where

$$
\begin{aligned}
\psi^{(-)}_{\boldsymbol{k}_\perp \nu s a\,\mathrm{FS}}(x) \underset{\tau\to 0^+}{=} & -\frac{e^{i\frac{\pi}{4}}}{\sqrt{M_k}} e^{i\nu\eta} \int \frac{d^2\boldsymbol{p}_\perp}{(2\pi)^2} \frac{e^{+i\boldsymbol{p}_\perp\cdot\boldsymbol{x}_\perp}}{M_p} \\
&\times \Bigg\{ e^{\frac{\pi\nu}{2}} \left(\frac{M_p^2\tau}{2M_k}\right)^{i\nu} \Gamma\left(\frac{1}{2} - i\nu\right) U_2^\dagger(\boldsymbol{x}_\perp)\widetilde{U}_2(\boldsymbol{p}_\perp + \boldsymbol{k}_\perp)\gamma^+ \\
&\quad + e^{-\frac{\nu\pi}{2}} \left(\frac{M_p^2\tau}{2M_k}\right)^{-i\nu} \Gamma\left(\frac{1}{2} + i\nu\right) U_1^\dagger(\boldsymbol{x}_\perp)\widetilde{U}_1(\boldsymbol{p}_\perp + \boldsymbol{k}_\perp)\gamma^- \Bigg\} (p^i\gamma^i + m) v_s(\boldsymbol{k}_\perp, y = 0)
\end{aligned}
\tag{4.40}
$$

the initial condition for the quark fields is obtained.

Chapter 5

Quark Spectrum in the Forward Light-Cone

To further understand what is actually observed and better interpret the measured charge asymmetry at heavy-ion collisions, one must characterize the evolution of axial charge taking into account the complex space-time evolution of the pre-equilibrium regime of the collision. Besides the remarkably short lifetime of magnetic fields expected at the collision, quark degrees of freedom, the necessary ingredient to discuss chirality are produced at the very early stages as well [60, 61]. Where it has been shown that QCD matter formed in the collision experiments is from the very beginning in local kinetic equilibrium and quark-antiquark pairs close to the chemically equilibration with the gluons. In this approach, the basis of mode functions used was expressed only in τ, y and z making the longitudinal boost invariance of the system highly non-obvious and the sum of modes in the expansion was only restricted to small subset. However, as discussed in the previous chapter, these short-comings have been overcomed and the initial condition has been recently worked out, providing the tools to correctly describe the quark fields in the forward light-cone [19]. The initial conditions for the quark field have been specified and now we are in interested in the quark spectrum. To that end, we first focus on the proper time evolution of the quark fields in the forward light-cone. Using the initial condition (4.40) for the quark wave functions and proceed to compute the resulting currents determined by the proper time evolved wave functions under a non-abelian constant background motivated by the CGC initial conditions. Finally, the generation of axial charge density is simulated in the expanding geometry and the effects arising from finite quark mass are discussed.

In this part, we focus on the analytical solution of the free Dirac equation in Bjorken coordinates $\{\tau, x_\perp, \eta\}$ where $t = \tau\cosh\eta$ and $z = \tau\sinh\eta$, with the purpose to establish basic definitions, conventions and notation used throughout this chapter. The starting point is of course,

$$\Big(i\gamma^\mu\partial_\mu - m\Big)\psi(x) = 0, \tag{5.1}$$

we can rewrite the derivatives,

$$\begin{pmatrix}\partial_0\\ \partial_3\end{pmatrix} = \begin{pmatrix}\cosh\eta & -\frac{1}{\tau}\sinh\eta\\ -\sinh\eta & \frac{1}{\tau}\cosh\eta\end{pmatrix}\begin{pmatrix}\partial_\tau\\ \partial_\eta\end{pmatrix}. \tag{5.2}$$

Changing the coordinates without taking into account the change of the spinor, leads us to the following form of the Dirac equation

$$\left[ie^{-\eta\gamma^0\gamma^3}\left(\gamma^0\partial_\tau + \frac{1}{\tau}\gamma^3\partial_\eta\right) + i\gamma^\perp\cdot\partial_\perp - m\right]\psi = 0. \tag{5.3}$$

Alternatively we can aim at solving,

$$\Big(i\gamma^a e^\mu_a[\partial_\mu + \Gamma_\mu] - m\Big)\psi(x) = 0, \tag{5.4}$$

using the usual choice for the vielbeins, the spin connection for this coordinate chart reads,

$$\Gamma_\mu = \frac{1}{8}[\gamma^a\gamma^b]e_{\nu a}(\partial_\mu e^\nu_b + \Gamma^\nu_{\mu\sigma}e^\sigma_b) \to \Gamma_\eta = \frac{1}{2}\gamma^0\gamma^3, \tag{5.5}$$

where only the longitudinal component provides a non-trivial contribution. This gives us the equation,

$$\left[i\left(\gamma^0\partial_\tau + \frac{1}{\tau}\gamma^3\partial_\eta + \frac{1}{2\tau}\gamma^0 + \gamma^\perp\cdot\partial_\perp\right) - m\right]\psi = 0. \tag{5.6}$$

At any case these two forms are related by the $\psi = e^{-\eta\gamma^0\gamma^3}\psi_{\text{flat}}$ where the later corresponds to the solution of equation (5.3). On the following section, we shall focus on solving (5.3).

5.1 The Free Solution

Squaring the Dirac operator as usual in these coordinates can be easily shown to reproduce the Bessel equation. However, to see each of its components, it is useful to consider instead,

$$\hat{\psi}_{\boldsymbol{k}_\perp ysa} = \sqrt{\tau} e^{-\frac{\eta}{2}\gamma^0\gamma^3} \psi_{\boldsymbol{k}_\perp ysa}. \tag{5.7}$$

The overall factor $\sqrt{\tau}$ has been introduce for convience as in this way the equation to solve is reduced to a much simpler form,

$$\left[i\left(\gamma^0 \partial_\tau + \frac{1}{\tau}\gamma^3 \partial_\eta + \gamma^\perp \cdot \partial_\perp \right) - m \right] \hat{\psi} = 0. \tag{5.8}$$

It is also useful to change from a basis of definite momentum rapidity y to one of fixed Fourier conjugate ν to the spacetime rapidity η.

$$\hat{\psi}^{(-)}_{\boldsymbol{k}_\perp \nu sa}(x) = \sqrt{\tau} e^{-\frac{\eta}{2}\gamma^0\gamma^3} \int_{-\infty}^{\infty} dy\, e^{i\nu y}\, \psi^{(-)}_{\boldsymbol{k}_\perp ysa}. \tag{5.9}$$

The advantage of such basis is obvious, ν is a conserved quantum number and Dirac equation obeyed by the spinors is effectively 2 dimensional. Its solution reads,

$$\begin{aligned} \hat{\psi}^{(-)}_{\boldsymbol{k}_\perp \nu sa}(x) = -i\pi \sqrt{\tau} e^{\frac{\pi\nu}{2}} e^{i\nu\eta - i\boldsymbol{k}_\perp \cdot \boldsymbol{x}_\perp} \Big\{ & e^{-i\frac{\pi}{4}} H^{(1)}_{-\frac{1}{2}-i\nu}(M_{\boldsymbol{k}}\tau)\, \mathscr{P}^+ \\ & + e^{i\frac{\pi}{4}} H^{(1)}_{\frac{1}{2}-i\nu}(M_{\boldsymbol{k}}\tau)\, \mathscr{P}^- \Big\} v_s(\boldsymbol{k}_\perp, y=0), \end{aligned} \tag{5.10}$$

where $\mathscr{P}^\pm$ correspond to the projector operators $\frac{1}{2}(1 \pm \gamma^0\gamma^3)$ and the negative energy spinor which can be computed from,

$$v_s(k) = \begin{pmatrix} \sqrt{(k\cdot\sigma)}\,\xi^s \\ -\sqrt{(k\cdot\bar{\sigma})}\,\xi^s \end{pmatrix} = \frac{1}{\sqrt{2(E+m)}} \begin{pmatrix} (k\cdot\sigma + m)\xi^s \\ -(k\cdot\bar{\sigma} + m)\xi^s \end{pmatrix}. \tag{5.11}$$

Choosing ξ^s eigenvalues of σ^3 and setting the longitudinal component of the momentum to zero, we

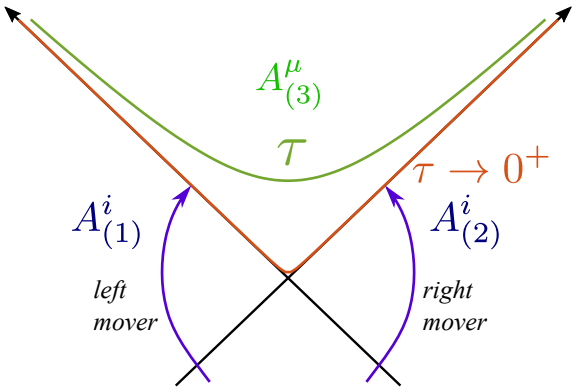

FIG. 5.1: Schematic picture of the setup of our simulation. The initial condition fot the proper time evolution is computed at [19] by evolving left/right partial waves through both sides of the light cone as they interact with the pure gauge field corresponding to the colliding nuclei.

can explicitly write down the spinor components,

$$v_{+}(\boldsymbol{k}_{\perp}, y=0) = -\frac{1}{\sqrt{2(M_{\boldsymbol{k}}+m)}}\begin{pmatrix} -(M_{\boldsymbol{k}}+m) \\ k_x + ik_y \\ M_{\boldsymbol{k}}+m \\ k_x + ik_y \end{pmatrix} \qquad v_{-}(\boldsymbol{k}_{\perp}, y=0) = -\frac{1}{\sqrt{2(M_{\boldsymbol{k}}+m)}}\begin{pmatrix} k_x - ik_y \\ -(M_{\boldsymbol{k}}+m) \\ k_x - ik_y \\ M_{\boldsymbol{k}}+m \end{pmatrix}, \tag{5.12}$$

using the proper asymptotic expansion of the Hankel funtions for $\tau \to 0^{+}$ one obtains the correct expression. The initial condition in presence of a background field can also be easily constructed in the Fock-Schwinger gauge by evolving the left-right movers partial waves through the $x^{-} > 0$, $x^{+} < 0$ and $x^{-} < 0$, $x^{+} > 0$ regions respectively where interacting with a background color gauge field induced by the nuclei moving along the $x^{\pm}$ axis, Fig. 5.1.

$$\begin{aligned}\hat{\psi}^{(-)}_{\boldsymbol{k}_\perp \nu s a\,\mathrm{FS}}(x) \underset{\tau\to 0^+}{=} & -\frac{e^{i\frac{\pi}{4}}}{\sqrt{M_{\boldsymbol{k}}}} e^{i\nu\eta} \int \frac{d^2\boldsymbol{p}_\perp}{(2\pi)^2} \frac{e^{+i\boldsymbol{p}_\perp\cdot\boldsymbol{x}_\perp}}{M_{\boldsymbol{p}}} \\ & \times \left\{ e^{\frac{\pi\nu}{2}} \left(\frac{M_{\boldsymbol{p}}^2\tau}{2M_{\boldsymbol{k}}}\right)^{i\nu} \Gamma\left(\frac{1}{2}-i\nu\right) U_2^\dagger(\boldsymbol{x}_\perp)\widetilde{U}_2(\boldsymbol{p}_\perp+\boldsymbol{k}_\perp)\gamma^+ \right. \\ & \left. + e^{-\frac{\nu\pi}{2}} \left(\frac{M_{\boldsymbol{p}}^2\tau}{2M_{\boldsymbol{k}}}\right)^{-i\nu} \Gamma\left(\frac{1}{2}+i\nu\right) U_1^\dagger(\boldsymbol{x}_\perp)\widetilde{U}_1(\boldsymbol{p}_\perp+\boldsymbol{k}_\perp)\gamma^- \right\} (p^i\gamma^i + m) v_s(\boldsymbol{k}_\perp, y=0).\end{aligned} \tag{5.13}$$

In the case of no background field the Wilson line becomes $U_{(1,2)}(\boldsymbol{x}_\perp) = 1$ and its Fourier transform $\tilde{U}_{(1,2)}(\boldsymbol{p}_\perp + \boldsymbol{k}_\perp) = (2\pi)^2\delta(\boldsymbol{p}_\perp + \boldsymbol{k}_\perp)$, one can trivially check that expression consides with that of the free spinor at $\tau \to 0^+$.

Let us now proceed to discretize the equation of motion for $\hat{\psi}$, the updated fields reads,

$$\begin{aligned}\hat{\psi}^{(-)}_{\tau+d\tau} = \left(1 - imd\tau\gamma^0\right)\hat{\psi}^{(-)}_\tau - \frac{d\tau}{2\,dx^i}\gamma^0\gamma^i\left(\hat{\psi}^{(-)x^i+dx^i}_\tau - \hat{\psi}^{(-)x^i-dx^i}_\tau\right) \\ - \frac{1}{2\tau}\frac{1}{d\eta}d\tau\gamma^0\gamma^3\left[\hat{\psi}^{(-)\eta+d\eta}_\tau - \hat{\psi}^{(-)\eta-d\eta}_\tau\right]\end{aligned}. \tag{5.14}$$

We apply periodic boundary conditions for along the transverse direction of the lattice while our treatment for the longitudinal dimension is trivial (we deal an effective 1+2 dimensional system) in the ν basis and so we can just simply solve for,

$$\begin{aligned}\hat{\psi}^{(-)}_{\tau+d\tau} = \left(1 - imd\tau\gamma^0\right)\hat{\psi}^{(-)}_\tau - \frac{d\tau}{2\,dx^i}\gamma^0\gamma^i\left(\hat{\psi}^{(-)x^i+dx^i}_\tau - \hat{\psi}^{(-)x^i-dx^i}_\tau\right) \\ - i\nu\frac{1}{\tau}d\tau\gamma^0\gamma^3\hat{\psi}^{(-)}_\tau\end{aligned}. \tag{5.15}$$

As a check of consistency we compared the analytical expression for free of interactions with the numeric solution corresponding to the initial condition (5.13). The approximation of the initial condition at is governed by the asymptotic behavior of the Hankel functions at early proper time. It is imperative to take a small enough τ to attain better accuracy, however due to the highly oscillatory behaviour of $H^{(1,2)}_{\pm\frac{1}{2}-i\nu}(M_{\boldsymbol{k}}\tau)$, a finer and finer discretization is required as $\tau \to 0$. Such fine cutting is

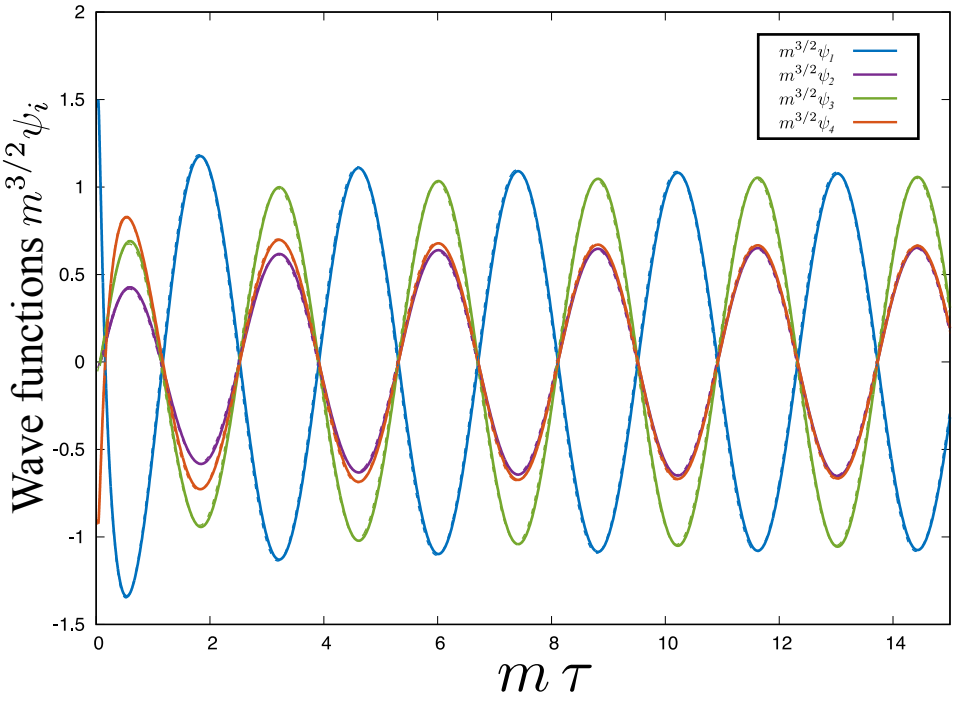

FIG. 5.2: Plots of the $\tau > 0$ evolution of the real part of the wavefunction $\hat{\psi}^{(-)}_{\boldsymbol{p}_\perp,\nu,+}(\tau, \boldsymbol{x}_{\perp 0})$ components at arbitrary point $\boldsymbol{x}_{\perp 0} = (1, 1)$ for mass $m = 0.5$ and momentum $n_x = 1$, $n_y = 2$, $\nu = 1$. The numerical/analytic solutions are denoted by solid/dashed lines. Lattice size $N_x = N_y = 4$. Initial tau τ_0 is set to 0.001. With τ in units of fm.

not needed and at larger τ and so we implement $d\tau$ as a function of τ that satisfies our purpose.

5.2 The Constant SU(2) Background Solution

In this section we study the wave-function in response to a constant SU(2) gauge field. We choose the two nuclei with different color configuration. This way, due to its non-abelian nature, we can expect a finite electric magnetic field and magnetic field as a result of a non-vanishing commutator.

$$\begin{aligned} A^1_{(1)} &= Q_0\sigma^1, \qquad A^2_{(1)} = Q_0\sigma^1, \\ A^1_{(2)} &= Q_0\sigma^2, \qquad A^2_{(2)} = 0, \end{aligned} \tag{5.16}$$

being Q_0, a constant. The general gauge link variables corresponding to a SU(2) configuration is

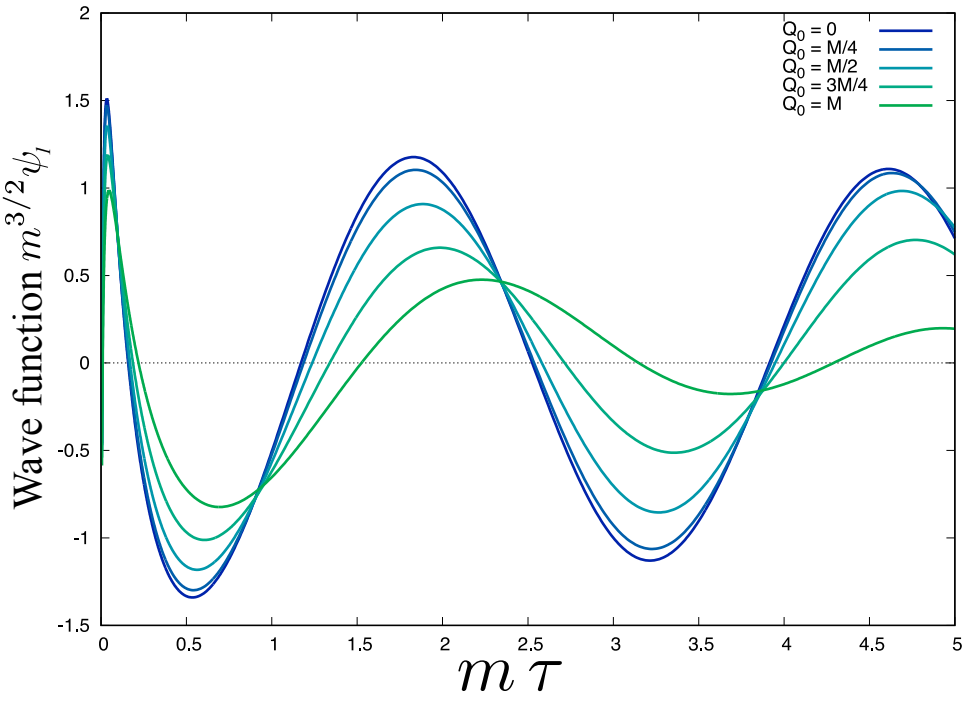

FIG. 5.3: Plots of the $\tau > 0$ evolution of the real part of first component of the wavefunction $\hat{\psi}^{(-)}_{\boldsymbol{p}_\perp,\nu,+}(\tau, \boldsymbol{x}_{\perp 0})$ at arbitrary point $\boldsymbol{x}_{\perp 0} = (1,1)$ for mass $m = 0.5$ and momentum $n_x = 1$, $n_y = 2$, $\nu = 1$ as in the figure (5.2) now for increasing magnitude of the Q_0 in mass units.

given by,

$$\begin{aligned}[U_\mu(\boldsymbol{x}_\perp)]_{ab} &= \exp\left(\frac{i}{2} g a A^a_\mu \sigma^a\right) \\ &= \delta_{ab} \cos\left(\frac{1}{2} g a \|A^a_\mu\|\right) + i(\vec{\sigma}\cdot\hat{e})_{ab} \sin\left(\frac{1}{2} g a \|A^b_\mu\|\right).\end{aligned} \tag{5.17}$$

As explicitly shown, the initial condition (5.13) depends on the Wilson lines $U_{(1,2)}$ given by,

$$U_{(m)}(\boldsymbol{x}_\perp) = \mathrm{P}\exp\left(\frac{i}{2} g \int_\gamma dz^\mu A^a_\mu \sigma^a\right). \tag{5.18}$$

The path γ is confined to the transverse plane and so it does not pick up a contribution from the longitudinal component of the gauge field, which in this case is non-vanishing. For this particular choice of the background the Wilson lines can be explicitly written as,

$$
\begin{aligned}
U_{(1)}(\boldsymbol{x}_\perp) &= e^{\frac{i}{2}gaQ_0(x+y)\sigma^1} = \cos\left(\frac{1}{2}gQ_0(x+y)\right) + i\sigma^1 \sin\left(\frac{1}{2}gQ_0(x+y)\right) \\
U_{(2)}(\boldsymbol{x}_\perp) &= e^{\frac{i}{2}gaQ_0x\sigma^1} = \cos\left(\frac{1}{2}gQ_0x\right) + i\sigma^2 \sin\left(\frac{1}{2}gQ_0x\right).
\end{aligned}
\tag{5.19}
$$

For the background acting on the quark fields in the forward light cone, we must define the appropriate minimal gauge link variable. One could naively consider the addition of the gauge field corresponding to both nuclei, however such a prescription fails to preserve unitarity, instead,

$$
U_i = (U_i^{(1)} + U_i^{(2)})(U_i^{(1)\dagger} + U_i^{(2)\dagger})^{-1}, \tag{5.20}
$$

one can easily confirm that such prescription is consistent at $\tau \to 0^+$ since the above expresion reduces to $U_i^{(1)}$ at $x^+ = 0$, $x^- > 0$ and to $U_i^{(2)}$ at $x^- = 0$, $x^+ > 0$ as it should. The discretization procedure that takes into account a nontrivial background should be expressed through the above defined link variables in the covariant derivatives, namely

$$
\begin{aligned}
\hat{\psi}^a_{\tau+d\tau} = \left(1 - imd\tau\gamma^0\right)\hat{\psi}^a_\tau - \frac{d\tau}{2\,dx^i}\gamma^0\gamma^i\left(U_i^{ab}(\boldsymbol{x}_\perp)\hat{\psi}^{b,\,x^i+dx^i}_\tau - U_i^{\dagger ab}(\boldsymbol{x}_\perp - \hat{i})\hat{\psi}^{b,\,x^i-dx^i}_\tau\right) \\
- i\nu\frac{1}{\tau}d\tau\gamma^0\gamma^3 U_i^{ab}(\boldsymbol{x}_\perp)\hat{\psi}^b_\tau,
\end{aligned}
\tag{5.21}
$$

the wavefunctions correspond to the negative energy solutions but for the sake of clearness of the notation we omit them from this point on. At $\tau \to 0^+$ the quark fields feel as a result a finite electric and magnetic field. The components $A^a_{(m)\mu}$ have the same color configuration and so the magnetic field easily follows from the commutator indicated below.

The gauge field at initial time is composed by the addition of the gauge vector of both nuclei,

$$
A^i(\tau = 0, \boldsymbol{x}_\perp) = A^i_{(1)}(\boldsymbol{x}_\perp) + A^i_{(2)}(\boldsymbol{x}_\perp). \tag{5.22}
$$

From the initial conditions we have both chromo -electric and -magnetic fields given by,

$$
\begin{aligned}
E^{\eta} &= ig\left([A_1^{(1)}, A_1^{(2)}] + [A_2^{(1)}, A_2^{(2)}]\right), \\
B^{\eta} &= -ig\left([A_1^{(1)}, A_2^{(2)}] + [A_1^{(2)}, A_2^{(1)}]\right).
\end{aligned}
\tag{5.23}
$$

With our parametrization for the constant SU(2) background gauge fields (5.16), the chromo -electric and -magnetic fields are $E^{\eta} = 2gQ_0^2\sigma^3$ and $B^{\eta} = 2gQ_0^2\sigma^3$ respectively. It is worth noting that we are no longer required to impose a time profile onto the gauge field configuration to achieve finite electric field as in the Abelian U(1) field case where $E^i = F^{0i}$. Instead we have finite longitudinal chromo-electric and magnetic fields arising from the commutator and so we are no longer bound to the unphysical switch on and switch off singularities from the previous simulation.

5.3 Expectation Values of the Currents

In this section we will compute some physical observables of interest such as number density currents produced as a response of the interaction. The quantized quark field operator in the forward light cone can be expanded as,

$$
\hat{\Psi}(x) = \sum_{a=1,2}\sum_{s=\pm}\int \frac{d^2\boldsymbol{k}_\perp d\nu}{2(2\pi)^4}\left[\hat{a}_{\boldsymbol{k}_\perp \nu s a}\,\psi^{(+)}_{\boldsymbol{k}_\perp \nu s a}(x) + \hat{b}^\dagger_{\boldsymbol{k}_\perp \nu s a}\,\psi^{(-)}_{\boldsymbol{k}_\perp \nu s a}(x)\right], \tag{5.24}
$$

$$
\hat{\overline{\Psi}}(x) = \sum_{a=1,2}\sum_{s=\pm}\int \frac{d^2\boldsymbol{k}_\perp d\nu}{2(2\pi)^4}\left[\hat{b}_{\boldsymbol{k}_\perp \nu s a}\,\overline{\psi}^{(+)}_{\boldsymbol{k}_\perp \nu s a}(x) + \hat{a}^\dagger_{\boldsymbol{k}_\perp \nu s a}\,\overline{\psi}^{(-)}_{\boldsymbol{k}_\perp \nu s a}(x)\right], \tag{5.25}
$$

where the hat notation over the wave-functions is omitted to avoid unnecessary confusion. The four-current operator is then given by $j^\mu(x) = \overline{\psi}\gamma^\mu\psi$ however we will find a divergence in its zero-component in order to avoid it, anti-symmetrization over pairs of fermion fields can get rid of this divergences. An expression of the form $\psi^\dagger_\alpha A_{\alpha\beta}\psi_\alpha$ with $A_{\alpha\beta}$ a matrix of complex numbers, then $1/2A_{\alpha\beta}(\psi^\dagger_\alpha\psi_\alpha - \psi_\alpha\psi^\dagger_\alpha) \equiv [\psi^\dagger, A\psi]$ We can evaluate the "vacuum" expectation of this current operator and find that only the $\hat{b}_{\boldsymbol{p}}\hat{b}^\dagger_{\boldsymbol{p}}$ term remains non-vanishingly as

$$J^{\mu} = g\tau \int d\eta d^2\boldsymbol{x}_{\perp} \overline{\psi}\gamma^{\mu}\psi \longrightarrow g\frac{\tau}{2}\int d\eta d^2\boldsymbol{x}_{\perp}\left[\overline{\psi}, \gamma^{\mu}\psi\right], \tag{5.26}$$

from where charge and vector currents can be computed,

$$Q = g\frac{\tau}{2}\int d\eta d^2\boldsymbol{x}_{\perp}\left[\psi^{\dagger}, \psi\right] \ , \quad J^{i} = g\frac{\tau}{2}\int d\eta d^2\boldsymbol{x}_{\perp}\left[\overline{\psi}, \gamma^{i}\psi\right]. \tag{5.27}$$

This is a standard calculation, it is not hard to show that the quantity above yields,

$$Q = g\sum_{a=1,2}\sum_{s=\pm}\int \frac{dvd^2\boldsymbol{k}_{\perp}}{2(2\pi)^4}\left[\hat{a}^{s\dagger}_{\boldsymbol{p}}\hat{a}^{s}_{\boldsymbol{p}} - \hat{b}^{s\dagger}_{\boldsymbol{p}}\hat{b}^{s}_{\boldsymbol{p}}\right]. \tag{5.28}$$

As expected the expectation value of the particle density operator vanishes in vacuum for the free particle case. As we shall see this is not the case when we introduce the homogeneous gauge $\boldsymbol{A}'$. Let us, perform the evaluation for the expectation value of the chiral charge $j^0_5(\tau)$ at a given τ. Since the mode functions satisfy the free initial condition, the creation and annihilation operators from (5.25) define the *in*-vacuum. The vacuum expectation of any bilinear operator, and in particular the currents, can be expressed in terms of the mode functions. For the operator in the form $\overline{\hat{\Psi}}(x)\mathrm{M}\hat{\Psi}(x)$ we compute its expectation value by expanding in the mode functions,

$$\langle 0|\overline{\hat{\Psi}}(x)\mathrm{M}\hat{\Psi}(x)|0\rangle = \sum_{s,a}\int \frac{dvd^2\boldsymbol{k}_{\perp}}{2(2\pi)^4}\hat{\psi}^{(-)\dagger}_{\boldsymbol{k}_{\perp}vsa}(x)\gamma^0\mathrm{M}\hat{\psi}^{(-)}_{\boldsymbol{k}_{\perp}vsa}(x), \tag{5.29}$$

where could be $\mathrm{M} = \gamma^m u$ or some other spin matrix, in our case of interest $\mathrm{M} = \gamma^{\mu}\gamma_5$. We are particularly interested in axial density current $j^{\mu}_5 = \langle 0|\overline{\Psi}(x)\gamma^{\mu}\gamma_5\Psi(x)|0\rangle$. However, since this current is defined in the Cartesian coordinates, the field operator that appears in the right hand side is as well. Ψ is related to its boosted counterpart $\hat{\Psi}$ in the same way its mode functions are in (5.7), that is,

$$\hat{\Psi} = \sqrt{\tau}e^{-\frac{\eta}{2}\gamma^0\gamma^3}\Psi, \tag{5.30}$$

rewritting the axial current in terms of these boosted field operator yields,

$$j_5^\mu(x) = \frac{1}{\tau}\langle 0|\overline{\Psi}(x)e^{-\frac{\eta}{2}\gamma^0\gamma^3}\gamma^\mu\gamma_5\, e^{\frac{\eta}{2}\gamma^0\gamma^3}\Psi(x)|0\rangle. \tag{5.31}$$

However we are considering a boost invariant expanding system and so it is more convenient to compute the current which is observed in the Bjorken frame. This can be achieved by simply applying a Lorentz boost to the previously defined current $\hat{j}_5^\mu = \Lambda^\mu_\nu j_5^\nu$, where the hat denotes a boosted quantity. In this way $\hat{j}_5^\mu(x) = \frac{1}{\tau}\langle 0|\overline{\hat{\Psi}}(x)\gamma^\mu\gamma_5\hat{\Psi}(x)|0\rangle$ the boosted current is no longer dependent on the η coordinate, since the η dependence of the wave functions also disappears when the background is boost invariant. The overall $1/\tau$ which appears in the currents is natural if one recalls that the quantity we are dealing with is a current density.

We are now interested in evolution of the chiral charge density which under the effect of a non-abelian $\mathcal{CP}$-odd background field. To this end we once more make use of the gauge field configuration as described in the previous section (5.16). First, let us compute the expectation value of j_5^0 when $\tau \to 0$ making use of the explicit expression for the initial condition (5.13),

$$\hat{j}_5^0(\tau) = \frac{1}{\tau}\langle 0|\overline{\hat{\Psi}}(x)\gamma^0\gamma_5\hat{\Psi}(x)|0\rangle = \frac{1}{\tau}\sum_{s,a}\int\frac{d\nu d^2\boldsymbol{k}_\perp}{2(2\pi)^4}\hat{\psi}^{(-)\dagger}_{\boldsymbol{k}_\perp\nu sa}(x)\gamma_5\hat{\psi}^{(-)}_{\boldsymbol{k}_\perp\nu sa}(x), \tag{5.32}$$

for this purpose let us compress the initial condition by making use of the following definitions,

$$\begin{aligned}
\phi_{\boldsymbol{p}}^{(1)} &= e^{-\frac{\nu\pi}{2}}\left(\frac{M_{\boldsymbol{p}}^2\tau}{2M_{\boldsymbol{k}}}\right)^{-i\nu}\Gamma\left(\frac{1}{2}+i\nu\right)U_1^\dagger(\boldsymbol{x}_\perp)\widetilde{U}_1(\boldsymbol{p}_\perp+\boldsymbol{k}_\perp)\\
\phi_{\boldsymbol{p}}^{(2)} &= e^{+\frac{\nu\pi}{2}}\left(\frac{M_{\boldsymbol{p}}^2\tau}{2M_{\boldsymbol{k}}}\right)^{+i\nu}\Gamma\left(\frac{1}{2}-i\nu\right)U_2^\dagger(\boldsymbol{x}_\perp)\widetilde{U}_2(\boldsymbol{p}_\perp+\boldsymbol{k}_\perp).
\end{aligned} \tag{5.33}$$

As it is now usual, we proceed to evaluate this quantity by making use of the explicit expression for negative energy wave function and performing the spin and color sums,

$$\begin{aligned}\sum_{s,a}\int \frac{dvd^2\boldsymbol{k}_\perp}{2(2\pi)^4}\overline{\hat{\psi}}^{(-)}_{\boldsymbol{k}_\perp vsa}\gamma^0\gamma_5\hat{\psi}^{(-)}_{\boldsymbol{k}_\perp vsa} &= \frac{1}{2(2\pi)^2}\sum_{s,a}\int dv \prod_{\sigma=\{\boldsymbol{k}_\perp,\boldsymbol{p}_\perp,\boldsymbol{q}_\perp\}}\int_\sigma \frac{1}{M_\sigma}e^{-i(\boldsymbol{p}_\perp-\boldsymbol{q}_\perp)\cdot\boldsymbol{x}_\perp} \\ &\times\chi_a^\dagger\bar{v}_s(\boldsymbol{k}_\perp,0)(p^i\gamma^i+m)\left(\phi_{\boldsymbol{p}}^{(1)\dagger}\gamma^+ + \phi_{\boldsymbol{p}}^{(2)\dagger}\gamma^-\right)\gamma^0\gamma_5\left(\phi_{\boldsymbol{q}}^{(1)}\gamma^+ + \phi_{\boldsymbol{q}}^{(2)}\gamma^-\right) \\ &\times(q^l\gamma^l+m)v_s(\boldsymbol{k}_\perp,0)\chi_a \\ &= \frac{1}{2(2\pi)^2}\int dv \prod_{\sigma=\{\boldsymbol{k}_\perp,\boldsymbol{p}_\perp,\boldsymbol{q}_\perp\}}\int_\sigma \frac{1}{M_\sigma}e^{-i(\boldsymbol{p}_\perp-\boldsymbol{q}_\perp)\cdot\boldsymbol{x}_\perp} \\ &\times \mathrm{tr}_{sp\times c}\Big[(p^i\gamma^i+m)(M_{\boldsymbol{k}}\gamma^0-k^j\gamma^j-m)(q^l\gamma^l+m) \\ &\qquad\times\left(\phi_{\boldsymbol{p}}^{(1)\dagger}\gamma^+ + \phi_{\boldsymbol{p}}^{(2)\dagger}\gamma^-\right)\gamma^0\gamma_5\left(\phi_{\boldsymbol{q}}^{(1)}\gamma^+ + \phi_{\boldsymbol{q}}^{(2)}\gamma^-\right)\Big],\end{aligned} \tag{5.34}$$

again, just like the calculation of the fermion number density j^0, we focus on the spin trace to break down this expression into a more compact form.

$$\begin{aligned}&\mathrm{tr}_{sp\times c}\left[(p^i\gamma^i+m)(M_{\boldsymbol{k}}\gamma^0-k^j\gamma^j-m)(q^l\gamma^l+m)\left(\phi_{\boldsymbol{p}}^{(1)\dagger}\gamma^+ + \phi_{\boldsymbol{p}}^{(2)\dagger}\gamma^-\right)\gamma^0\gamma_5\left(\phi_{\boldsymbol{q}}^{(1)}\gamma^+ + \phi_{\boldsymbol{q}}^{(2)}\gamma^-\right)\right] \\ &= i\,\mathrm{tr}_{sp\times c}\left[\gamma^0(p^i\gamma^i+m)(M_{\boldsymbol{k}}\gamma^0-k^j\gamma^j-m)(q^l\gamma^l+m)\gamma^1\gamma^2\left(\phi_{\boldsymbol{p}}^{(1)\dagger}\gamma^+ + \phi_{\boldsymbol{p}}^{(2)\dagger}\gamma^-\right)\gamma^3\left(\phi_{\boldsymbol{q}}^{(1)}\gamma^+ + \phi_{\boldsymbol{q}}^{(2)}\gamma^-\right)\gamma^0\right].\end{aligned} \tag{5.35}$$

Here, let us rewrite the last portion of the trace,

$$\left(\phi_{\boldsymbol{p}}^{(1)\dagger}\gamma^+ + \phi_{\boldsymbol{p}}^{(2)\dagger}\gamma^-\right)\gamma^3\left(\phi_{\boldsymbol{q}}^{(1)}\gamma^+ + \phi_{\boldsymbol{q}}^{(2)}\gamma^-\right)\gamma^0 = \left(\phi_{\boldsymbol{p}}^{(1)\dagger}\phi_{\boldsymbol{q}}^{(1)} - \phi_{\boldsymbol{p}}^{(2)\dagger}\phi_{\boldsymbol{p}}^{(2)}\right) + \gamma^0\gamma^3\left(\phi_{\boldsymbol{p}}^{(1)\dagger}\phi_{\boldsymbol{q}}^{(1)} + \phi_{\boldsymbol{p}}^{(2)\dagger}\phi_{\boldsymbol{p}}^{(2)}\right) \tag{5.36}$$

From this point it is not hard to see that the spin trace picking up the later term will automatically vanish as neither i,j or l involve the third component and thus such term can be dropped. Terms with pair number of gamma matrices survive, out of these, only the term proportional to $M_{\boldsymbol{k}}$ survives, this leads to,

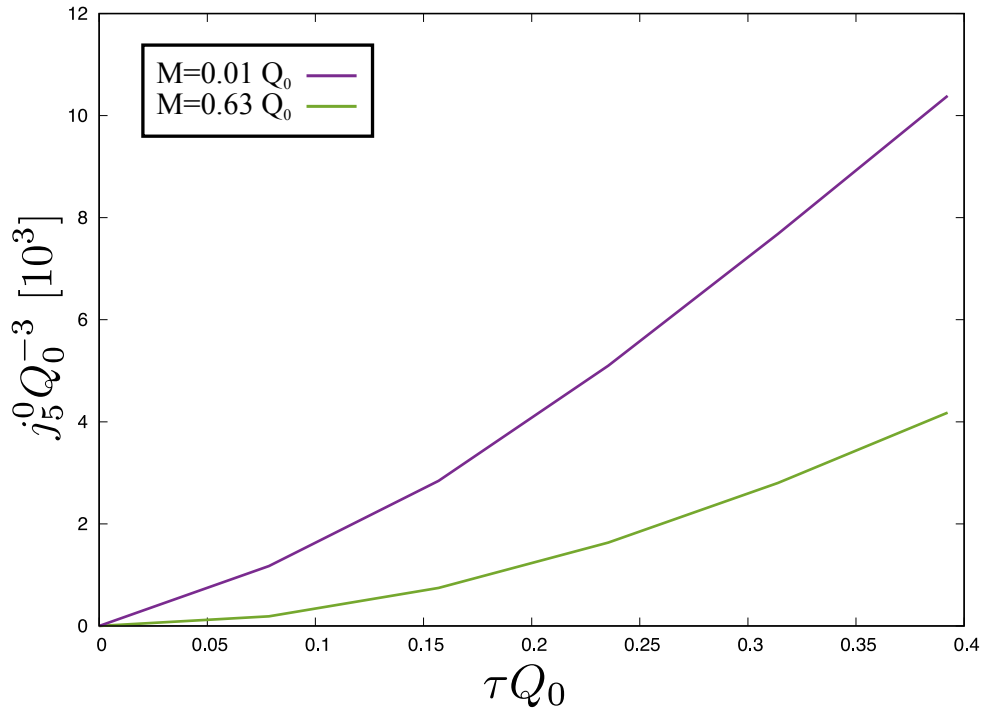

FIG. 5.4: $\tau > 0$ evolution of the expectation value of $j_5^0(\tau)$ computed by means of the τ-evolved wave function at arbitrary point $\boldsymbol{x}_\perp = (1, 1)$, $\eta = 1$ under constant SU(2) background field parametrized by $Q_0 = 0.5$. The lattice volume 8^3, i.e. $N_{x,y,\eta} = 8$. $\tau_0 = 10^{-5}$ was considered for the initial wave function 5.13. Axial charge and proper time were scale to dimensionless units by Q_0.

$$\hat{j}_5^0 = \frac{1}{2(2\pi)^2}\tau^{-1}\int d\nu \prod_{\sigma=\{\boldsymbol{p}_\perp,\boldsymbol{q}_\perp\}}\int_\sigma \frac{1}{M_\sigma} e^{-i(\boldsymbol{p}_\perp-\boldsymbol{q}_\perp)\cdot\boldsymbol{x}_\perp} 4i(q^1p^2 - q^2p^1)\int_{\{\boldsymbol{k}_\perp\}} \mathrm{tr}_c\left(\phi_{\boldsymbol{p}}^{(1)\dagger}\phi_{\boldsymbol{q}}^{(1)} - \phi_{\boldsymbol{p}}^{(2)\dagger}\phi_{\boldsymbol{p}}^{(2)}\right) = 0. \tag{5.37}$$

Here, the integration of $\boldsymbol{k}_\perp$ integration in the right side can be carried out explicitly by making use of the explicit form of $\phi_{\boldsymbol{p}}^{(1,2)}$ defined at (5.33). However, for arbitrary gauge configurations, due to the unitarity of the U-matrices the following relation holds,

$$\int_{\{\boldsymbol{k}_\perp\}} \widetilde{U}_i^\dagger(\boldsymbol{p}_\perp + \boldsymbol{k}_\perp)\widetilde{U}_i(\boldsymbol{q}_\perp + \boldsymbol{k}_\perp) = (2\pi)^2\delta^2(\boldsymbol{p}_\perp - \boldsymbol{q}_\perp), \tag{5.38}$$

from where it is evident that j_5^0 will vanish as the $\boldsymbol{k}_\perp$ integration implies through Eq. (5.38) that $\boldsymbol{p}_\perp = \boldsymbol{q}_\perp$ and thus the is exactly zero for $\tau \to 0$.

While the electric current can be obtained by an analogous expression. In the latter case its zero-component should tell us about the time evolution of the particle number density. Whatever the case, since we are working with massive quark fields. For the numerical computation, we restricted the momentum domain only to half of the first Brillouin zone as to avoid cancellation of the anomaly by the doublers. The longitudinal momentum integration has been performed discretizing the η direction where periodic boundary conditions where imposed.

Let us finally see how the axial charge density responds to finite mass. As it can be seen from the numerical simulation shown at 5.4, the proper time evolution of j_5^0 is damped by the finite mass. This is very non-trivial as it cannot be directly inferred from axial Ward identity,

$$\partial_\mu j_5^\mu = -\frac{g^2}{16\pi^2}\,\mathrm{tr}\{F_{\mu\nu}\tilde{F}^{\mu\nu}\} + 2m\bar{\psi}i\gamma^5\psi, \tag{5.39}$$

where the time integrated zero component yields,

$$j_5^0 = -\frac{g^2}{4\pi^2}\int_0^t \langle \boldsymbol{E}^a \cdot \boldsymbol{B}^a \rangle\, dt' + 2im\int_0^t \left\langle \bar{\psi}\gamma^5\psi \right\rangle dt', \tag{5.40}$$

on the right hand side we recognize the first term as the contribution coming from the chiral anomaly responsible for the axial charge non-conservation in the massless limit and the second term proportional to the quark mass responsible for the mixing of different chiral components. However, given the proper conditions chirality might be conserved. For instance, in the case electromagnetic -electric and -magnetic fields explored in the previous chapter, no axial charge is generated for perpendicular fields even for massive quarks starting from the vacuum state. The chirality for a massive quark is a Lorentz-frame dependent quantity and therefore not necessarily conserved in every frame. The mass term is usually neglected in the axial Ward identity, e.g. when studying the axial charge, however we do know that from the Schwinger pair production, as discussed in the previous chapter, that the quark mass can considerably suppress pair production and hence affect chirality imbalance. The quark initial conditions (5.13) are crucial to the description of j_5^0, in Fig. 5.4 we present the production of chirality imbalance for different quark masses as a function of proper time.

All quantities have been scaled by the intensity of the gauge field Q_0. To get an order of magnitude

estimates we have to set the scale, let us assume chromo-electric and chromo-magnetic field intensities of the order of the gluon saturation scale, i.e. $g|\boldsymbol{E}^a| = g|\boldsymbol{B}^a| \sim Q_{sat}^2$ [67, 68]. Considering the RHIC values for the gluon saturation momentum $Q_{\rm sat} \sim 1$ GeV, implies $Q_0 \sim 0.7$ GeV. This translates in Fig. 5.4 as quark mass values $m = 7$ MeV of the order of the up and down quark masses in the upper plot and for $m = 420$ MeV between the strange and bottom quark mass at the bottom. The magnitude of the axial charge follows in the same manner; $\tau Q_0 = 0.4$, which means proper time $\tau \sim 0.1$ fm where the axial charge density is $j_5^0 \sim 10^{-2} Q_0^3$, for our value of Q_0, this means $j_5^0 \sim 3.5 \times 10^{-3}\text{GeV}^3$ for the light sector. This estimate falls in line with the initial profile of axial charges used in the anomalous hydrodynamic simulations [14] where by assuming spatially random configuration for the axial charge density. In [14], the charge-dependent correlation functions γ_{++}, γ_{--} and γ_{+-} are computed as a function of centrality included in the profile of the magnetic field via impact parameter b and compared to the STAR data Fig. 2.9. The results in show qualitative agreement however are inevitably subject of large uncertainties coming from the lack of knowledge on the initial configuration which arises from the dynamics at the early-time regime. The initial distribution of axial charges is indispensable to the observed charge asymmetry at the relativistic heavy ion collisions. It is not known how to disentangle the signal from background effects in the observable $\gamma_{\alpha\beta}$ with $\alpha, \beta \in \{+, -\}$ proposed for observations. In fact, model calculations have shown that under certain circumstances the background contributions could in principle mimic the observed charge asymmetry at the STAR data [69], and it is therefore imperative to improve the description of the early-time regime dynamics.

We have here provided the first real-time simulation of axial charge production in the expanding geometry and studied the systems response to finite quark mass. We have assumed for simplicity a constant SU(2) background field, the non-abelian nature of the background allowed us to get rid of the unphysical ambiguity of the sudden switch on and switch off as it is no longer necessary to impose a time profile as in the abelian case. However, it would be interesting to enhance this picture by introducing dynamical soft gluon modes instead. This extension is can be readily implemented in our formulation and represents the immediate follow-up to this work, to presented elsewhere. Further

extensions including non-trivial interplay with external electromagnetic U(1) fields would be of interest, as it would provide a way to study chiral plasma instabilities within the heavy-ion collision setup that must be explored. With this work, we attempt to provide a better understanding on the dynamics of axial charge generation within the early-stages of the heavy-ion collisions with CGC motivated setups, considering for the expanding geometry and its response to finite quark mass.

Chapter 6

Conclusion

The ultra-relativistic heavy-ion collision experiments represent a unique laboratory for the most intriguing phenomena unique to strong interacting systems. The Chiral Magnetic Effect has been the focus of attention for several years now, providing a promising path to test the topologically non-trivial vacuum and it could denote a signal for deconfinement in heavy ion collisions. Given its implications, it is highly desirable to search for signals of the vector current within heavy ion experiments. The CME current requires strong magnetic fields on top chirallity imbalanced medium. There have been several studies in which by means of anomalous hydrodynamics and chiral kinetic theory approaches attempt to characterize the CME current. The intensities of the magnetic fields generated at the peripheral collisions are indeed enough to trigger the current generation, however, they are short lived. The lifetime of the transient magnetic fields is as short as $Q_{sat}^{-1} \sim 0.2$ fm/c for RHIC and $Q_{sat}^{-1} \sim 0.1$ fm/c for LHC. On top of this, most of quarks and antiquark pairs are produced from the very beginning [19]. This implies that the relevant the production of the current should be studied in the early-time regime of the collision whose dynamics is governed by the Color-Glass-Condensate framework. In this thesis, the dynamics of axial charge density was addressed in terms of quark production using CGC-motivated setups. Previous studies usually neglect the mass term contribution, however, fermion pair production is severely suppressed as it can be understood from Schwinger effect. We showed the suppression of axial charge by finite quark mass in a finite box and expanding systems. The generation of the dynamical Chiral Magnetic Effect current was simulated, enhanced

by finite perpendicular component of the magnetic field on top of chirally imbalanced medium but inheriting the same exponential damping behaviour induced by finite mass. Discretization of Dirac equation inevitably gives rise to unphysical doublers which cancelling the chiral anomaly according to the Nielsen-Ninomiya theorem. In order to pick up the right contribution from the anomaly, the effect coming from the unphysical doublers were studied. The simulations were performed by introducing a cut-off in momentum space restricting to only half of the Brillouin zone. The validity for this prescription was established by contrasting the naive fermion set-up in the half-cut Brillouin and a system of Wilson fermions in the full Brillouin zone. This is quite non-trivial as the smearing of the particle distribution functions in momentum space by the magnetic field could in principle be contaminated by the doublers if the distribution does not decay rapidly enough at the edges.

The effects of the quantum anomaly in out-of-equilibrium system are believed to be of crucial importance in the astrophysical context [70] where it has been reported that the exchange of fermionic chirality and magnetic helicity could lead to instability of the system, phenomenon known as chiral plasma instability [71, 72]. In these scenarios the fermion mass is believed to have the role suppressing the production of chirality and must be taken into account when studying chiral plasma instability [73]. Such a situation might also take place in ultra-relativistic heavy-ion collisions as well, hence, characterizing the damping effect of the axial charge by finite quark mass becomes necessary. Besides the finite box system, we showed in this thesis, that the damping effect perdures in the expanding geometry. Using the quark initial conditions at $\tau \to 0^+$ recently reported in [19], simulations of the axial charge density were performed for constant SU(2) background field. The non-abelian nature of the background gauge fields allowed implement longitudinal chromo -electric and magnetic fields without the need to impose a time profile onto them as one would in the U(1) case. In this way we disposed of the unphysical singularity coming from the sudden switch on and off of the background manifested in the oscillations of the momentum distribution.

As an extension of this work, it is of interest to see whether the observed mass effect hold in more realistic setups considering the dynamical color fields from the CGC framework, characterizing the proper time scales and magnitudes relevant to the anomalous transport in a more quantitative way. It

is of interest is see how the CGC color fields affect pair production and the proving this setup with external electromagnetic fields attaining a more realistic frame that addresses the ultra-relativistic heavy ion collision experiments. It would be amusing to extend our real-time simulations of out-of-equilibrium axial charge density performed here to scenarios of electroweak baryogenesis [74] as well.

Appendix A

Concistenty Checks

A.1 Computation of the j^0 Expectation Value

First let us restrict to the case of vanishing external fields. In this case, we have that both positive and negative energy wave functions are described by Hankel functions of first (second) type. j_0 can be explitly obtained,

$$\hat{j}^0(\tau) = \frac{1}{\tau}\sum_{s,a}\int \frac{dv d^2\boldsymbol{k}_\perp}{2(2\pi)^4}\left(|\widehat{\psi}^{(-)}_{\boldsymbol{k}_\perp v s a}|^2 - |\hat{\psi}^{(+)}_{\boldsymbol{k}_\perp v s a}|^2\right). \tag{A.1}$$

For the sake of brevity we adopt the notation $\int_{\{\boldsymbol{k}_\perp\}} = \int \frac{d^2\boldsymbol{k}_\perp}{(2\pi)^2}$. The explicit form of the negative energy quark field in the absence of a backgauge field reads,

$$\begin{aligned}\hat{\psi}^{(-)}_{\boldsymbol{k}_\perp v s a}(x) = -i\pi\sqrt{\tau}e^{\frac{\pi v}{2}}e^{iv\eta - i\boldsymbol{k}_\perp\cdot\boldsymbol{x}_\perp}\Big\{&e^{-i\frac{\pi}{4}}H^{(1)}_{-\frac{1}{2}-iv}(M_{\boldsymbol{k}}\tau)\,\mathscr{P}^+ \\ &+ e^{i\frac{\pi}{4}}H^{(1)}_{\frac{1}{2}-iv}(M_{\boldsymbol{k}}\tau)\,\mathscr{P}^-\Big\}v_s(\boldsymbol{k}_\perp, y=0),\end{aligned} \tag{A.2}$$

where the positive energy free quark field is similarly obtained, in terms of second type Hankel functions. Taken into account these two expressions the zero component of the vector current (A.1) yields,

$$\hat{j}^0(\tau) = \frac{\pi^2}{2(2\pi)^2}\sum_{s,a}\int d\nu \int_{\{\boldsymbol{k}_\perp\}} \chi_a^\dagger \Big[e^{\pi\nu}\bar{v}_s(\boldsymbol{k}_\perp,0)\gamma^0\Big(|H^{(1)}_{-\frac{1}{2}-i\nu}(M_{\boldsymbol{k}}\tau)|^2\mathscr{P}^+ + |H^{(1)}_{\frac{1}{2}-i\nu}(M_{\boldsymbol{k}}\tau)|^2\mathscr{P}^-\Big)v_s(\boldsymbol{k}_\perp,0) \\ -e^{-\pi\nu}\bar{u}_s(\boldsymbol{k}_\perp,0)\gamma^0\Big(|H^{(2)}_{-\frac{1}{2}-i\nu}(M_{\boldsymbol{k}}\tau)|^2\mathscr{P}^+ + |H^{(2)}_{\frac{1}{2}-i\nu}(M_{\boldsymbol{k}}\tau)|^2\mathscr{P}^-\Big)u_s(\boldsymbol{k}_\perp,0)\Big]\chi_a. \tag{A.3}$$

We can readily perform the spin and color sums of this operator resulting into the following trace,

$$\hat{j}^0(\tau) = \frac{1}{8}\int d\nu \int_{\{\boldsymbol{k}_\perp\}} \mathrm{tr}_{sp\times c}\Big[e^{\pi\nu}\gamma^0\Big(|H^{(1)}_{-\frac{1}{2}-i\nu}(M_{\boldsymbol{k}}\tau)|^2\mathscr{P}^+ + |H^{(1)}_{\frac{1}{2}-i\nu}(M_{\boldsymbol{k}}\tau)|^2\mathscr{P}^-\Big)(M_{\boldsymbol{k}}\gamma^0 - p^i\gamma^i - m) \\ -e^{-\pi\nu}\gamma^0\Big(|H^{(2)}_{-\frac{1}{2}-i\nu}(M_{\boldsymbol{k}}\tau)|^2\mathscr{P}^+ + |H^{(2)}_{\frac{1}{2}-i\nu}(M_{\boldsymbol{k}}\tau)|^2\mathscr{P}^-\Big)(M_{\boldsymbol{k}}\gamma^0 - p^i\gamma^i + m)\Big]. \tag{A.4}$$

Because of the spin trace only terms most terms vanish and the only term that contributes comes from $M_{\boldsymbol{k}}\gamma^0$,

$$\hat{j}^0(\tau) = \frac{N_c}{8}\int d\nu \int_{\{\boldsymbol{k}_\perp\}} M_{\boldsymbol{k}}\,\mathrm{tr}_{sp}\Big[e^{\pi\nu}\Big(|H^{(1)}_{-\frac{1}{2}-i\nu}(M_{\boldsymbol{k}}\tau)|^2 + |H^{(1)}_{\frac{1}{2}-i\nu}(M_{\boldsymbol{k}}\tau)|^2\Big) \\ -e^{-\pi\nu}\Big(|H^{(2)}_{-\frac{1}{2}-i\nu}(M_{\boldsymbol{k}}\tau)|^2 + |H^{(2)}_{\frac{1}{2}-i\nu}(M_{\boldsymbol{k}}\tau)|^2\Big)\Big]. \tag{A.5}$$

On the first term we perform the change of variable $\nu \to -\nu$,

$$\hat{j}^0(\tau) = \frac{N_c}{2}\int d\nu \int_{\{\boldsymbol{k}_\perp\}} M_{\boldsymbol{k}}\Big[e^{-\pi\nu}|H^{(1)}_{-\frac{1}{2}+i\nu}(M_{\boldsymbol{k}}\tau)|^2 + e^{\pi\nu}|H^{(1)}_{\frac{1}{2}-i\nu}(M_{\boldsymbol{k}}\tau)|^2 \\ -e^{-\pi\nu}|H^{(2)}_{-\frac{1}{2}-i\nu}(M_{\boldsymbol{k}}\tau)|^2 - e^{\pi\nu}|H^{(2)}_{\frac{1}{2}+i\nu}(M_{\boldsymbol{k}}\tau)|^2\Big]. \tag{A.6}$$

At this point by noting that analityc continuation of these Hankel functions, i.e. $[H^{(1,2)}_w(z)]^* = H^{(2,1)}_{w^*}(z^*)$, we can readily see how the cancellation takes place,

$$\hat{j}^0(\tau) = \frac{N_c}{2}\int d\nu \int_{\{\boldsymbol{k}_\perp\}} M_{\boldsymbol{k}} \Big[e^{-\pi\nu} H^{(2)}_{-\frac{1}{2}-i\nu}(M_{\boldsymbol{k}}\tau) H^{(1)}_{-\frac{1}{2}+i\nu}(M_{\boldsymbol{k}}\tau) + e^{\pi\nu} H^{(2)}_{\frac{1}{2}+i\nu}(M_{\boldsymbol{k}}\tau) H^{(1)}_{\frac{1}{2}-i\nu}(M_{\boldsymbol{k}}\tau) - e^{-\pi\nu} H^{(1)}_{-\frac{1}{2}+i\nu}(M_{\boldsymbol{k}}\tau) H^{(2)}_{-\frac{1}{2}-i\nu}(M_{\boldsymbol{k}}\tau) - e^{\pi\nu} H^{(1)}_{\frac{1}{2}-i\nu}(M_{\boldsymbol{k}}\tau) H^{(2)}_{\frac{1}{2}+i\nu}(M_{\boldsymbol{k}}\tau) \Big] = 0. \tag{A.7}$$

In the case of finite external fields we can still calculate analytically once obtained the explicit expresions for the wave function of both positive and negative energy wave functions. That is from the initial condition of the quark field Eq. (5.13) and

$$\hat{\psi}^{(+)}_{\boldsymbol{k}_\perp \nu s a\,\mathrm{FS}}(x) \underset{\tau\to 0^+}{=} \pi e^{-i\frac{\pi}{4}} U_1^\dagger(\boldsymbol{x}_\perp) U_2^\dagger(\boldsymbol{x}_\perp) \sqrt{\frac{2}{M_{\boldsymbol{k}}}} \frac{e^{i\nu\eta} e^{+i\boldsymbol{k}_\perp\cdot\boldsymbol{x}_\perp}}{\cosh(\pi\nu)} \times \left\{ \frac{e^{\frac{\pi\nu}{2}}}{\Gamma\left(\frac{1}{2}-i\nu\right)} \left(\frac{M_{\boldsymbol{k}}\tau}{2}\right)^{-i\nu} \mathscr{P}^+ + \frac{e^{-\frac{\pi\nu}{2}}}{\Gamma\left(\frac{1}{2}+i\nu\right)} \left(\frac{M_{\boldsymbol{k}}\tau}{2}\right)^{i\nu} \mathscr{P}^- \right\} u_s(\boldsymbol{k}_\perp, y=0). \tag{A.8}$$

Let us examine the $\hat{\psi}^{(+)}_{\boldsymbol{k}_\perp \nu s a}(x)$ and $\hat{\psi}^{(-)}_{\boldsymbol{k}_\perp \nu s a}(x)$ separately, just as observed in the previous case we expect cancellation between this two parts at the end,

$$\begin{aligned}
\sum_{s,a}\int \frac{d\nu d^2\boldsymbol{k}_\perp}{2(2\pi)^4} |\hat{\psi}^{(-)}_{\boldsymbol{k}_\perp \nu s a}|^2 &= \frac{1}{2(2\pi)^2}\sum_{s,a}\int d\nu \prod_{\sigma=\{\boldsymbol{k}_\perp,\boldsymbol{p}_\perp,\boldsymbol{q}_\perp\}} \int_\sigma \frac{1}{M_\sigma} e^{-i(\boldsymbol{p}_\perp-\boldsymbol{q}_\perp)\cdot\boldsymbol{x}_\perp} \chi_a^\dagger \bar{v}_s(\boldsymbol{k}_\perp, 0) \\
&\times (p^i\gamma^i + m)\left(\phi^{(1)\dagger}_{\boldsymbol{p}}\gamma^+ + \phi^{(2)\dagger}_{\boldsymbol{p}}\gamma^-\right)\gamma^0\left(\phi^{(1)}_{\boldsymbol{q}}\gamma^+ + \phi^{(2)}_{\boldsymbol{q}}\gamma^-\right)(q^l\gamma^l + m) v_s(\boldsymbol{k}_\perp, 0)\chi_a \\
&= \frac{1}{2(2\pi)^2}\int d\nu \prod_{\sigma=\{\boldsymbol{k}_\perp,\boldsymbol{p}_\perp,\boldsymbol{q}_\perp\}} \int_\sigma \frac{1}{M_\sigma} e^{-i(\boldsymbol{p}_\perp-\boldsymbol{q}_\perp)\cdot\boldsymbol{x}_\perp} \\
&\times \mathrm{tr}_{sp\times c}\left[(p^i\gamma^i + m)(M_{\boldsymbol{k}}\gamma^0 - k^j\gamma^j - m)(q^l\gamma^l + m)\left(\phi^{(1)\dagger}_{\boldsymbol{p}}\gamma^+ + \phi^{(2)\dagger}_{\boldsymbol{p}}\gamma^-\right)\gamma^0\left(\phi^{(1)}_{\boldsymbol{q}}\gamma^+ + \phi^{(2)}_{\boldsymbol{q}}\gamma^-\right)\right],
\end{aligned} \tag{A.9}$$

where we have used the following definitions,

$$\begin{aligned}\phi_{\boldsymbol{p}}^{(1)} &= e^{-\frac{\nu\pi}{2}}\left(\frac{M_p^2\tau}{2M_k}\right)^{-i\nu}\Gamma\left(\frac{1}{2}+i\nu\right)U_1^{\dagger}(\boldsymbol{x}_\perp)\widetilde{U}_1(\boldsymbol{p}_\perp+\boldsymbol{k}_\perp)\\ \phi_{\boldsymbol{p}}^{(2)} &= e^{+\frac{\nu\pi}{2}}\left(\frac{M_p^2\tau}{2M_k}\right)^{+i\nu}\Gamma\left(\frac{1}{2}-i\nu\right)U_2^{\dagger}(\boldsymbol{x}_\perp)\widetilde{U}_2(\boldsymbol{p}_\perp+\boldsymbol{k}_\perp).\end{aligned} \tag{A.10}$$

By evaluating the trace above one obtains,

$$\begin{aligned}\sum_{s,a}\int\frac{d\nu d^2\boldsymbol{k}_\perp}{2(2\pi)^4}|\hat{\psi}^{(-)}_{\boldsymbol{k}_\perp\nu sa}|^2 &= \frac{1}{2(2\pi)^2}\int d\nu\prod_{\sigma=\{\boldsymbol{k}_\perp,\boldsymbol{p}_\perp,\boldsymbol{q}_\perp\}}\int_\sigma\frac{1}{M_\sigma}e^{-i(\boldsymbol{p}_\perp-\boldsymbol{q}_\perp)\cdot\boldsymbol{x}_\perp}\\ &\quad\times\mathrm{tr}_{sp\times c}\Big[(p^i\gamma^i+m)(M_{\boldsymbol{k}}\gamma^0-k^j\gamma^j-m)(q^l\gamma^l+m)\gamma^0\\ &\qquad\times\left(\phi_{\boldsymbol{p}}^{(2)\dagger}\phi_{\boldsymbol{q}}^{(2)}\gamma^-\gamma^+ + \phi_{\boldsymbol{p}}^{(1)\dagger}\phi_{\boldsymbol{q}}^{(1)}\gamma^+\gamma^-\right)\Big]\\ &= \frac{2}{(2\pi)^2}\int d\nu\int_{\{\boldsymbol{k}_\perp\}}\int_{\{\boldsymbol{p}_\perp\}}\frac{1}{M_{\boldsymbol{p}}}\int_{\{\boldsymbol{q}_\perp\}}\frac{1}{M_{\boldsymbol{q}}}e^{-i(\boldsymbol{p}_\perp-\boldsymbol{q}_\perp)\cdot\boldsymbol{x}_\perp}(\boldsymbol{q}_\perp\cdot\boldsymbol{p}_\perp+m^2)\\ &\quad\times\mathrm{tr}_c\left[\phi_{\boldsymbol{p}}^{(2)\dagger}\phi_{\boldsymbol{q}}^{(2)}+\phi_{\boldsymbol{p}}^{(1)\dagger}\phi_{\boldsymbol{q}}^{(1)}\right].\end{aligned} \tag{A.11}$$

The integrand depends on $\boldsymbol{k}_\perp$ only through the gauge fields and so in can be its integral can be explicitly performed,

$$\int_{\{\boldsymbol{k}_\perp\}}\widetilde{U}_i^{\dagger}(\boldsymbol{p}_\perp+\boldsymbol{k}_\perp)\widetilde{U}_i(\boldsymbol{q}_\perp+\boldsymbol{k}_\perp) = (2\pi)^2\delta^2(\boldsymbol{p}_\perp-\boldsymbol{q}_\perp), \tag{A.12}$$

$$\begin{aligned}\sum_{s,a}\int\frac{d\nu d^2\boldsymbol{k}_\perp}{2(2\pi)^4}|\hat{\psi}^{(-)}_{\boldsymbol{k}_\perp\nu sa}|^2 &= \frac{4N_c}{(2\pi)^2}\int d\nu\int_{\{\boldsymbol{p}_\perp\}}\frac{\cosh(\nu\pi)}{M_{\boldsymbol{p}}^2}\left|\Gamma\left(\frac{1}{2}-i\nu\right)\right|^2(\boldsymbol{p}_\perp^2+m^2)\\ &= \frac{4N_c}{(2\pi)^2}\int d\nu\int_{\{\boldsymbol{p}_\perp\}}\left|\Gamma\left(\frac{1}{2}-i\nu\right)\right|^2\cosh(\nu\pi) = \frac{N_c}{\pi}\int d\nu\int_{\{\boldsymbol{p}_\perp\}},\end{aligned} \tag{A.13}$$

where we have made use of the identity,

$$\Gamma\left(\frac{1}{2}-i\nu\right)\Gamma\left(\frac{1}{2}+i\nu\right) = \frac{\pi}{\cosh(\pi\nu)}. \tag{A.14}$$

Similarly we compute the contribution from the positive energy wave function to the j^0,

$$\begin{aligned}\sum_{s,a}\int\frac{dvd^2\boldsymbol{k}_\perp}{2(2\pi)^4}|\hat{\psi}^{(+)}_{\boldsymbol{k}_\perp\nu sa}|^2 &= \frac{1}{4}\sum_{s,a}\int d\nu\int_{\{\boldsymbol{k}_\perp\}}\frac{1}{M_{\boldsymbol{k}}}\chi_a^\dagger\bar{u}_s(\boldsymbol{k}_\perp,0)\gamma^0\\ &\times\frac{1}{\cosh(\pi\nu)^2}\left\{\frac{e^{\frac{\pi\nu}{2}}}{\Gamma\left(\frac{1}{2}-i\nu\right)}\left(\frac{M_{\boldsymbol{k}}\tau}{2}\right)^{-i\nu}\mathscr{P}^+ + \frac{e^{-\frac{\pi\nu}{2}}}{\Gamma\left(\frac{1}{2}+i\nu\right)}\left(\frac{M_{\boldsymbol{k}}\tau}{2}\right)^{i\nu}\mathscr{P}^-\right\}\\ &\times\left\{\frac{e^{\frac{\pi\nu}{2}}}{\Gamma\left(\frac{1}{2}-i\nu\right)}\left(\frac{M_{\boldsymbol{k}}\tau}{2}\right)^{-i\nu}\mathscr{P}^+ + \frac{e^{-\frac{\pi\nu}{2}}}{\Gamma\left(\frac{1}{2}+i\nu\right)}\left(\frac{M_{\boldsymbol{k}}\tau}{2}\right)^{i\nu}\mathscr{P}^-\right\}u_s(\boldsymbol{k}_\perp,0)\chi_a,\end{aligned}\tag{A.15}$$

due the projectors in the integrand this quantity can be readily be written a compact form,

$$\begin{aligned}\sum_{s,a}\int\frac{dvd^2\boldsymbol{k}_\perp}{2(2\pi)^4}|\hat{\psi}^{(+)}_{\boldsymbol{k}_\perp\nu sa}|^2 &= \frac{1}{4}\sum_{s,a}\int d\nu\int_{\{\boldsymbol{k}_\perp\}}\frac{1}{M_{\boldsymbol{k}}}\frac{1}{\cosh(\pi\nu)^2}\chi_a^\dagger\bar{u}_s(\boldsymbol{k}_\perp,0)\gamma^0\\ &\times\frac{1}{\left|\Gamma\left(\frac{1}{2}+i\nu\right)\right|^2}\left(e^{\pi\nu}\mathscr{P}^+ + e^{-\pi\nu}\mathscr{P}^-\right)u_s(\boldsymbol{k}_\perp,0)\chi_a.\end{aligned}\tag{A.16}$$

Now we take the spin and color sums as usual which yields,

$$\begin{aligned}\sum_{s,a}\int\frac{dvd^2\boldsymbol{k}_\perp}{2(2\pi)^4}|\hat{\psi}^{(+)}_{\boldsymbol{k}_\perp\nu sa}|^2 &= \frac{1}{4}\int d\nu\int_{\{\boldsymbol{k}_\perp\}}\frac{1}{M_{\boldsymbol{k}}}\frac{1}{\cosh(\pi\nu)^2}\frac{1}{\left|\Gamma\left(\frac{1}{2}+i\nu\right)\right|^2}\\ &\times\mathrm{tr}_{sp\times c}\left[(M_{\boldsymbol{k}}\gamma^0-k^j\gamma^j+m)(\gamma^0\cosh(\pi\nu)+\gamma^3\sinh(\pi\nu))\right]\\ &= N_c\int d\nu\int_{\{\boldsymbol{k}_\perp\}}\frac{1}{\cosh(\pi\nu)}\frac{1}{\left|\Gamma\left(\frac{1}{2}+i\nu\right)\right|^2} = \frac{N_c}{\pi}\int d\nu\int_{\{\boldsymbol{k}_\perp\}},\end{aligned}\tag{A.17}$$

and so we can clearly see how at $\tau\to 0^+$ both contributions from the negative and positive energy wave functions are independant of the background gauge field and cancel each other our resulting in vanishing fermion number j^0.

A.2 Orthogonality Relation

The quark fields in the forward light-cone are orthonormal under the conserved inner product at the constant τ hypersurface, defined as

$$\left(\psi\middle|\chi\right)_\tau = \tau \int d\eta d^2\boldsymbol{x}'_\perp \hat{\psi}^\dagger(\tau, \boldsymbol{x}'_\perp, \eta)\hat{\chi}(\tau, \boldsymbol{x}'_\perp, \eta), \tag{A.18}$$

where the hat notation denotes that we are dealing with the boosted spinors. The orthonormality of the quark fields under this product follows as,

$$\left(\psi^{(-)}_{\boldsymbol{k}_\perp \nu s a}\middle|\psi^{(-)}_{\boldsymbol{k}'_\perp \nu' s' a'}\right) = 2(2\pi)^4\delta(\boldsymbol{k}_\perp - \boldsymbol{k}'_\perp)\delta(\nu - \nu')\delta_{ss'}\delta_{aa'}. \tag{A.19}$$

Bibliography

[1] I. Ya. Pomeranchuk. On the theory of multiple particle production in a single collision. *Dokl. Akad. Nauk Ser. Fiz.*, 78:889–891, 1951.

[2] R. Hagedorn. Statistical thermodynamics of strong interactions at high-energies. *Nuovo Cim. Suppl.*, 3:147–186, 1965.

[3] Siegfried Bethke. Experimental tests of asymptotic freedom. *Prog. Part. Nucl. Phys.*, 58:351–386, 2007. doi: 10.1016/j.ppnp.2006.06.001.

[4] Kenneth G. Wilson. Confinement of Quarks. *Phys. Rev.*, D10:2445–2459, 1974. doi: 10.1103/PhysRevD.10.2445. [,45(1974)].

[5] John C. Collins and M. J. Perry. Superdense Matter: Neutrons Or Asymptotically Free Quarks? *Phys. Rev. Lett.*, 34:1353, 1975. doi: 10.1103/PhysRevLett.34.1353.

[6] N. Cabibbo and G. Parisi. Exponential Hadronic Spectrum and Quark Liberation. *Phys. Lett.*, 59B:67–69, 1975. doi: 10.1016/0370-2693(75)90158-6.

[7] V. Skokov, A. Yu. Illarionov, and V. Toneev. Estimate of the magnetic field strength in heavy-ion collisions. *Int. J. Mod. Phys.*, A24:5925–5932, 2009. doi: 10.1142/S0217751X09047570.

[8] Kenji Fukushima, Dmitri E. Kharzeev, and Harmen J. Warringa. The Chiral Magnetic Effect. *Phys. Rev.*, D78:074033, 2008. doi: 10.1103/PhysRevD.78.074033.

[9] Harmen J. Warringa. Dynamics of the Chiral Magnetic Effect in a weak magnetic field. *Phys. Rev.*, D86:085029, 2012. doi: 10.1103/PhysRevD.86.085029.

[10] Dmitri E. Kharzeev and Ho-Ung Yee. Chiral Magnetic Wave. *Phys. Rev.*, D83:085007, 2011. doi: 10.1103/PhysRevD.83.085007.

[11] Dam T. Son and Piotr Surowka. Hydrodynamics with Triangle Anomalies. *Phys. Rev. Lett.*, 103:191601, 2009. doi: 10.1103/PhysRevLett.103.191601.

[12] Qiang Li, Dmitri E. Kharzeev, Cheng Zhang, Yuan Huang, I. Pletikosic, A. V. Fedorov, R. D. Zhong, J. A. Schneeloch, G. D. Gu, and T. Valla. Chiral magnetic effect in zrte5. *Nat Phys*, advance online publication:–, 02 2016. URL http://dx.doi.org/10.1038/nphys3648.

[13] A. V. Sadofyev and M. V. Isachenkov. The Chiral magnetic effect in hydrodynamical approach. *Phys. Lett.*, B697:404–406, 2011. doi: 10.1016/j.physletb.2011.02.041.

[14] Yuji Hirono, Tetsufumi Hirano, and Dmitri E. Kharzeev. The chiral magnetic effect in heavy-ion collisions from event-by-event anomalous hydrodynamics. 2014.

[15] M. A. Stephanov and Y. Yin. Chiral Kinetic Theory. *Phys. Rev. Lett.*, 109:162001, 2012. doi: 10.1103/PhysRevLett.109.162001.

[16] Dam Thanh Son and Naoki Yamamoto. Berry Curvature, Triangle Anomalies, and the Chiral Magnetic Effect in Fermi Liquids. *Phys. Rev. Lett.*, 109:181602, 2012. doi: 10.1103/PhysRevLett.109.181602.

[17] Larry D. McLerran and Raju Venugopalan. Gluon distribution functions for very large nuclei at small transverse momentum. *Phys. Rev.*, D49:3352–3355, 1994. doi: 10.1103/PhysRevD.49.3352.

[18] Larry D. McLerran and Raju Venugopalan. Computing quark and gluon distribution functions for very large nuclei. *Phys. Rev.*, D49:2233–2241, 1994. doi: 10.1103/PhysRevD.49.2233.

[19] Francois Gelis and Naoto Tanji. Quark production in heavy ion collisions: formalism and boost invariant fermionic light-cone mode functions. *JHEP*, 02:126, 2016. doi: 10.1007/JHEP02(2016)126.

[20] David J. Gross and Frank Wilczek. Ultraviolet Behavior of Nonabelian Gauge Theories. *Phys. Rev. Lett.*, 30:1343–1346, 1973. doi: 10.1103/PhysRevLett.30.1343.

[21] Gerard 't Hooft. How Instantons Solve the U(1) Problem. *Phys. Rept.*, 142:357–387, 1986. doi: 10.1016/0370-1573(86)90117-1.

[22] Steven Weinberg. The U(1) Problem. *Phys. Rev.*, D11:3583–3593, 1975. doi: 10.1103/PhysRevD.11.3583.

[23] Gerard 't Hooft. Symmetry Breaking Through Bell-Jackiw Anomalies. *Phys. Rev. Lett.*, 37: 8–11, 1976. doi: 10.1103/PhysRevLett.37.8.

[24] Kazuo Fujikawa. Path Integral Measure for Gauge Invariant Fermion Theories. *Phys. Rev. Lett.*, 42:1195–1198, 1979. doi: 10.1103/PhysRevLett.42.1195.

[25] Kazuo Fujikawa. Path Integral for Gauge Theories with Fermions. *Phys. Rev.*, D21: 2848, 1980. doi: 10.1103/PhysRevD.21.2848,10.1103/PhysRevD.22.1499. [Erratum: Phys. Rev.D22,1499(1980)].

[26] R. Jackiw and C. Rebbi. Vacuum Periodicity in a Yang-Mills Quantum Theory. *Phys. Rev. Lett.*, 37:172–175, 1976. doi: 10.1103/PhysRevLett.37.172.

[27] Kenji Fukushima. QCD matter in extreme environments. *J. Phys.*, G39:013101, 2012. doi: 10.1088/0954-3899/39/1/013101.

[28] D. E. Kharzeev, J. Liao, S. A. Voloshin, and G. Wang. Chiral magnetic and vortical effects in high-energy nuclear collisions—A status report. *Prog. Part. Nucl. Phys.*, 88:1–28, 2016. doi: 10.1016/j.ppnp.2016.01.001.

[29] C. A. Baker et al. An Improved experimental limit on the electric dipole moment of the neutron. *Phys. Rev. Lett.*, 97:131801, 2006. doi: 10.1103/PhysRevLett.97.131801.

[30] R. D. Peccei and Helen R. Quinn. Constraints Imposed by CP Conservation in the Presence of Instantons. *Phys. Rev.*, D16:1791–1797, 1977. doi: 10.1103/PhysRevD.16.1791.

[31] R. D. Peccei and Helen R. Quinn. CP Conservation in the Presence of Instantons. *Phys. Rev. Lett.*, 38:1440–1443, 1977. doi: 10.1103/PhysRevLett.38.1440.

[32] Frank Wilczek. Problem of Strong p and t Invariance in the Presence of Instantons. *Phys. Rev. Lett.*, 40:279–282, 1978. doi: 10.1103/PhysRevLett.40.279.

[33] Steven Weinberg. A New Light Boson? *Phys. Rev. Lett.*, 40:223–226, 1978. doi: 10.1103/PhysRevLett.40.223.

[34] Dmitri E. Kharzeev. Topologically induced local P and CP violation in QCD x QED. *Annals Phys.*, 325:205–218, 2010. doi: 10.1016/j.aop.2009.11.002.

[35] Kenji Fukushima, Dmitri E. Kharzeev, and Harmen J. Warringa. Real-time dynamics of the Chiral Magnetic Effect. *Phys. Rev. Lett.*, 104:212001, 2010. doi: 10.1103/PhysRevLett.104.212001.

[36] David J. Gross, Robert D. Pisarski, and Laurence G. Yaffe. QCD and Instantons at Finite Temperature. *Rev. Mod. Phys.*, 53:43, 1981. doi: 10.1103/RevModPhys.53.43.

[37] Guy D. Moore, Chao-ran Hu, and Berndt Muller. Chern-Simons number diffusion with hard thermal loops. *Phys. Rev.*, D58:045001, 1998. doi: 10.1103/PhysRevD.58.045001.

[38] D. Bodeker, Guy D. Moore, and K. Rummukainen. Chern-Simons number diffusion and hard thermal loops on the lattice. *Phys. Rev.*, D61:056003, 2000. doi: 10.1103/PhysRevD.61.056003.

[39] Larry McLerran, Emil Mottola, and Mikhail E. Shaposhnikov. Sphalerons and axion dynamics in high-temperature qcd. *Phys. Rev. D*, 43:2027–2035, Mar 1991. doi: 10.1103/PhysRevD.43.2027. URL https://link.aps.org/doi/10.1103/PhysRevD.43.2027.

[40] Kenji Fukushima and Pablo Morales. Spatial modulation and topological current in holographic QCD matter. *Phys. Rev. Lett.*, 111:051601, 2013. doi: 10.1103/PhysRevLett.111.051601.

[41] Karl Landsteiner, Eugenio Megias, Luis Melgar, and Francisco Pena-Benitez. Holographic Gravitational Anomaly and Chiral Vortical Effect. *JHEP*, 09:121, 2011. doi: 10.1007/JHEP09(2011)121.

[42] Dmitri E. Kharzeev and Dam T. Son. Testing the chiral magnetic and chiral vortical effects in heavy ion collisions. *Phys. Rev. Lett.*, 106:062301, 2011. doi: 10.1103/PhysRevLett.106.062301.

[43] Arthur M. Poskanzer and S. A. Voloshin. Methods for analyzing anisotropic flow in relativistic nuclear collisions. *Phys. Rev.*, C58:1671–1678, 1998. doi: 10.1103/PhysRevC.58.1671.

[44] Sergei A. Voloshin. Parity violation in hot QCD: How to detect it. *Phys. Rev.*, C70:057901, 2004. doi: 10.1103/PhysRevC.70.057901.

[45] R. A. Lacey. (PHENIX Collaboration) N. N. Ajitanand, S. Esumi. P- and CP-odd effects in hot and dense matter - 2010 (Proc.). *Proc. of the RBRC Workshops*, 96 230.

[46] Betty Abelev et al. Pseudorapidity density of charged particles in p + Pb collisions at $\sqrt{s_{NN}}$ = 5.02 TeV. *Phys. Rev. Lett.*, 110(3):032301, 2013. doi: 10.1103/PhysRevLett.110.032301.

[47] B. I. Abelev et al. Azimuthal Charged-Particle Correlations and Possible Local Strong Parity Violation. *Phys. Rev. Lett.*, 103:251601, 2009. doi: 10.1103/PhysRevLett.103.251601.

[48] Volker Koch, Soeren Schlichting, Vladimir Skokov, Paul Sorensen, Jim Thomas, Sergei Voloshin, Gang Wang, and Ho-Ung Yee. Status of the chiral magnetic effect and collisions of isobars. *Chin. Phys.*, C41(7):072001, 2017. doi: 10.1088/1674-1137/41/7/072001.

[49] Fred Cooper and Graham Frye. Single-particle distribution in the hydrodynamic and statistical thermodynamic models of multiparticle production. *Phys. Rev. D*, 10:186–189, Jul 1974. doi: 10.1103/PhysRevD.10.186. URL https://link.aps.org/doi/10.1103/PhysRevD.10.186.

[50] F. D. Aaron et al. Combined Measurement and QCD Analysis of the Inclusive e+- p Scattering Cross Sections at HERA. *JHEP*, 01:109, 2010. doi: 10.1007/JHEP01(2010)109.

[51] V.S. Fadin E.A. Kuraev, L.N. Lipatov. Multiregge processes in the Yang–Mills theory. *Sov. Phys. JETP*, 45:45, 199–204, 1977.

[52] L.N. Lipatov I. Balitsky. *Sov. J. Nucl. Phys.*, 28:822, 1978.

[53] I. Balitsky. Operator expansion for high-energy scattering. *Nucl. Phys.*, B463:99–160, 1996. doi: 10.1016/0550-3213(95)00638-9.

[54] Yuri V. Kovchegov. Small-x F_2 structure function of a nucleus including multiple pomeron exchanges. *Phys. Rev. D*, 60:034008, Jun 1999. doi: 10.1103/PhysRevD.60.034008. URL https://link.aps.org/doi/10.1103/PhysRevD.60.034008.

[55] Jamal Jalilian-Marian, Alex Kovner, Larry D. McLerran, and Heribert Weigert. The Intrinsic glue distribution at very small x. *Phys. Rev.*, D55:5414–5428, 1997. doi: 10.1103/PhysRevD.55.5414.

[56] Jamal Jalilian-Marian, Alex Kovner, and Heribert Weigert. The Wilson renormalization group for low x physics: Gluon evolution at finite parton density. *Phys. Rev.*, D59:014015, 1998. doi: 10.1103/PhysRevD.59.014015.

[57] Edmond Iancu, Andrei Leonidov, and Larry D. McLerran. The Renormalization group equation for the color glass condensate. *Phys. Lett.*, B510:133–144, 2001. doi: 10.1016/S0370-2693(01)00524-X.

[58] Elena Ferreiro, Edmond Iancu, Andrei Leonidov, and Larry McLerran. Nonlinear gluon evolution in the color glass condensate. 2. *Nucl. Phys.*, A703:489–538, 2002. doi: 10.1016/S0375-9474(01)01329-X.

[59] Kenji Fukushima. Evolving Glasma and Kolmogorov Spectrum. *Acta Phys. Polon.*, B42:2697–2715, 2011. doi: 10.5506/APhysPolB.42.2697.

[60] F. Gelis, K. Kajantie, and T. Lappi. Quark-antiquark production from classical fields in heavy ion collisions: 1+1 dimensions. *Phys. Rev.*, C71:024904, 2005. doi: 10.1103/PhysRevC.71.024904.

[61] F. Gelis, K. Kajantie, and T. Lappi. Chemical thermalization in relativistic heavy ion collisions. *Phys. Rev. Lett.*, 96:032304, 2006. doi: 10.1103/PhysRevLett.96.032304.

[62] A. I. Nikishov. Barrier scattering in field theory removal of klein paradox. *Nucl. Phys.*, B21: 346–358, 1970. doi: 10.1016/0550-3213(70)90527-4.

[63] Thomas D. Cohen and David A. McGady. The Schwinger mechanism revisited. *Phys. Rev.*, D78:036008, 2008. doi: 10.1103/PhysRevD.78.036008.

[64] Kenji Fukushima. Simulating net particle production and chiral magnetic current in a CP-odd domain. *Phys. Rev.*, D92(5):054009, 2015. doi: 10.1103/PhysRevD.92.054009.

[65] Holger Bech Nielsen and M. Ninomiya. No Go Theorem for Regularizing Chiral Fermions. *Phys. Lett.*, 105B:219–223, 1981. doi: 10.1016/0370-2693(81)91026-1.

[66] K.G. Wilson. Quarks and strings on a lattice. *New Phenomena In Subnuclear Physics*, Part. A: 69, 1977.

[67] Dmitri Kharzeev and Marzia Nardi. Hadron production in nuclear collisions at RHIC and high density QCD. *Phys. Lett.*, B507:121–128, 2001. doi: 10.1016/S0370-2693(01)00457-9.

[68] Dmitri Kharzeev and Eugene Levin. Manifestations of high density QCD in the first RHIC data. *Phys. Lett.*, B523:79–87, 2001. doi: 10.1016/S0370-2693(01)01309-0.

[69] Soren Schlichting and Scott Pratt. Charge conservation at energies available at the BNL Relativistic Heavy Ion Collider and contributions to local parity violation observables. *Phys. Rev.*, C83:014913, 2011. doi: 10.1103/PhysRevC.83.014913.

[70] James Charbonneau and Ariel Zhitnitsky. Topological Currents in Neutron Stars: Kicks, Precession, Toroidal Fields, and Magnetic Helicity. *JCAP*, 1008:010, 2010. doi: 10.1088/1475-7516/2010/08/010.

[71] Dorota Grabowska, David B. Kaplan, and Sanjay Reddy. Role of the electron mass in damping chiral plasma instability in Supernovae and neutron stars. *Phys. Rev.*, D91(8):085035, 2015. doi: 10.1103/PhysRevD.91.085035.

[72] Yukinao Akamatsu and Naoki Yamamoto. Chiral Plasma Instabilities. *Phys. Rev. Lett.*, 111: 052002, 2013. doi: 10.1103/PhysRevLett.111.052002.

[73] Er-dong Guo and Shu Lin. Quark mass effect on axial charge dynamics. *Phys. Rev.*, D93(10): 105001, 2016. doi: 10.1103/PhysRevD.93.105001.

[74] Paul M. Saffin and Anders Tranberg. Dynamical simulations of electroweak baryogenesis with fermions. *JHEP*, 02:102, 2012. doi: 10.1007/JHEP02(2012)102.